ACCELERATING NATURAL PRODUCT DISCOVERY AND SYNTHETIC BIOLOGY WORKFLOWS USING MULTIDIMENSIONAL MOLECULAR PHENOTYPING

By

Berkley M. Ellis

Dissertation
Submitted to the Faculty of the
Graduate School of Vanderbilt University
in partial fulfillment of the requirements
for the degree of
DOCTOR OF PHILOSOPHY
in
Chemistry
June 30, 2021
Nashville, Tennessee

Approved:

John A. McLean, Ph.D.

Renã A.S. Robinson, Ph.D.

David E. Cliffel, Ph.D.

Kevin L. Schey, Ph.D.

DEDICATION

This work is dedicated to Steve Koudelka.
Without your mentorship and example this would not have been possible.

ACKNOWLEDGMENTS

I would like to thank my dissertation advisor, Dr. John A. McLean, for his guidance and support. I am thankful for the opportunities that Dr. McLean and his research provided me whether it is traveling to conferences or working with cutting edge instrumentation. My time within this group is marked by hard work, good friends, and fun times. Throughout my experience in this group, I have been able to grow as a scientist, professional, and a person. It has been a pleasure working within this group and with such a great team of people.

I would also like to thank my committee members, Dr. Renã A.S. Robinson, Dr. David E. Cliffel, and Dr. Kevin L. Schey for all of their mentorship and conversations. Their insight and motivation have enabled me to become a better scientist.

All of the work within this document would not be possible without my friends in the McLean group. These graduate students, postdocs, and professors have pushed me to become better and supported me throughout all of my endeavors. I would like thank Dr. Stacy D. Sherrod for challenging me in sub-group meetings to answer tough questions and apply myself. I would like to acknowledge Dr. James C. Poland for his mentorship and teaching me to be objective and understanding. Thank you Dr. Jacqueline A. Picache for all of the lunches, conversations, laughter, and coding. I would especially like to thank Andrzej Ballinski for his technical help, mentorship, challenging conversations, and friendship. The list of group members that have helped me is quite long, but I would like to highlight Dr. James N. Dodds, Dr. Sarah M. Stow, and Dr. Nichole M. Laureau for paving the way within the McLean group and being role models, mentors, and friends.

I would like to acknowledge my friends and family for their love and support. To my father, Cole, you are truly one of my best friends and have always been a role model that I have looked up to. Your industrious attitude and confidence are intangible characteristics that I have tried to incorporate within myself. Our conversations on my walk home every day from work gave me the necessary perspective and laughter to stay the path of my graduate career. To my mother, Michele, you have always understood me better than anyone else and accepted me for who I am. Aside from your love and support, you taught me attention to detail, which has been

invaluable in my pursuits as a scientist. To my sister, Jenna, your selflessness and love have inspired me and helped me along this journey. You have been a true teammate in navigating the COVID-19 pandemic. Our friendship and daily conversations have quailed so much anxiety and brought so much joy into my life. I would also like to thank my friends Todd Galvin, Adam Davey, and all of those in the Lynchburg Men's Lacrosse Program for teaching me to enjoy the struggle of progress and live in the moment. I would like to acknowledge my teachers at St. Charles Preparatory School, particularly Dr. Penny Bostic, Mr. Dominic Cavello, and Mr. Joseph Moyer for challenging me at an early age and instilling a work ethic inside me. Finally, thank you William A. Weldon, and Benjamin D. Mackessy for all of the good times, support, and love.

I would be remised if I didn't acknowledge my friends that I have met here in Nashville. Caleb T. West, you have been such a great and loving friend. Without you, the growth that I have had as a person in my time in graduate school would not have been possible. Zachary R. Austin, from our time spent in professional development to comedy clubs and golf courses, you have always been a much-needed source of optimism and fun. To all of the members of Father Ryan Lacrosse, Rise Lacrosse and Nashville Ignite, my time spent with all of you has helped me persevere through graduate school, given me life lessons, and countless good times that I will never forget.

Lastly, I would like to acknowledge the funding sources for my research: the National Institute of Heath, the Department of Energy, the College of Arts and Science, and the Center for Innovative Technologies.

TABLE OF CONTENTS

Page

DEDICATION ii

ACKNOWLEDGMENTS iii

LIST OF TABLES viii

LIST OF FIGURES ix

CHAPTERS

1 INTRODUCTION: MASS SPECTROMETRY TO ACCELERATE SYNTHETIC BIOLOGY WORKFLOWS AND PROBE MOLECULAR STRUCTURE 1

1.1 Introduction 1
1.2 Chapter Overviews 2
1.2.1 Spatiochemically Profiling Intermicrobial Interactions with Desorption Electrospray Ionization-Ion Mobility-Imaging Mass Spectrometry and Unsupervised Segmentation 2
1.2.2 Accelerating Strain Engineering Using Desorption Electrospray Ionization-Imaging Mass Spectrometry and Untargeted Molecular Analysis of Intact Microbial Colonies 4
1.2.3 Chiral Separation of Diastereomers of the Cyclic Nonapeptides Vasopressin and Desmopressin by Uniform Field Ion Mobility-Mass Spectrometry 6
1.3 Acknowledgments 6
1.4 References 7

2 SPATIOCHEMICALLY PROFILING MICROBIAL INTERACTIONS WITH DESORPTION ELECTROSPRAY IONIZATION-ION MOBILITY-MASS SPECTROMETRY AND UNSUPERVISED SEGMENTATION 8

2.1 Introduction 8
2.2 Experimental Methods 10
2.2.1 Strains 10
2.2.2 Culture and Growth Conditions 11
2.2.3 Sample Preparation 11
2.2.4 Acquisitions 11
2.2.5 Data Processing and Analysis 12
2.3 Results and Discussion 15
2.3.1 Sampling Methodology 15
2.3.2 Unsupervised Segmentation of Microbial Predation 19
2.3.3 Application To WT, *M. xanthus Δta1* and Phase Variants 22
2.4 Conclusions 25

2.5 Acknowledgements 27
2.6 References 27

3 ACCELERATING STRAIN ENGINEERING USING DESORPTION ELECTROSPRAY IONIZATION-IMAGING MASS SPECTROMETRY AND UNTARGETED MOLECULAR ANALYSIS OF INTACT MICROBIAL COLONIES 30

3.1 Introduction 30
3.2 Experimental Methods 32
3.2.1 Strains and Culture Conditions 32
3.2.2 Sample Preparation and Acquisitions 33
3.2.3 Data Processing and Analysis 34
3.2.4 Confirmation of Strain Genotype via PCR 34
3.3 Results and Discussion 35
3.3.1 Rapid Metabolic Phenotyping of Free Fatty Acid Overproducing *E. coli* 35
3.3.2 Untargeted Molecular Phenotyping via Unsupervised Segmentation 40
3.3.3 Unsupervised Segmentation Elucidates the Underlying Biology of Engineered Microorganisms 44
3.4 Conclusions 47
3.5 Acknowledgements 48
3.6 References 49

4 CHIRAL SEPARATION OF DIASTEREOMERS OF THE CYCLIC NONAPEPTIDES VASOPRESSIN AND DESMOPRESSIN BY UNIFORM FIELD ION MOBILITY MASS SPECTROMETRY 52

4.1 Introduction 52
4.2 Experimental Methods 55
4.3 Results and Discussion 55
4.4 Conclusions 60
4.5 Acknowledgements 61
4.6 References 61

5 CONSPECTUS AND OUTLOOK 63

5.1 Conspectus 63
5.2 Outlook and Future Directions 64
5.2.1 DESI-IM-IMS to Enhance Feature Annotation 65
5.2.2 IM-IMS to Increase Metabolite Identification Confidence 67
5.2.3 DESI-IM-IMS to Accelerate Natural Product Discovery 69
5.3 Concluding Remarks 71
5.4 Acknowledgements 71

5.5 References 72

APPENDIX

A. References of Adaptation for Chapters 74

B. Supplementary Material for Chapter 2 76

C. Supplementary Material for Chapter 3 131

D. Supplementary Material for Chapter 4 140

LIST OF TABLES

Table Page

1. 2.1 Sampling Metrics Across DESI-IMS Preparation Methods 15
2. 4.1 Abbreviations and Designations of Chirality for Diastereomers 54
3. B.1 Calculated Values Annotating DESI-IMS Preparation Method Efficiency..... 78
4. B.2 Measured features using DESI-IMS with tentative metabolite identifications and annotations 79
5. C.1 List of Engineered *E. coli* strains, genotype, and primer used for PCR Validation..... 139
6. D.1 A summary of the drift tube CCS measurements of nonapeptides..... 141

LIST OF FIGURES

Figure Page

1. 1.1 Photograph of DESI process at atmospheric conditions 3
2. 1.2 Diagram of Waters Synapt G2-S Instrument 5
3. 2.1 Diagram of microbial predation and evaluation of tested sample preparation methods .. 14
4. 2.2 Unsupervised segmentation of microbial predation corroborated by PCA 18
5. 2.3 Unsupervised segmentation results of microbial predation with outputs 21
6. 2.4 Optical Images, ion overlays, and segmentation results of *M. xanthus* sample types.. 24
7. 3.1 Sample preparation and acquisition workflow to profile microbial biosynthesis..... 36
8. 3.2 DESI-IMS results from a single acquisition of TY05 and NHL17 co-culture 38
9. 3.3 Unsupervised segmentation to phenotype four engineered *E. coli* strains 43
10. 3.4 PCA and Volcano plots highlighting unique molecular profiles of strains 46
11. 4.1 Chemical scaffold of nonapeptide hormones desmopressin and vasopressin..... 53
12. 4.2 Ion mobility spectra of nonapeptides with representations of intramolecular folding. 57
13. 4.3 Structural representations and theoretical conformations on nonapeptides..... 58
14. 5.1 Nesting of analytical timescales based on speed of separation of IM-MS acquistions 66
15. 5.2 DESI-IM-IMS data highlighting IM separation of similar m/z values 68
16. 5.3 Ion mobility as a means for natural product discovery and prioritization..... 70
17. B.1 Venn Diagram of DESI-IMS and LC-MS features from microbial co-cultures 124
18. B.2 Fragmentation spectra of identified metabolites from microbial co-cultures 125
19. B.3 Average mass spectra of DESI-IMS preparation methods..... 126
20. B.4 Biological replicates of unsupervised segmentation from MMS DESI-IMS 127
21. B.5 Natural product discovery workflow using unsupervised segmentation. 128
22. B.6 Biological replicas of natural product biosynthesis across *M. xanthus* sample types 129
23. B.7 Drift time vs relative intensity of WT and *M. xanthus* sample types 130
24. C.1 Evaluation of raster rate on sampling time and dodecanoic acid measurement..... 133
25. C.2 Comparison of IMS data analysis techniques 134

26. C.3 Segment fatty acid profiles of engineered *E. coli* strains 135
27. C.4 Confirmation of unsupervised segmentation results using PCR genotyping 136
28. C.5 PCA loadings plot highlighting features contributing to strain phenotypes 137
29. C.6 MS/MS spectra of identified lipids using DESI-MS/MS 138
30. D.1 Ion mobility fragmentation data for 8L-vasopressin 142
31. D.2 Mobility selected mass spectra for vasopressin diastereomers 143
32. D.3 Ion mobility spectra of protonated vasopressin diastereomers and a mixture of both144
33. D.4 Drift time distributions of 8L-vasopressin in Helium 145
34. D.5 RMSD clustering analysis of 8L-vasopressin theoretical structures 146
35. D.6 Distribution of theoretical structures based on calculated CCS values 147

LIST OF ABBREVIATIONS

MAGE ..... Multiplexed Automated Genome Engineering

MS ..... Mass Spectrometry

GC-MS ..... Gas Chromatography-Mass Spectrometry

LC-MS ..... Liquid Chromatography-Mass Spectrometry

DESI-MS ..... Desorption Electrospray Ionization- Mass Spectrometry

DESI-IMS ..... Desorption Electrospray Ionization-Imaging Mass Spectrometry

MS/MS ..... Tandem Mass Spectrometry

IM ..... Ion Mobility

MMS ..... Microporous Membrane Scaffold

MALDI ..... Matrix assisted laser desorption ionization

LC-ESI-MS ..... Liquid Chromatography- Electrospray Ionization- Mass Spectrometry

E. coli ..... *Escherichia coli*

IM-MS ..... Ion Mobility- Mass Spectrometry

MRSA ..... Methicilin-resistant- *Staphylococcus aureus*

RPLC-ESI-MS ..... Reversed Phase- LC-ESI-MS

IMS ..... Imaging Mass Spectrometry

LESA ..... Liquid Extraction Surface Analysis

Nano-DESI ..... Nanospray- Desorption Electrospray Ionization

M. xanthus ..... *Myxococcus xanthus*

CYE ..... Casitone Yeast Extract

LysoPE ..... Lysophosphatidylethanolamine

SocA ..... Short-chain Alcohol Dehydrogenase

s/n ..... signal-to-noise ratio

PCA .....Principal Component Analysis

PV.....Phase Variation

WT..... Wild Type

MMS- DESI-IMS.....Microporous Membrane Scaffolded- DESI-IMS

FFA .....Free Fatty Acid

PG..... Phosphatidylglycerol

m/z.....mass-to-charge ratio

IPTG.....Isopropyl-β-D-thiogalactopyranoside

LB..... Luria Bertani

DESI-MS/MS..... Desorption Electrospray Ionization-Tandem Mass Spectrometry

RMS ..... Root Mean Square

ACP .....Acyl Carrier Protein

FAB ..... Fatty Acid Biosynthesis

ROI..... Region of Interest

FA.....Fatty Acid

PCR ..... Polymerase Chain Reaction

PE ..... Phosphatidylethanolamine

CCS .....Collision Cross Section

μm. ..... micrometer

μs..... microsecond

VP..... Vasopressin

DP..... Desmopressin

RMSD.....Root-mean-square-deviation

ppm.....parts per million

CHAPTER 1

ACCELERATING SYNTHETIC BIOLOGY AND BIOSYNTHETIC WORKFLOWS USING DESI-IMS AND IM-MS

1.1 Introduction

Synthetic biology and natural product discovery workflows employ natural constructs such as bacteria for the production and discovery of chemical commodities. Bacterial chassis are a primary focus due to their seemingly untapped biosynthetic potential. Synthetic biology strategies aim to engineer microbial cell factories that produce chemicals ranging from fuels to therapeutics using renewable feedstocks and biomass. Alternatively, natural product discovery leverages the millions of years of microbial evolution to identify and isolate novel chemical structures that possess potent bioactivity (i.e. anticancer and antibiotic properties). Fully realized, these fields can address global challenges across medical, environmental, energy, and economic sectors.[1]

Given the significant advances in genomic and biologic sciences, synthetic biology and biosynthetic workflows are no longer inhibited by reading and writing DNA.[2] The current rate-limiting step in these fields are analytical methods that characterize the metabolic and biosynthetic outcomes of genetic editing events.[2] Directed evolution experiments and screening strain libraries are techniques proven to isolate genes and properties of biological systems with enhanced performance. These workflows can yield upwards of 10^{10} genetic variants with technologies like multiplexed automated genome engineering (MAGE) capable of producing over 4.3 billion combinatorial variants in a day.[2,3] In contrast, contemporary analytical methods measuring phenotypes are limited to ca. 10^2 samples per day. Natural product discovery workflows share a similar bottleneck. However, instead of directing efforts solely towards the generation of new strains, these workflows test numerous growth conditions (co-cultures, media composition, etc.) of different species to activate silent gene clusters encoding secondary

metabolite synthesis.[4] To accelerate these workflows and their ultimate commercial utility, rapid analytical methods comprehensively characterizing biosynthetic production are required.

Mass spectrometry-based techniques address these challenges by simultaneously measuring the intrinsic property of mass-to-charge ratio (m/z) of molecular species with high sensitivity and at rates consummate with high throughput analysis.[5] Contemporary mass spectrometry (MS) methods to investigate biosynthetic production typically use gas chromatography-mass spectrometry (GC-MS) or liquid chromatography-mass spectrometry (LC-MS).[6,7] However, the chromatography and sample preparation required by these sequential strategies greatly limit throughput. For these reasons, we have developed desorption electrospray ionization – imaging mass spectrometry (DESI-IMS) workflows to characterize microbial biosynthesis. DESI is an ambient ionization technique that reduces sample preparation by directly sampling biological tissues without sample pretreatment and under ambient conditions (Figure 1.1). Using a Waters Synapt G2-S MS (Waters, Manchester UK), DESI-IMS is amenable to both tandem mass-spectrometry (MS/MS) and ion mobility (IM) experiments measuring the molecular composition and conformations of biomolecules, respectively (Figure 1.2). The utility of these techniques in profiling microbial biosynthesis and even measuring chirality are described within this dissertation.

1.2 Chapter Overviews

In the following chapters, we describe the application of DESI-IMS, DESI-IM-IMS, and IM-MS to characterize biomolecules. In particular, we highlight the value of DESI-IMS to accelerate biosynthetic workflows.

1.2.1 *Spatiochemical Profiling Microbial Interactions with Membrane Scaffolded Desorption Electrospray Ionization-Ion Mobility-Imaging Mass Spectrometry and Unsupervised Segmentation*

Specifically, Chapter 2 details the development of a novel DESI-IMS method for probing natural product synthesis in microbial co-cultures.

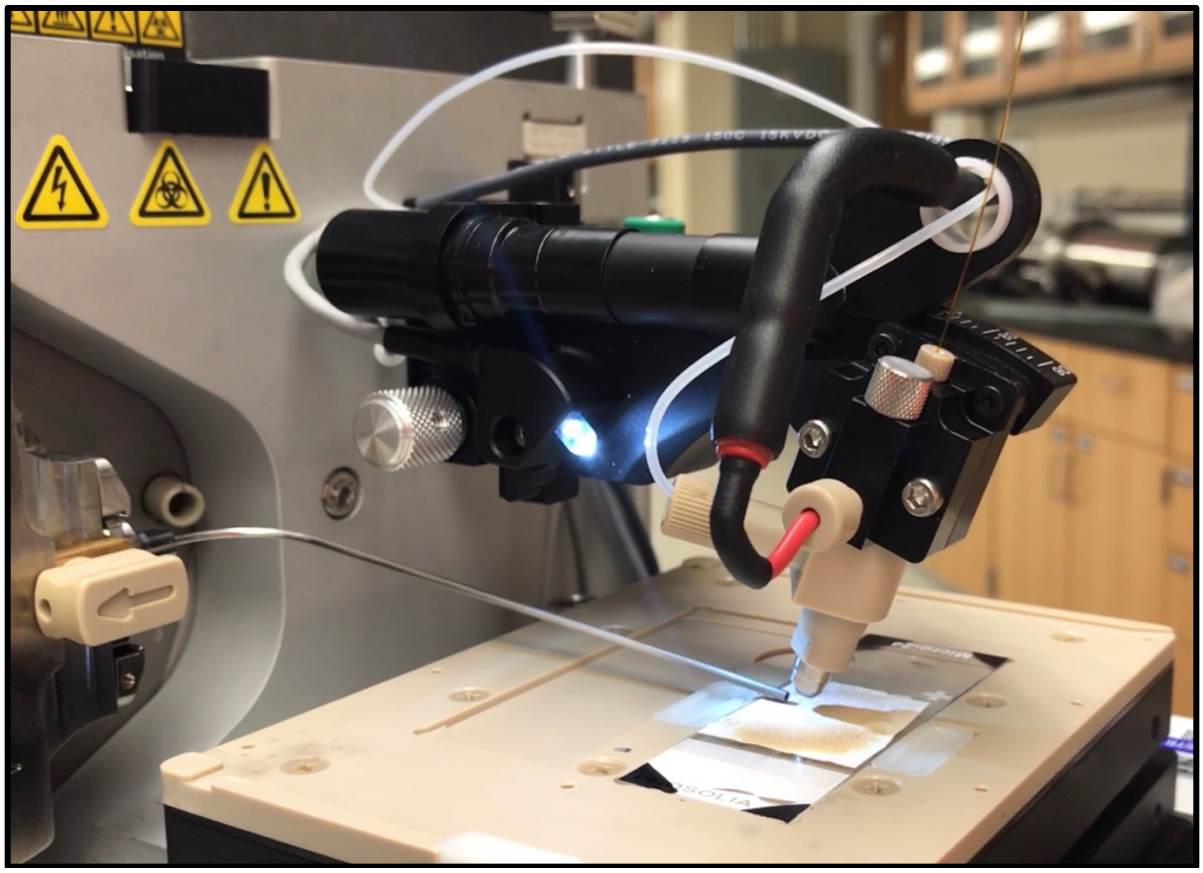

Figure 1.1. Photograph of DESI sampling under ambient conditions.

We demonstrate that DESI-IMS using microporous membrane scaffolds (MMS) enables enhanced spatiochemical analyses of interacting microbes amongst tested sample preparation techniques. Membrane scaffolded DESI-IMS has inherent advantages compared to matrix-assisted laser desorption ionization (MALDI) and other IMS methods through direct IMS analyses of microbial chemistry *in situ*. This rapid imaging method yields sensitive MS analyses with unique m/z measurements when compared to liquid chromatography- electrospray ionization-mass spectrometry (LC-ESI-MS) via unmediated sampling by MMS DESI-IMS. Unsupervised segmentation imaging analysis of acquired DESI-IMS data reveals distinct chemical regions corresponding to intermicrobial phenomenon such as predation and communication. We validate the method by linking Myxovirescin A and DKxanthene-560 to their known biological roles of predation and phase variation, respectively. In addition to providing the first topographic locations of known natural products, we prioritize 47 unknown features using segmentation within the region of predation. Thus, DESI-IMS and unsupervised segmentation spatially annotates the known biology of myxobacteria and provides functional exploration of newly uncharacterized small molecules.

1.2.2 *Accelerating Strain Engineering Using Desorption Electrospray Ionization-Imaging Mass Spectrometry and Untargeted Molecular Analysis of Intact Microbial Colonies* Chapter 3 details the application of the MMS DESI-IMS method to accelerate synthetic biology workflows. We applied DESI-IMS for rapid analytical measurements characterizing phenotypes resulting from genetic edits by directly sampling microorganisms. This technology increases the throughput of metabolic measurements by reducing sample preparation and analyzing organisms in a multiplexed fashion. To further accelerate synthetic biology workflows, we utilized untargeted acquisitions and unsupervised analytics to provide multiple targets for future engineering strategies within a single acquisition. We demonstrate the utility of the developed method using *Escherichia coli* strains engineered to overproduce free fatty acids. Using unsupervised data analytics, we determined discrete metabolic phenotypes associated with each strain, which includes the primary product, relative production levels, and specificity within biosynthetic production.

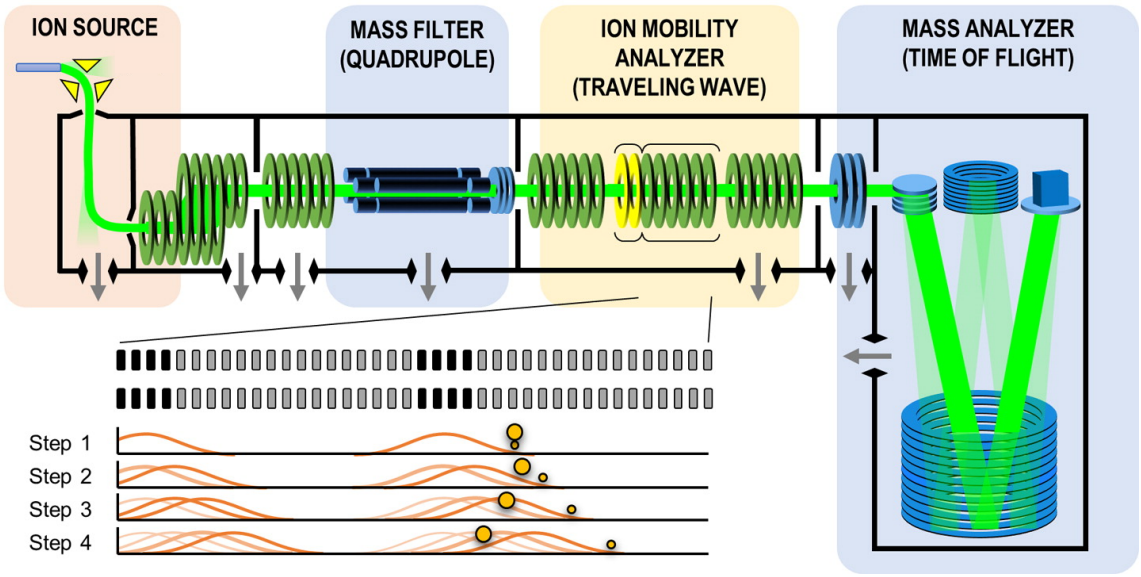

Figure 1.2. Diagram of Waters Synapt-G2S High Definition Mass Spectrometer. Ion mobility separations of molecular size and shape are performed via traveling wave separations. Adapted with permission from May, J.C.; McLean, J.A., "Ion Mobility-Mass Spectrometry: Time-Dispersive Instrumentation" *Anal. Chem*, **2015**, 87 (3), 1422-1436. https://pubs.acs.org/doi/10.1021/ac504720m.

The determined metabolic phenotypes additionally detail the broader biology of the microorganisms. Within our *E. coli* panel, we measured changes in membrane lipid composition, which affects cell viability. In sum, we present an analytical method to accelerate synthetic biology workflows through rapid, untargeted, and multiplexed analyses.

1.2.3 *Chiral Separation of Diastereomers of the Cyclic Nonapeptides Vasopressin and Desmopressin by Uniform Field Ion Mobility Mass Spectrometry* Chapter 4 highlights the utility of IM-MS to probe molecular conformations and chirality within MS workflows. In this study IM-MS is used to distinguish chiral diastereomers of the nonapeptides desmopressin and vasopressin. The differences in gas phase cross sectional area (*ca.* 2%) were sufficient to directly resolve the enantiomers present in a binary mixture. Results from computational modeling indicate that chiral recognition by IM-MS for nonapeptides is possible due to enantiomer-specific conformations in the gas-phase, namely a compact ring-tail conformer specific to the L-enantiomer forms.

1.3 Acknowledgments

This dissertation chapter was adapted from the abstracts of several published manuscripts including "Spatiochemical Profiling Microbial Interactions with Membrane Scaffolded Desorption Electrospray Ionization-Ion Mobility-Imaging Mass Spectrometry and Unsupervised Segmentation" by Berkley M. Ellis, Caleb N. Fischer, Leroy B. Martin, Brian O. Bachmann, and John A. McLean published in *Analytical Chemistry* **2019**, 91 (21), 13703-13711; "Accelerating Strain Engineering Using Desorption Electrospray Ionization-Imaging Mass Spectrometry and Untargeted Molecular Analysis of Intact Microbial Colonies" by Berkley M. Ellis, Piyoosh Babele, Jody C. May, Carl H. Johnson, Brian F. Pfleger, Jamey D. Young, and John A. McLean, preprinted on Biorxiv server at https://doi.org/10.1101/2021.04.01.438078; and "Chiral Separation of Diastereomers of the Cyclic Nonapeptides Vasopressin and Desmopressin by Uniform Field Ion Mobility Mass Spectrometry" by Shawn T. Philips, James N. Dodds, Berkley, M. Ellis, Jody C. May, and John A . McLean published in *Chemical Communications* **2018**, 54 (68), 9398-9401.

Financial support for this research was provided by the U.S. Department of Energy, Office of Science, Biological and Environmental Research Division under award number DE-SC00019404. Financial support for aspects of this research was also provided by The National Institutes of Health (Grants NIH NIGMS R01GM092218, NIGMS R37GM067152, NCI R03CA222-452-01 and NCI 1F32GM128344-01), the U.S. Environmental Protection Agency under Assistance Agreement 83573601, and the U.S. Army Research Office and the Defense Advanced Research Projects Agency (DARPA) under Cooperative Agreement W911 NF-14-2-0022. This work has not been formally reviewed by the EPA. The views expressed in this document are solely those of the authors and do not necessarily reflect those of the funding agencies and organizations. EPA, DARPA, and the U.S. Government do not endorse any products or commercial services mentioned in this publication.

1.4 References

(1) National Research Council. 2015. Industrialization of Biology: A Roadmap to Accelerate the Advanced Manufacturing of Chemicals. Washington, DC: The National Academies Press. **2015**.

(2) Pfleger, B. F.; Prather, K. L. J. *Nat. Biotechnol*., **2015**, 33 (11), 1148-1149.

(3) Wang, H. H.; Isaacs, F.J.; Carr, P. A.; Sun, Z. Z.; Xu, G.; Forest, C. R.; Church, G. M. *Nature*, **2009**, 460 (7257), 894-898.

(4) Covington, B. C.; Spraggins, J. M.; Ynigez-Gutierrez, A. E.; Hylton, Z. B.; Bachmann, B. O. *Appl. Environ. Microbiol.,* **2018**, 84 (19), e01125-18.

(5) May, J.C.; McLean, J. A. *Ann. Rev. Anal. Chem*., **2016**, 9, 387-409.

(6) Gajewski, J.; Pavlovic, R.; Fischer, M.; Boles, E.;Grininger, M. *Nat. Comm.*, **2017**, 8, 14650.

(7) Rigouin, C.; Gueroult, M.; Croux, C.; Dubois, G.; Borsenberger, V.; Barbe, S.; Bordes, F. *Microb. Cell Fact*., **2018**, 17 (1), 142.

CHAPTER 2

SPATIOCHEMICALLY PROFILING MICROBIAL INTERACTIONS DESORPTION-ELECTROSPRAY IONIZATION-ION MOBILITY-IMAGING MASS SPECTROMETRY AND UNSUPERVISED SEGMENTATION

2.1 Introduction

A significant means by which microorganisms maintain interactions within ecological communities is through producing primary and secondary metabolites.[1] In human-microbiome interactions, *Escherichia coli* was shown to secrete colibactin, which intercalates into host DNA. This demonstrated how human gut microbiota composition can be connected to carcinogenesis.[2-4] In insects, volatile metabolites emitted from microbe-microbe interactions constitute a symbiotic relationship modulating insect behavior.[5] Leaf cutting ants harbor symbiotic actinomycetes on their carapace that produce antifungal compounds, which allow the ants to prevent pathogenic strains from invading the fungal gardens they use as a food source.[6] An anti-methicilin-resistant *Staphylococcus aureus* (MRSA) metabolite lugdunin is produced by *Staphylococcus lugdunensis* and mediates interspecies *Staphylococcus* interactions in human nares.[7] The importance of microbial secondary metabolites in maintaining complex interkingdom, interspecies, and intergeneric chemical ecologies may be one reason that microbial natural products have become a major source of therapeutic antibiotics and anticancer agents in human medicine.

Historically, the discovery of secondary metabolites has been conducted via bioassay guided isolation from microbial liquid monocultures.[8–10] However, recent innovations in natural product discovery have demonstrated novel secondary metabolite production from microbes in solid-phase growth.[11] Indeed, microbial competition and other mixed culture phenomena induce broad changes in the measurable metabolome in comparison to individual monocultures.[12–14] Typically, metabolomic changes are measured via reversed phase liquid chromatography-electrospray ionization-mass spectrometry (RPLC-ESI-MS).[9,12,13] However, in these

experiments, there is a loss of the spatial expression patterns of metabolites, which may reveal functional roles. Thus, developing tools that provide detailed spatial maps of secondary metabolites during co-culture conditions on surfaces are an active area of research. Fully realized, these promise to both advance natural product discovery as well as detail the functional roles of primary and secondary metabolite dynamics in microbial chemical ecology.

Imaging mass spectrometry (IMS) is conducive to sampling microbes under planar solid-phase growth conditions. This technique can be used to assess chemical-spatial phenotypes by correlating the location of measured metabolites to observed microbial morphologies.[11] These spatial correlations provide a significant advantage in assessing the functional roles of natural products. For instance, homospermidine lipids were correlated to myxobacteria fruiting body formation using matrix assisted laser desorption ionization (MALDI) imaging MS.[11] Indeed, MALDI was the first technique used to map secondary metabolites from microorganisms.[15] Subsequently, an array of imaging MS techniques have been developed including liquid extraction surface analysis (LESA), desorption electrospray ionization (DESI), and nanospray-DESI (nano-DESI) to analyze microbial metabolites.[16–22] DESI-IMS methods to sample microbial communities are of particular interest for screening purposes due to rapid data acquisition and minimal sample preparation associated with ambient sampling.[22] Removing the vacuum requirements from ionization increases throughput and provides some flexibility in the state of the sample to be interrogated. Therefore, ambient sampling provides a means for the direct measurements of secondary metabolites within the microbial environment in situ. For these reasons, we describe DESI-IMS to spatially profile secondary metabolites of microbial communities in co-culture conditions.

Herein, we have developed and evaluated a process for DESI-IMS based analysis of spatially-resolved molecular patterns associated with interacting microbes grown on surfaces. The most promising workflow combines a microporous membrane scaffold (MMS) and an unsupervised image segmentation chemoinformatics platform for data analysis. Spatial segmentation has been applied to MALDI-IMS data of microbial relations, setting a precedence for spatiochemical phenotyping of microorganisms in response to co-culture conditions.[23-25]

Further, membrane scaffolds have been used in microbiology and DESI-IMS in particular to study biofilm formation and metabolite production.[26,27] We developed a membrane scaffolded DESI-IMS workflow with unsupervised segmentation using the model predator-prey system of *Myxococcus xanthus* DK1622 and *Escherichia coli*. Using the MMS DESI-IMS method, we observed the significant accumulation of the myxobacterial secondary metabolites DKxnathene-560 and Myxovirescin A within the region of interaction.[28–31] To our knowledge DESI-IMS and unsupervised image segmentation provides the first topographic location of these metabolites during surface predation. We demonstrate the utility of the method in natural product discovery by measuring and spatially prioritizing unknown features within this designated region of predation. Therefore, DESI-IMS and unsupervised segmentation can be used to elucidate previously unreported molecules with implicated roles in secondary metabolism and predation. Comparing *M. xanthus* mutants and chemotypes, we validate previous reports of Myxovirescin A within myxobacterial predation of *E. coli* and further probe phase variation within this phenomenon via DKxanthene-560.[28–31] In sum, we present a workflow that effectively evaluates microbe-microbe interactions and correlates spatial location of metabolites to biological function.

2.2 Experimental Methods

2.2.1 *Strains Escherichia coli* B/R was obtained from a plate of the amoeba *Dictyostelium discoideum* AX-2. A *D. discoideum* AX-2 stock was obtained from the Dicty Stock Center at Northwestern University (Chicago, IL). The original plates containing both *D. discoideum* AX-2 and *E. coli* B/R were restreaked on CYE agar until pure *E. coli* B/R colonies were obtained. The *Myxococcocus xanthus* DK1622 and Δta1 strains were kindly donated to our laboratories by Dr. Daniel Wall (University of Wyoming, Laramie, WY). *M. xanthus* DK1622 undergoes phase variation, a process by which predominantly yellow or tan subpopulations appear due to changes in gene expression.[28-30] Phenotypic studies show increased DKxanthene production resulting in variants by streaking out *M. xanthus* Dk1622 and then picking individual colonies that were either yellow or tan in appearance.

2.2.2 *Culture and Growth Conditions* The prey *E. coli* was grown in casitone yeast extract (CYE) liquid medium (1% casitone, 0.5 % yeast extract, 8 mM MgSO4, 10 mM MOPS, pH 7.6) for 16-24 h. After growth, *E. coli* was spun down and concentrated 10- 20 fold. 50 μL of the prey was spotted onto 10 % (carbon sources of yeast extract and casitone) CYE medium and allowed to dry for 1-2 h prior to placement of the predator myxobacteria. Predator seed cultures were inoculated into CYE liquid medium and shaken at 200 rpm for 48 h at 30 ºC (New Brunswick Scientific, Innova 4900 Multi-tier Environmental Shaker). After growth, the cultures were spun down, concentrated 10-20 fold, and 50 μL was spotted adjacent to the dried *E. coli*. After the myxobacteria dried, each sample was placed into a 30 ºC incubator and allowed to grow for four days. After the allotted time, they were stored at 4 ºC until sampled.

2.2.3 *Sample Preparation* We evaluated three methods of sample preparation for the detection of microbially produced small molecules via DESI-IMS. *Dried agar* samples were prepared by first placing a glass slide in the Petri dish below the growth medium, such that predator and prey colonies were spotted on the agar directly above the glass slide. After growth the samples were allowed to dry for 8 hours. The glass slide was then removed from the Petri dish by detaching any medium outside of the slide area. The resulting dried medium and colonies were sampled.[21] *Imprinting* samples were constructed by placing a glass slide on top of the grown microbial colonies on agar and applying uniform pressure for 10-20 seconds. The transferred colonies were allowed to dry for an hour before sampling.[19] *The microporous membrane scaffold* (MMS) method entailed spotting predator and prey onto a sterile nylon membrane (Sigma-Aldrich, 0.45 μM pore size, 47 mm diameter) and placing the membrane on top of the medium. This system was kept intact within the incubator and during the growth period. Prior to sampling, the membrane was removed from the medium, dried for 10 minutes, and adhered to a glass slide using double-sided scotch tape. Membranes were incubated on agar without colonies to provide blanks for the MMS method.

2.2.4 *Acquisitions* A Waters Synapt G2S High Definition Mass Spectrometer (Waters Corporation, Milford MA) was used with a Waters x-y directional stage and DESI source described by *Tilner et al*.[32] The system was mass calibrated with sodium formate salt clusters to

a 95% confidence band and root mean square (RMS) residual mass ≤ 0.5 ppm. This resulted in experimental mass accuracies of generally 2-5 ppm ± 3 ppm and mass resolving powers circa 11,000. Ion mobility calibrations were performed using polyalanine to achieve RMS CCS ≤ 0.5%. Optimized DESI source conditions were found to be a –3 kV capillary voltage, 110 °C desolvation temperature, 0.5 mPa N2 gas flow, and a cone voltage of 40 V. The sprayer was set at a 70 ° angle, with the x, y, z, settings at -2, +2, and +2.75, respectively. Ionization solvent was comprised of 90/10 acetonitrile/water (Optima grade, Fisher Scientific) solution with 0.1% NH_4OH and 0.2 ng/μL leucine-enkephalin for lock mass and normalization purposes. Optical images were taken using a 12-megapixel camera. Imaging acquisitions were prepared using the HDImaging software. All images were acquired using a 50 x 200 μm pixel size with a raster rate of 100 μm/s equating to ~30,000 pixels per image at a 0.485 s scan rate. All analyses were performed in negative ion mode in the mass range of m/z 50-1200. Ion mobility (IM) experiments were performed using a nitrogen buffer gas. DESI-MS/MS experiments were individually performed to putatively identify natural products and metabolites. All acquisitions were performed in triplicate. Parameters for RPLC-ESI-IM-MS experiments can be found in figure B.1.

2.2.5 *Data Processing and Analysis* All raw imaging files were processed using HDImaging software. The 4,000 most abundant features of each experiment were investigated. Mass measurements for these features were lock mass adjusted in 2-minute intervals throughout each experiment to the leucine enkephalin internal standard. During this processing step for DESI-IM-IMS files, a temporary raw file was created that consists of the mobility drift time plotted against m/z. This file was directly imported into Progenesis QI. These 4,000 most abundant features result in an average of 1,670 features when peak picked across replicates. Further, ~300 features were observed in blank samples, leaving ~1,400 quality features to search and dereplicate against an in-house myxobacteria database consisting of 280 natural product entries as well as the online repositories KEGG, Chemspider, MassBank, *E. coli* Metabolome Database, Yeast Metabolome Database, Natural Product Updates, Natural Products Discovery Institute, and NIST. Tentative identifications were made on a threshold of 10 ppm mass accuracy and 80%

isotopic similarity according to the level system proposed by Schrimpe-Rutledge *et al*.[33] Level 2 identifications of natural products and other metabolites were made using DESI-MS/MS acquisitions (figure B.2).

Unsupervised spatial prioritization used an imaging text file created by the HDImaging program. The generated text file was imported into R and Cardinal MSI. Feature intensities were normalized to the TIC and then subsequently normalized to the internal standard leucine-enkephalin intensity for each pixel across the image to account for substrate-dependent ionization, or differential ionization in regards to the various structures and surfaces within an IMS experiment. Features were peak picked using a 10 ppm window. Prior to unsupervised segmentation via spatial shrunken centroids analysis, the initial number of families (k) and the shrinkage parameter (s) were determined empirically for each experiment as described by Bemis et al.[33,34] The significant features within each segment of interest were dereplicated against online repositories and the myxobacteria database to prioritize unreported natural products.

2.3 Results and Discussion

2.3.1 *Sampling Methodology* To effectively measure intermicrobial interactions using IMS, three regions representing the two microbial communities and their interface must first be resolved spatially (figure 2.1A). Second, the measured metabolites from each of the separate regions must be unique. Thus, these regions that we refer to as predator, prey, and predation must have discrete locations and chemical profiles to successfully evaluate microbe-microbe relations. While these regions are visually quite distinct, capturing these differences via IMS remains a challenge. This is mainly due to the relatively fragile nature of microbial colonies, which must be rigid for effective ionization. For this reason, sample preparation is the primary factor influencing the ability to analyze microbial communities. The extent of retained spatial and chemical information of the microbial environment ultimately determines the ability to distinguish between distinct phenotypic regions within intermicrobial interactions.

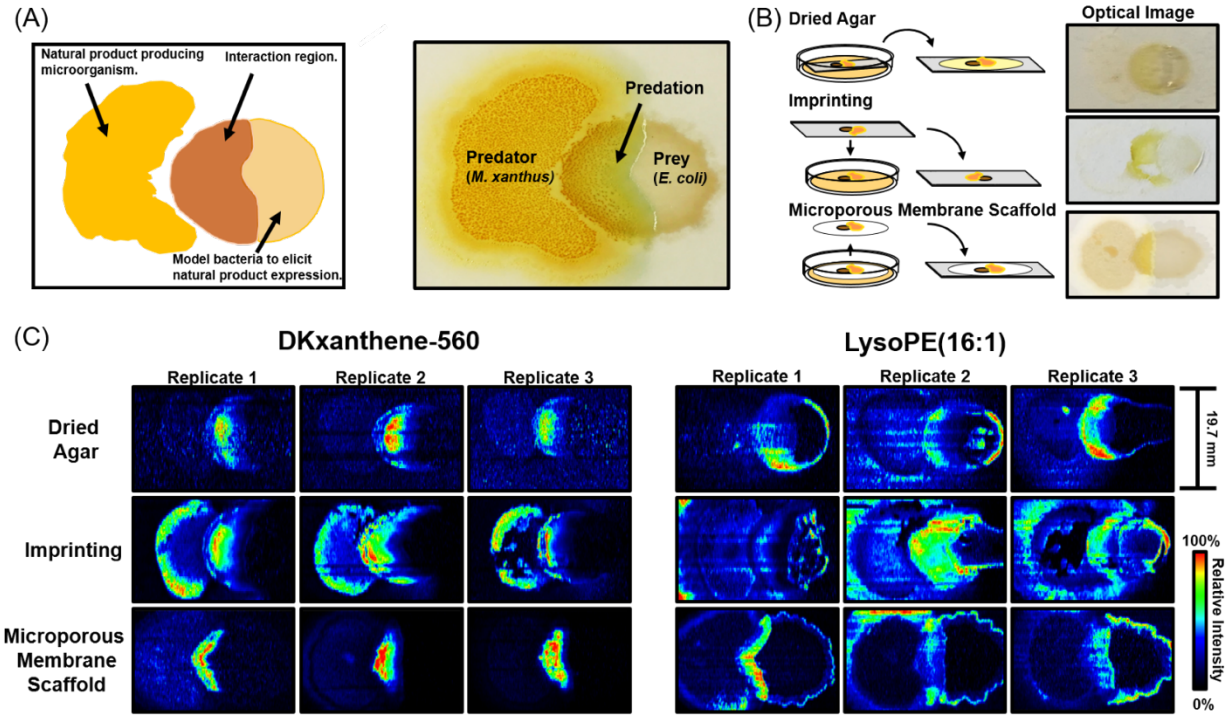

Figure 2 .1 (A) Diagram of microbial predation experiments and annotation of optical image. **(B)** Visual representation of sample preparation methods and optical images of microbial colonies prior to acquisitions. **(C)** Ion images of DKxanthene-560 and lysoPE 16:1 of biological replicates.

Table 2.1. Sampling metrics across DESI-IMS preparation methods.

Method	Sensitivity[a]	Repeatability[b,c]	Analyte Localization[c]
Dried agar	-	+	+
Imprinting	+	-	-
Microporous Membrane Scaffold	+	++	++

[a] Comparison of significant features with s/n ≥ 3 (Table s1)
[b] Evaluation of percent covariance of feature intensities (Table s1)
[c] Visual comparison of ion images in figure 2.1C.

Therefore, methods that avoid analyte delocalization and degradation during the sample preparation process will provide the most repeatable and comprehensive analysis. We evaluated the dried agar, imprinting, and MMS sample preparation methods depicted in figure 2.1B using sensitivity, repeatability, and analyte delocalization as performance metrics. The optical images, which qualitatively represent the outcome of these preparative methods, demonstrate the varying levels of retained spatial and chemical information (figure 2.1B).

The delocalization of small molecules within predation experiments across the dried agar, imprinting, and MMS methods is shown by the ion images of DKxanthene-560and lysophosphatidylethanolamine 16:1 (lysoPE 16:1) across biological replicates (figure 2.1C). The ion images of the reported *M. xanthus* natural product DKxanthene-560 highlight the increased spatial preservation of the dried agar and MMS methods compared to imprinting. The MMS and dried agar methods avoid an indirect spatial readout, minimizing the delocalization of observed metabolites. The ion images of lysoPE 16:1 differentiated the dried agar and MMS methods. This lipid was investigated for its defined role as a SocA (a short-chain alcohol dehydrogenase) substrate within myxobacterial intercellular signaling and refined localization within predation experiments.[36] Within this comparison, we observe more resolved and repeatable ion images from the MMS versus the dried agar method, which is attributed to the drying process of the latter. When agar gel is removed from humid culturing conditions and dried, it tends to shrink, resulting in some changes in metabolite abundance and localization. It is important to note that analyte recovery was not evaluated in this study. Varying localizations may be attributed to analyte extraction efficiency or ion suppression effects across each method. Substrate-dependent ionization and other sampling artifacts affecting signal intensity within each IMS image was addressed by normalizing feature intensities to the lock mass intensity for each pixel, which may account for the horizontal stripes within ion images (figure 2.1C). Considering these factors, the MMS method showed the least amount of metabolite delocalization within ion images (figure 2.1C). Therefore, this sampling technique avoids spatially perturbing the microbial environment, which allows for *in situ* IMS measurements of microbially produced small molecules in co-culture conditions.

Preserving metabolite localizations in IMS sample preparation is necessary to spatially distinguish the regions in microbial predation experiments. However, sensitive and reproducible MS measurements are necessary to determine the underlying molecular changes within each region of the experiment. Imprinting and MMS methods exhibit increased sensitivity compared to dried agar with 340 and 355 features having signal-to-noise ratios (s/n) greater than or equal to 3, respectively (table B.1). The increased sensitivity of the imprinting and MMS method are attributed to avoiding the matrix effects associated with sampling from agar. These methods are distinguished by the average mass spectrum and in particular the m/z range from 400 to 800, by which the MMS method yielded more comprehensive measurements (figure B.3). Lastly, across the normalized intensities of select features the dried agar, imprinting and MMS methods yielded 44.1%, 54.6%, and 20.2% covariances, respectively (table B.1). Thus, the MMS method not only provides the best spatial analyses, but also the most sensitive and repeatable MS measurements. A summary of these results exhibits the comprehensive increase in sampling capabilities using the microporous membrane scaffolded DESI-IMS within microbial predation experiments (table 2.1). The MMS method retains analyte localization by directly sampling metabolites from the microbial environment with minimal matrix effects.

2.3.2 *Unsupervised Segmentation of Microbial Predation In situ* spatial annotations and sensitive chemical measurements allowed for the development of an untargeted IMS data analytics workflow. To accomplish this, we used spatial shrunken centroids to perform unsupervised segmentation.[34,35] Spatial shrunken centroids analysis provides unique segmentation, such that it entails statistical regularization to extract subsets of informative features (i.e., removing features that do not change across the image), which reduces the amount of features from ~1,700 to ~600 for spatial analyses.[34,35] Spatial shrunken centroids analysis also accounts for the spatial structure of the data during the segmentation process as opposed to post hoc correlations.[34,35] This allows for the assignment of pixels into unique, homogeneous regions on the basis of mass spectral similarities across the most significant features within an IMS image.[34,35] Thus, each of the unique segments resulting from this analysis have both unique locations and chemical profiles. The most significant features within each segment are

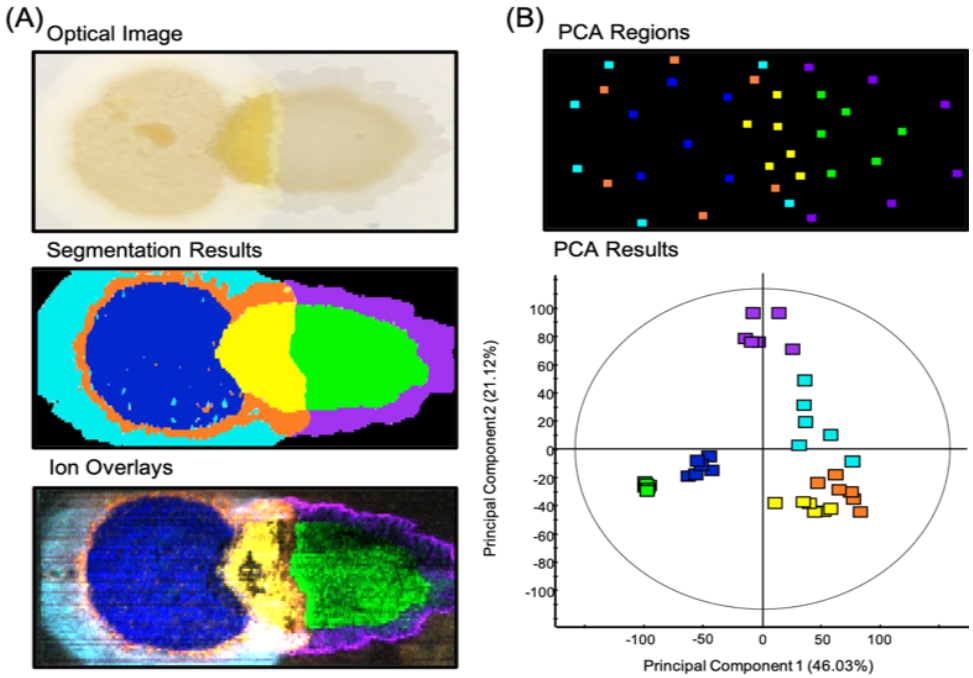

Figure 2.2. (A) Optical image, unsupervised segmentation results, and ion overlays of prioritized using segmentation. Features for ion overlays and replicates of segmentation results are shown in figure B.4. **(B)** Six mass spectra were extracted throughout the location of each segment with locations shown in PCA regions. The PCA of these mass spectra demonstrate the discrete chemical profiles of each segment.

determined using a "t-statistics" value. We used these "t-statistics" to determine the contributing features to each segment and rank them for untargeted spatial prioritization. Unsupervised segmentation of acquired IMS data from microbial predation experiments provides an unbiased evaluation of the homogeneous segments contributing to the heterogeneous phenotypes within these experiments. The assessment of chemical-spatial phenotypes using this technology facilitates the investigation of the underlying mechanisms by which microorganisms predate, communicate, and interact.

When unsupervised segmentation was applied to microbial predation experiments, we typically observed 7 segments (including the membrane background) represented by the different colored regions within the segmentation results (figure 2.2A). The ion images of the most significant features within each segment were overlaid using similar colors to confirm the authenticity and localization of output features (figure 2.2A). The distinct localizations within the ion overlay image nearly match that of the segmentation results, which demonstrates accurate spatial analyses via segmentation (figure 2.2A). We demonstrated the repeatability of unsupervised segmentation and annotate the primary features contributing to each segment across replicates (figure B.4). We also validated the ability of unsupervised segmentation to chemically distinguish these distinct regions via spatially directed principle component analysis (PCA) (figure 2.2B). Six replicates taken across the area of each proposed segment group together within the PCA displaying the chemical homogeneity of each segment (figure 2.2B). Further, each segment's unique chemical profile is demonstrated by these grouping and their distinct separations (figure 2.2B). Principle Component 1, which represents 46% of the data, differentiates the predator and prey communities (blue and green) from the region of interaction and those areas surrounding them (purple, cyan, orange, and yellow). This distinction asserts that the primary observed chemical difference lies between inactive and active secondary metabolism. These results validate the ability to use unsupervised segmentation as a chemoinformatics platform to spatially assess the chemical profile of discrete phenotypes within microbial predation experiments.

The chemical-spatial phenotypes resulting from unsupervised segmentation were investigated using "t-statistics" and the average mass spectrum (figure 2.3A). Statistically enriched features yielded positive "t-statistics", while those systemically absent resulted in negative values. Within the well-studied *M. xanthus* DK1622 species, we were able to use these "t-statistic" values to annotate reported natural products and validate the prioritization of biologically appropriate molecules with associated segments. DKxanthene-560, which has been reported in phase variation and fruiting body formation, was used as a benchmark for secondary metabolism.[28-30] The myxobacterial antibiotic Myxovirescin A produced in interactions with *E. coli* was used to determine the location of predation.[31] Both these natural products were prioritized within the yellow interaction segment demonstrating the ability to discern the location of predation and activated secondary metabolism (figure 2.3B). These positive controls define the yellow segment as the region where secondary metabolism was activated. Therefore, other measured features and unknowns including m/z 668.52 and m/z 596.47 may also be secondary metabolites associated with predation (figure 2.3B). We observed 52 other unknown features within the predation segment when dereplicated against our in-house myxobacteria database and online repositories (figure 2.3B).

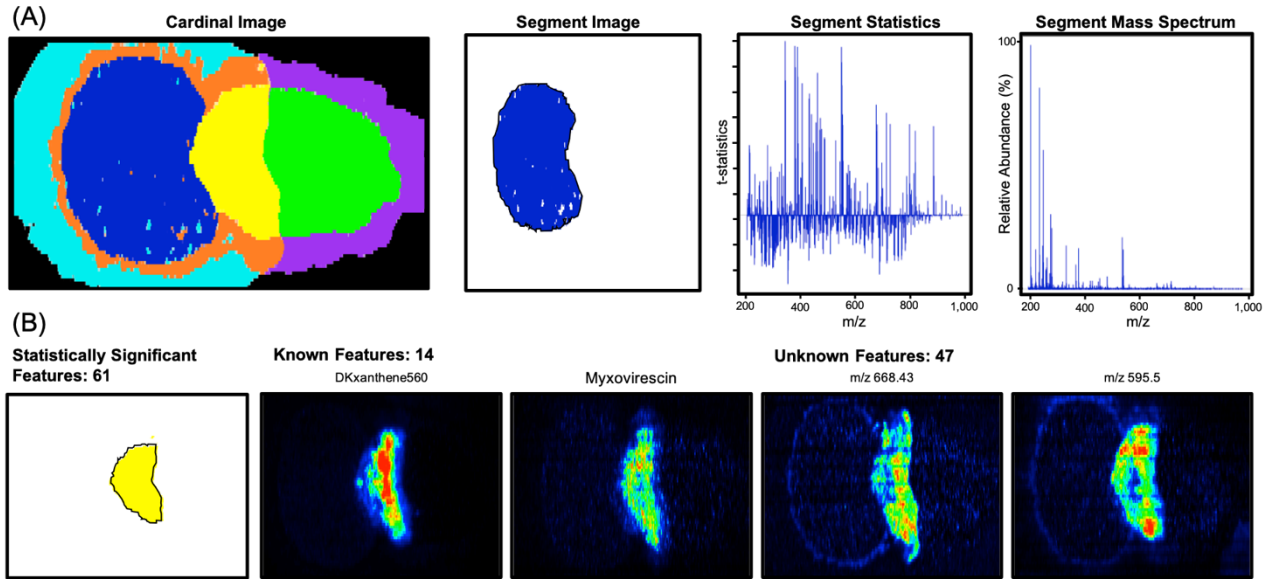

Figure 2.3. (A) Unsupervised segmentation results with outputs. The segmentation image represents the pixels that make up the segment, the segment statistics show the contribution of features using "t-statistics", and average mass spectrum of the segment. **(B)** Predation segment with known and unknown features. Myxovirescin and DKxanthene-560 represent known secondary metabolites, which validate the predation and phase variation in the yellow segment. Unknown highlight the application of this system to prioritize unreported natural products.

These previously unreported features suggest the potential for measurement and prioritization of novel natural products. Spatially prioritizing these unknowns has implications in drug discovery by removing features that are not localized to areas of activated secondary metabolism. Coupling spatial prioritization and dereplication simplifies the number of candidate masses from 4,000 total features to 54 unknowns associated with predation. This technology yields a natural product discovery workflow that incorporates spatial location and thus proposed function into the prioritization process (figure B.5). The segmentation results also validate the ability to successfully evaluate microbe-microbe interactions using microporous membrane scaffolded DESI-IMS and unsupervised segmentation. We were able to measure 6 chemically unique regions within these experiments where only three regions (predator, prey, and predation) were defined as necessary to effectively measure microbial relations (figure 2.1A). These capabilities were validated across replicates with ion overlays, PCA, and the spatial prioritization of predation and secondary metabolism with biologically appropriate natural products.

2.3.3 *Application to WT, M. xanthus Δta1 and Phase Variants* The developed method for characterizing microbe-microbe interactions was applied to wild type (WT), mutated *M. xanthus Δta1* strains, and respective phase variants. *M. xanthus Δta1* strains lack the megasynthetase responsible for Myxovirescin A (Antibiotic TA) production.[37] Phase variation (PV) in myxobacteria results from environmental stimulation, which cues the expression of genes and secondary metabolites in a given population of cells, some of which are important for predation.[28-30, 38] For example, myxobacterial yellow PVs have increased DKxanthene production (resulting in a yellow pigment) and swarming abilities whereas tan phase variants display little DKxanthene production and limited swarming abilities.[28-30,38] Using the developed DESI-IMS sampling method and data analysis protocol we distinguish between WT and *M. xanthus Δta1* strains and associated phase variants using Myxovirescin A and DKxanthene-560, respectively.

Unsupervised segmentation was used to evaluate the distinct predations of the *M. xanthus* strains and PVs (figure 2.4). In comparing WT and *M. xanthus Δta1* strains we measured the differential production of Myxovirescin A, which is demonstrated by the ion images in figure

2.4. This distinction was observed across biological replicates of all sample types and validates the feature prioritization process as well as the capabilities to sample natural product antibiotics from microbial communities using the MMS DESI-IMS method (figure B.6). However, many features were conserved in the predation segment between *M. xanthus Δta1* and WT. The unknown feature m/z 668.52 shares a similar localization to Myxovirescin A, which may indicate a role in predation (figure 2.4). The conservation of this feature in both strains may be the product of an additional biosynthetic gene cluster activated during predation outside of the TA megasynthetase. It is of interest that *M. xanthus Δta1* species were able to predate *E. coli* despite the mutation (figure 2.4).[37] While mutants predated slower than WT, this infers a variety of predatory mechanisms, which may be linked to measured unidentified features. More broadly, the measurement of unknown features associated with predation demonstrates the method's capabilities towards natural product discovery.

Further analysis of unsupervised segmentation results by comparing PVs provides insight into the role of PV within predation (figure 2.4). In tan PVs, we observed DKxanthene-560 and m/z 668.52 as well as Myxovirescin A in WT within the predation segment. Since DKxanthene-560 and Myxovirescin A are co-localized in tan PVs, this suggests that predation and phase variation occur at similar localizations and timescales within the predation process. In yellow PVs, however, DKxanthene-560 was not co-localized to Myxovirescin A and m/z 668.52, which infers that DKxanthene-560 is not directly involved in predation. This comparison suggests that predation may cause the switch from tan PV to yellow PV. Yellow PVs have been shown to be more motile, resistant to heat, and active than tan variants, which is a predatory advantage.[28-30, 38] Also, PV has been reported in other processes requiring secondary metabolism such as sporulation, which suggests a higher amount of secondary metabolism activated within yellow PVs.[28-30, 38] Our data support a model whereby tan PVs undergo phase variation prior to predation (figure 2.4)

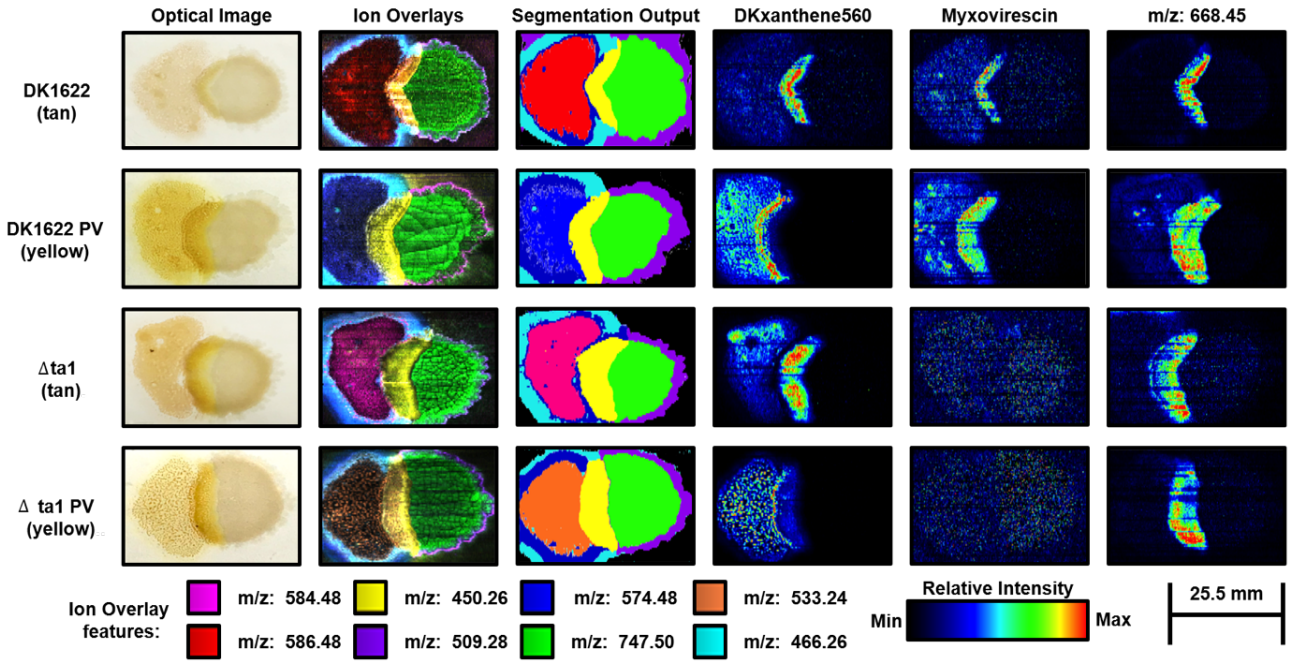

Figure 2.4 Optical images, ion overlays, and unsupervised segmentation results of WT and *M. xanthus Δta1* strains and respective phase variants (PV). Using unsupervised segmentation results we highlight the differential expression of DKxanthene-560 and Myxovirsecin as well as similar production of m/z 668.45. Colored boxes represent features in ion overlays.

Despite annotating the differences associated with WT and *M. xanthus Δta1* strains along with respective PVs, the majority of metabolic spatial expressions represented by segments were conserved throughout sample types, which is shown in the similar localizations in ion overlays and unsupervised segmentation outputs (figure 2.4). These similarities across all sample types elucidate some of the dynamic biosynthetic processes associated within *M. xanthus* predation and the chemical-spatial phenotypes that facilitate them. For example, the cyan segment may be associated with myxobacteria continuing to explore the surrounding environment despite predation. This segment and others may provide insight to myxobacterial predation as *M. xanthus* species have been reported to undergo a series of processes during predation including predataxis, or cellular reversals to increase contact with prey organisms, fruiting body formation, and "wolfpack" motility.[10,39] Thus, the combination of unsupervised segmentation and microporous membrane scaffolded DESI-IMS sampling presents the opportunity to unbiasedly investigate the molecular mediators by which microorganisms interact with others and the surrounding environment.

2.4 Conclusions

We demonstrate that DESI-IMS using MMS is an effective sampling method for evaluating interspecies microbial interactions. The robust and minimalistic preparation via this method provided sensitive analyses of secondary metabolites while preserving the *in situ* localization of microbially produced small molecules. The low covariance of metabolite intensities and repeatable ion images across replicates afforded consistent access to the chemical and spatial information between interspecies metabolite exchange. Capitalizing on this advantage, we developed a chemoinformatics platform capable of discerning chemically unique phenotypic regions using unsupervised segmentation. This imaging analysis presents a powerful tool in exploring the chemical ecology of microorganisms in an unbiased manner. Segmentation results were validated using ion overlays and PCA as well as the spatial prioritization of biologically appropriate natural products. These results highlight the ability to unbiasedly elucidate the molecular mediators in microbial relations by correlating spatially resolved and chemically unique regions to phenotypes within predation. The combination of microporous

membrane scaffolded DESI-IMS and unsupervised segmentation present unprecedented capabilities to investigate the roles of small molecules within microbial chemical ecology.

The application of this innovation to WT and *M. xanthus Δta1* strains along with yellow and tan phase variants validated the sampling and feature prioritization processes using the natural products DKxanthene-560 and Myxovirescin A. We used Myxovirescin A to differentiate between the WT and mutant strains and validate the predation segment within our analyses. DKxanthene-560 was used as a marker for phase variation and activated secondary metabolism. By comparing these secondary metabolites, we were able to probe the role of phase variation in myxobacterial predation, such that tan PVs turn to yellow PVs to predate more effectively. These assertions reflect the ability of this method to unbiasedly assess underlying ecological roles of natural products. We also add to the known myxobacterial chemistry by sampling unreported natural products with suggested roles in predation and secondary metabolism via our assignment of the predation segment. Lastly, other segments and features were measured outside of the predation region, which combine to represent the multiplicity of phenotypes within microbial predation. These segments may or may not be contributing to the overarching predatory process, but represent the ability of this technology to probe the chemical mechanisms of microbial behavior.

The developed technology presents an innovation in annotating microbially produced small molecules by combining the spatial location of DESI-IMS to the orthogonal detection capabilities of RPLC-ESI-MS. Using unsupervised segmentation, location can be used as a means for prioritization, which significantly reduces the number of prioritized features and provides insight to biological function. DESI-IMS MMS method is not limited to co-culture experiments, but can be applied to measuring the chemical crosstalk within other systems such as host-pathogen relations, tumor and tissue heterogeneity, and microbiome studies. The presented microporous membrane scaffolded DESI-IMS method and unsupervised segmentation is a novel method for molecular discovery and the unbiased assessment of small molecules within chemical ecology.

2.5 Acknowledgements

Financial support for aspects of this research was provided by The National Institutes of Health (Grants NIH NIGMS R01GM092218, NCI R03CA222452 and NIH NIGMS 1F32GM128344), the U.S. Environmental Protection Agency under Assistance Agreement 83573601, and the U.S. Army Research Office and the Defense Advanced Research Projects Agency (DARPA) under Cooperative Agreement W911 NF-14-2-0022. The views expressed in this document are solely those of the authors and do not necessarily reflect those of the funding agencies and organizations

2.6 References

(1) Mcfall-Ngai, M.; Hadfield, M. G.; Bosch, T. C. G.; Carey, H. V; Domazet-Lo, T.; Douglas, A. E.; Dubilier, N.; Eberl, G.; Fu-kami, T.; Gilbert, S. F.; Hentschel, U.; King, N.; Kjelleberg, S.; Knoll, A. H.; Kremer, N.; Mazmanian, S. K.; Metcalf, J. L.; Nealson, K.; Pierce, N. E.; Rawls, J. F.; Ried, A.; Ruby, E. G.; Rumpho, M.; Sanders, J. G.; Tautz, D.; Wernegreen, J. J. *Proc. Natl. Acad. Sci.*, **2013**, 110 (9), 3229-3236.

(2) Wilson, M. R.; Jiang, Y.; Villalta, P. W.; Stornetta, A.; Bou-dreau, P. D.; Carrá, A.; Brennan, C. A.; Chun, E.; Ngo, L.; Samson, L. D.; Engleward B. P.; Garrett, W. S.; Balbo, S.; Balskus, E. P. *Science*, **2019**, 363 (6428), eaar7785.

(3) Vizcaino, M. I.; Crawford, J. M. *Nat. Chem*. **2015**, 7 (5), 411–417.

(4) Xue, M; Kim, C. S.; Healy, A. R.; Wernke, K. M.; Wang, Z.; Frischling, M. C.; Shine, E. E.; Wang, W.; Herzon, S. B.; Craw-ford, J. M. *Science*, **2019**, 365 (6457), eaax2685.

(5) Fischer, C. N.; Trautman, E. P.; Crawford, J. M.; Stabb, E. V; Handelsman, J.; Broderick, N. A. *Elife*, **2017**, 6.

(6) Currie, C. R.; Scott, J. A.; Summerbell, R. C.; Malloch, D. Erratum: *Nature*, **1999**, 398 (6729), 701–704.

(7) Zipperer, A.; Konnerth, M. C.; Laux, C.; Berscheid, A.; Janek, D.; Weidenmaier, C.; Burian, M.; Schilling, N. A.; Slavetinsky, C.; Marschal, M.; Willmann, M.; Kalbacher, H.; Schittek, B.; Brotz-Oesterhelt, H.; Grond, S.; Peschel, A.; Krismer, B. *Nature*, **2016**, 535 (7613), 511–516.

(8) Newman, D. J.; Cragg, G. M. *J. Nat. Prod.,* **1997**, 79, 629-661.

(9) Covington, B. C.; Mclean, J. A.; Bachmann, B. O. *Nat. Prod. Rep.,* **2017**, 34 (1), 6-24.

(10) Findlay, B. L. *ACS Chem. Biol.,* **2016**, 11 (6), 1502-1510.

(11) Hoffmann, M.; Auerbach, D.; Panter, F.; Hoffmann, T.; Dorrestein, P. C.; Müller, R. *ACS Chem. Biol.,* **2018**, 13 (1), 273-280.

(12) Covington, B. C.; Spraggins, J. M.; Ynigez-Gutierrez, A. E.; Hylton, Z. B.; Bachmann, B. O. *Appl. Environ. Microbiol.,* **2018**, 84 (19), e01125-18.

(13) Derewacz, D. K.; Covington, B. C.; Mclean, J. A.; Bachmann, B. O. *ACS Chem. Biol.,* **2015**, 10 (9), 1998-2006.

(14) Derewacz, D. K.; Goodwin, C. R.; McNees, C. R.; McLean, J. A.; Bachmann, B. O. *Proc. Natl. Acad. Sci.,* **2013**, 110 (6), 2336–2341.

(15) Yang, Y.-L.; Xu, Y.; Straight, P.; Dorrestein, P. C. *Nat. Chem. Biol.,* **2009**, 5 (12), 885-887.

(16) Watrous, J.; Roach, P.; Alexandrov, T.; Heath, B. S.; Yang, J. Y.; Kersten, R. D.; Van Der Voort, M.; Pogliano, K.; Gross, H.; Raaijmakers, J. M.; Moore, B. S.; Laskin, J.; Bandeira, N.; Dorrestein, P. C. *Proc. Natl. Acad. Sci*., **2012**, E1743-E1752.

(17) Watrous, J.; Roach, P.; Heath, B.; Alexandrov, T.; Laskin, J.; Dorrestein, P. C.. *Anal. Chem.,* **2013**, 85 (21), 10385-10391.

(18) Araújo, F. D. S.; Vieira, R. L.; Molano, E. P. L.; Aximo, H. J.; Dalio, R. J. D.; Vendramini, P. H.; Ará Ujo D, W. L.; Eberlin, M. N. *RSC Adv*., **2017**, 7, 29953-29958.

(19) Tata, A.; Perez, C.; Campos, M. L.; Bayfield, M. A.; Eberlin, M. N.; Ifa, D. R.. *Anal. Chem.,* **2015**, 87 (24), 12298-12305.

(20) Menezes, R. C.; Kai, M.; Krause, K.; Matthäus, C.; Svatoš, A.; Popp, J.; Kothe, E. *Anal. Bioanal. Chem.,* **2015**, 407 (8), 2273–2282.

(21) Fernando, C.; Angolini, F.; Vendramini, P. H.; Arauo, F. D. S.; Arauo, W. L.; Augusti, R.; Eberlin, M. N.; Gonzaga De Oliveira, L. *Anal. Chem*., **2015**, 87 (13), 6925-6930.

(22) Yan, C.; Parmeggiani, F.; Jones, E.A.; Claude, E.; Hussain, S.A.; Turner, N.J.; Flitsch, S.L.; Barran, P.E. *J. Am. Chem. Soc.,* **2017**, 139 (4), 1408-1411.

(23) Song, X.; Mazzola, M.; Cheng X.; Oetjen, J.; Alexandrov, T.; Dorrestein, P. C.; Watrous, J.; Van der Voort, M.; Raaijmakers, J. M*Sci. Rep.,* **2015**, 5:12837.

(24) Alexandrov, T. *BMC Bioinformatics*, **2012**, 13 (S16): S11.

(25) Rath, C. M.; Alexandrov, T.; Higginbottom, S. K.; Song, J.; Mila, M.; Fischbach, M.; Sonnenburg, J. L.; Dorrestein, P. C. *Anal Chem*., **2012**, 84 (21), 9529-9267.

(26) Ravindran S. J.; Kumar, R.; Srimany, A.; Philip, L.; Pradeep, T. *Anal Chem.,* **2018**, 90, 988-997.

(27) Powell, L. C.; Pritchard, M. F.; Ferguson, E. L.; Powell, K. A.; Patel, S. U.; Rye, P. D.; Sakellakou, S.; Buurma, N. J.; Bril-lant, C. D.; Menzies, G. E.; Lewis, P. D.; Hill, K. E.; Thomwas, D. W. *NPJ Biofilms Microbiomes.*, **2018**, 4, 13.

(28) Meiser, P.; Weissman, K. J.; Bode, H. B.; Krug, D.; Dickschat, J. S.; Sandmann, A.; Mülller, R. *Chem. Biol.,* **2008**, 15 (8), 771-781.

(28) Dziewanowska, K.; Settles, M.; Hunter, S.; Linquist, I.; Schilkey, F.; Hartzell, P. L.; Hoskisson, P. *PLoS One*, **2014**, 9 (4), e95189.

(30) Meiser, P.; Bode, H. B.; Müller, R. *Proc. Natl. Acad. Sci.,* **2006**, 103 (50), 19128-19133.

(31) Xiao, Y.; Wei, X.; Ebright, R.; Wall, D. *J. Bacteriol*., **2011**, 193 (18), 4626–4633.

(32) Tillner, J.; Wu, V.; Jones, E. A.; Pringle, S. D.; Karancsi, T.; Dannhorn, A.; Veselkov, K.; McKenzie, J. S.; Takats, Z. *J. Am. Soc. Mass Spectrom*., **2017**, 28 (10), 2090–2098.

(33) Schrimpe-Rutledge, A.C.; Codreanu, S. G.; Sherrod, S. D.; McLean, J. A. *J. Am. Soc. Mass Spectrom*., **2016**, 27 (12), 1897-1905.

(34) Bemis, K. D.; Harry, A.; Eberlin, L. S.; Ferreira, C. R.; van de Ven, S. M.; Mallick, P.; Stolowitz, M.; Vitek, O. *Mol. Cell. Proteomics,* **2016**, 15 (5), 1761–1772.

(35) Bemis, K. D.; Harry, A.; Eberlin, L. S.; Ferreira, C.; Van De Ven, S. M.; Mallick, P.; Stolowitz, M.; Vitek, O. *Bioinformatics*, **2015**, 31 (14), 2418-2420.

(36) Avadhani, M.; Geyer, R.; White, D. C.; Shimkets, L. J. *J. Bacteriol*., **2006**, 188 (24), 8543–8550.

(37) Korp, J.; Vela Gurovic, M. S.; Nett, M. *Beilstein J. Org. Chem.,* **2016**, 12, 594–607.

(38) Dahl, J. L.; Ulrich, C. H.; Kroft, T. L. *J. Bacteriol*., **2011**, 193 (19), 5081–5089.

(39) Muñoz-Dorado, J.; Marcos-Torres, F. J.; García-Bravo, E.; Moraleda-Muñoz, A.; Pérez. *J. Font. Microbiol*., **2016**, 7, 781.

CHAPTER 3

ACCELERATING STRAIN ENGINEERING USING DESOPRTION ELECTROSPRAY IONIZATION-IMAGING MASS SPECTROMETRY AND UNTARGETED MOLECULAR ANALYSIS OF INTACT MICROBIAL COLONIES

3.1 Introduction

Engineering microorganisms for the renewable manufacturing of chemicals is becoming increasingly viable given major advancements in genome and biological sciences. Biosynthetic production of commodity chemicals as an alternate path to traditional chemical synthesis has the potential to address global challenges across medical, environmental, energy, and economic sectors.[1-3] However, engineering microorganisms, such as bacteria, with the efficiency and low cost of commercial chemical syntheses remains a significant challenge. Despite the ability to rapidly alter and edit bacterial genomes, directing these alterations to elicit specific biological changes is hindered by the rate at which phenotypic outcomes can be measured from individual gene edits.[2,4-6] In part, this is due to a fundamental mismatch in the throughput with which genetic editing can be performed versus how quickly the metabolic consequences can be determined. Comprehensive chemical characterization of engineered strains is considered one of the grand challenges in synthetic biology.[2,7,8] Thus, increasing the throughput and molecular breadth of analytical readouts provides opportunities to accelerate metabolic engineering and ultimately promote commercial feasibility of microbial cell factories.

Contemporary synthetic biology workflows for optimizing microbial biosynthesis are rooted in functional genomics, directed evolution, and metabolic flux studies all of which depend on chemical measurements. To effectively support these applications, the analytical method utilized must be rapid, minimally invasive to microbial colonies, and broadly amenable to many molecular classes. Label free sampling provides a more rapid and robust annotation of the microorganism's chemical productivity by alleviating the need for additional engineering steps encoding sensors, or probes, and further perturbing the system. Fluorescence spectroscopy

methods are rapid and highly sensitive, however, the majority of biomolecules do not intrinsically fluoresce, which limits the chemistries that can be targeted.[6,9] Techniques such as riboswitches, RNA aptamers, ligand responsive transcription factors, or coupled enzyme reactions can also be used for rapid screening of a wider variety of chemistries, but at the cost of additional engineering steps that may confound readout of the biological system being investigated.[6] Furthermore, the methods reported thus far have been tailored towards specific products that are not yet fully generalizable.[6] Mass spectrometry-based techniques address many of these challenges and limitations by simultaneously measuring the intrinsic property of mass-to-charge ratio (m/z) of a large breadth of molecular species with high sensitivity and at rates commensurate with high throughput analyses.[8]

Most mass spectrometry (MS) methods to investigate synthetic biology use gas chromatography-mass spectrometry (GC-MS) or liquid chromatography-mass spectrometry (LC-MS) to target specific endpoint molecules arising from microbial biosynthesis.[10,11] Both GC-MS and LC-MS typically require several steps of sample handling prior to MS analysis, including analyte extraction, liquid sample preparation procedures, and, in some instances, chemical derivatization to enhance sensitivity for minimally volatile analytes. Furthermore, GC-MS and LC-MS methods can only analyze one sample (e.g. strain extract) at a time, and chromatographic separations necessitate several minutes to complete per sample.[10,11] To reduce sample handling and increase throughput, a recently developed MS method using matrix assisted laser desorption/ionization (MALDI) provided rapid sampling from a 96-well plate of bacterial samples.[12] However, this sequential MALDI strategy is not conducive to analyzing most small molecules due to matrix interferences and the need for vacuum-based sampling, which otherwise restricts the ability to measure labile and volatile analytes.[12,13] Additionally, these chromatography and MALDI-based methods are not amenable to direct sampling of microbial colonies. Previously, Barran and coworkers described a targeted method based on desorption electrospray ionization (DESI) with MS analysis to measure biocatalysis from live bacterial colonies.[14] Whereas this approach enabled the direct sampling of microorganisms, the targeted assay focused exclusively on tracking the conversion of specific molecules and did not examine

the broader metabolome of the microorganisms. We have recently described an aligned DESI-MS strategy operated in an imaging MS (IMS) mode for rapid and reproducible analysis of microbially produced metabolites and chemicals in situ.[15] Building on this approach, we have tailored this sampling method for the simultaneous analysis of many bacterial colonies including multiple strains and biosynthetic products in a spatially-resolved manner. Herein, we describe the application of DESI-IMS and unsupervised analytics to untargeted metabolomic characterization of engineered microorganisms. With this technique, we obtain analytical information simultaneously for both the targeted biosynthetic products and also global metabolites detailing the broader biology of the organisms. We demonstrate the capabilities of this DESI-IMS workflow using *Escherichia coli* strains that have been genetically engineered to overproduce free fatty acids (FFA) with defined chain-lengths by expressing different thioesterase enzymes.[16-19] We highlight the advantages of untargeted acquisitions to provide specific readouts of secondary fatty acid production, as well as broader insight into the molecular profiles of the microorganisms via lipidomics analyses to reveal variations in membrane lipid saturation, which has been shown to affect cell viability.[20]

3.2 Experimental Methods

3.2.1 *Strains and Culture Conditions* Engineering strategies for the TY05, TY06, NHL17, and WT-TesA can be found in the respective publications.[16-18] Briefly, TY05 (K-12 MG1655 ΔfadD::trcBTE, ΔfadE::trcBTE, ΔfadAB::trcBTE) was engineered to preferentially produce dodecanoic acid (C12:0) by inserting three copies of a codon-optimized acyl-acyl carrier protein thioesterase from *Umbellularia californica* (BTE) under the control of an isopropyl-β-D-thiogalactopyranoside (IPTG)-inducible promoter. These changes were integrated into chromosomal loci of B-oxidation genes (fadD, fadE, and fadAB).[17] The same gene deletions were also made in a negative-control strain (TY06) containing three copies of BTE with an active-site mutation (BTE-H204A) that renders the protein nonfunctional.[17] NHL17 (K-12 MG1655 ΔaraBAD ΔfadD::trcCpFatB1.2-M4-287) was augmented for enhanced octanoic acid (C8:0) production by inserting a single chromosomal copy of an optimized thioesterase under

IPTG induction.[16] The WT-TesA strain expresses a native thioesterase (TesA), which produces fatty acids with a range of chain-length distributions from C8-C14.[18] For DESI-IMS analysis of co-cultures, single colonies of each strain were inoculated from freezer stocks into 3 mL of Luria-Bertani (LB) and incubated overnight at 37°C with shaking. An equal volume (500 µL each) of each strain culture with equal OD600 of 0.3 were mixed thoroughly in a sterile tube. Mixed culture was serially diluted 3-fold using sterile LB media. 100 µL of mixed culture was plated on the microporous membrane scaffold placed on the top of LB agar Petri dish with isopropyl β-D-1-thiogalactopyranoside (IPTG) (1 mM final concentration). All plates were incubated at 37°C for 30 h for FFA production.

3.2.2 *Sample Preparation and Acquisitions* Membranes used for the microporous membrane scaffold method were 0.45 µM pore size and 47 mm diameter (Sigma-Aldrich). Prior to sampling, the membrane was removed from the medium, dried for 5 minutes, and adhered to a glass slide using double-sided scotch tape. DESI-IMS and DESI-MS/MS acquisitions were performed using a Waters Synapt G2S High Definition Mass Spectrometer (Waters Corporation, Manchester, UK) with a Waters x-y directional stage and DESI source described by *Tilner et al*.[21] The system was mass calibrated with sodium formate salt clusters to a 95% confidence band and root mean square (RMS) residual mass ≤ 0.5 ppm. This resulted in experimental mass accuracies of generally 2-5 ppm and mass resolving powers circa 11,000. Optimized DESI source conditions were found to be a –5 kv capillary voltage, 110 ^{o}C desolvation temperature, 0.5 mPa N_2 gas flow, and a cone voltage of 40 V. The sprayer was set at a 70^{o} angle, with the x, y, z, settings at -2, +2, and +2.75, respectively. Ionization solvent was comprised of 90/10 acetonitrile/water (Optima grade, Fisher Scientific) solution with 0.5% NH_4OH with 0.2 ng/µL leucine-enkephalin for lock mass purposes and 0.2 ng/µL pentadecanoic acid for spatial normalization. Optical images were taken using a 12-megapixel camera. Imaging acquisitions were prepared using the HDImaging software. All images were acquired using a 50 x 250 µm pixel size with a raster rate of 100 µm/s. All analyses were performed in negative ion mode in the mass range of m/z 50-1200. DESI-MS/MS experiments were performed from *E. coli* colonies while selectively fragmenting a single ion of interest for identification purposes.

3.2.3 *Data Processing and Analysis* All imaging files were processed using the HDImaging software. The 1,000 most abundant features from each experiment were investigated. Mass measurements for the features were lock mass adjusted in 2-minute intervals to the leucine enkephalin internal standard. During this processing step an imaging text file was created by the HDImaging program. This text file was imported into R and Cardinal MSI.[22,23] Feature intensities were normalized to the TIC and subsequently spatially normalized to the pentadecanoic acid (C15:0) internal standard intensity for each pixel to account for substrate-dependent ionization, or differential ionization in regards to the various areas and surfaces within the IMS experiment. This is a pivotal step in the normalization process as there is considerable fatty acid noise within DESI-MS analyses most likely due to the ambient conditions, which can interfere with the spatial intensities of fatty acids of interest. Features were then assigned using a 5 parts-per-million (ppm) mass measurement window.

Unsupervised segmentation using spatial shrunken centroids analysis in the Cardinal R package was used to distinguish the strains unbiasedly.[22,23] Initial segmentation trials used a higher number of families (8-10) with varying shrinkage parameters (1-3) and radii (1-3) to remove background interferences and resolve strain identities into segments. Strains were identified using the significance and average intensity of biosynthetic products and metabolites.

DESI-ion mobility-MS and DESI-MS/MS data were used to identify measured metabolites. The HDImaging program generates a temporary data file that consists of the drift time plotted against m/z. This file was able to be directly imported into Progenesis QI for metabolite identification. The imported features were normalized to the TIC, deconvoluted, and searched against the online repositories KEGG and Chemspider. Search parameters for tentative matches were made on a threshold of 10 ppm mass accuracy and 80% isotopic similarity. Tentatively identified features using this process were subsequently fragmented via DESI-MS/MS analysis of microbial colonies to achieve putative identifications.

3.2.4 *Confirmation of strain genotype via PCR* To confirm the genotype of selected strains replica plates were prepared by streaking selected colonies on a fresh LB media plate. The

identities of the replicate colonies were validated and confirmed by colony PCR using primers listed in Table C.1. Oligonucleotide primers were purchased from Integrated DNA Technologies, Inc. (Coralville, IA).

3.3 Results and Discussion

3.3.1 *Rapid metabolic phenotyping of FFA overproducing E. coli* Engineering *E. coli* fatty acid metabolism has led to the production of high-energy density, liquid transportation fuels and high-value oleochemicals from renewable feedstocks.[24,25] With reported amounts reaching up to 70% of the theoretical yield, engineers have achieved higher production of FFA than any other downstream products.[24,25] If these yields can approach theoretical limits, then processes may be developed to replace current petrochemical production strategies.[25] Acyl-acyl carrier protein (ACP) thioesterases are some of the primary targets for engineering FFA production.[25,26] These enzymes regulate the catalytic link between fatty acid biosynthesis (FAB) and a product sink, increase flux by depleting the primary regulatory signaling molecules, and control the composition and chain length of the final products.[26] To enhance the activity of these enzymes and thus create more productive strains directed evolution or mutagenesis studies can be performed.[27,28] In particular, screening libraries with varying modifications to acyl-ACP thioesterases can provide pivotal insight to controlling chain lengths and compositions of free fatty acids, which is a challenge within this field.[29]

A previously developed microporous membrane scaffold method was adapted to sample a mixed culture of engineered *E. coli* strains (figure 3.1).[15] Briefly, microorganisms were grown on a membrane scaffold placed on top of an agar substrate, which facilitated the uptake of nutrients to support microbial growth and production, while retaining microorganisms and their excreted biosynthetic products on the scaffold surface. At desired timepoints, the membrane was removed from the agar and affixed to a glass microscope slide to provide a solid support on which DESI can be performed directly with no further sample pretreatment. The typical DESI-IMS pixel size used in these experiments was 50 x 250 μm. Using conventional parameters, we were able to completely sample 42 colonies in 356 minutes.

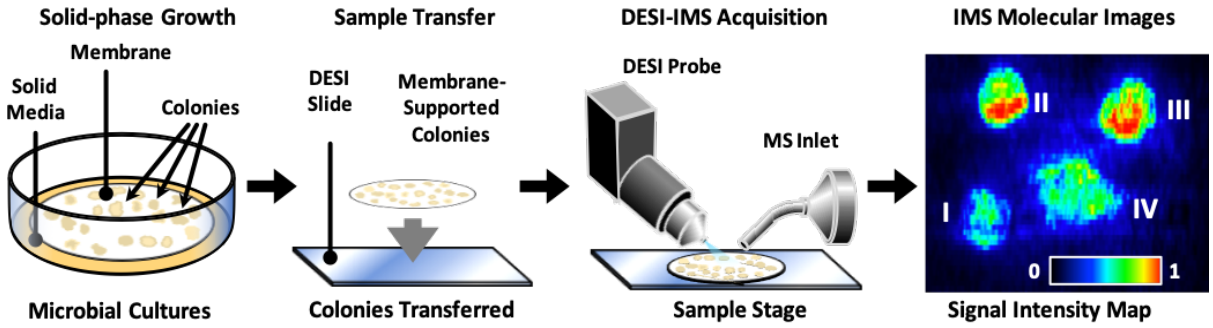

Figure 3.1. Sample preparation and acquisition workflow to profile microbial biosynthesis. Microorganisms are grown on a membrane scaffold placed on top of agar. The microorganisms and scaffold are removed from the agar and adhered to a glass slide. The DESI directly samples the microorganisms, biosynthetic products, and metabolites from the scaffold in a spatially resolved MS analysis (IMS). The resulting IMS image maps the relative amounts of different chemical products and metabolites to spatial positions (e.g., within each colony).

Considering the time needed to transfer the samples onto the DESI slide (ca. 10 minutes), the sample throughput was 8 minutes per microbial colony from solid-phase growth to acquired data. Faster raster rates yielding the same data fidelity are also possible (figure C.1). While MALDI-MS is capable of very fast acquisition speeds on the orders of seconds, there are additional throughput restraints imposed by colony picking, matrix application, and sample loading that are not generally reported in these workflows.[12,13] Thus, we concluded that the 8 minutes needed to obtain the full MS images of each colony was suitable for rapid screening applications.

DESI-IMS facilitates the direct analysis of microbial colonies, while acquiring chemical information on biosynthetic products including relatively volatile analytes (e.g., short and medium chain fatty acids). Additionally, IMS is inherently a multiplexed technique through the acquisition of full MS spectra at each sampling location. We demonstrate these multiplexing and volatile analyte detection capabilities for the DESI-IMS analysis of a co-culture of two engineered *E. coli* strains TY05 and NHL17 (figure 3.2). In a co-culture with isopropyl-D-thiogalactopyranoside (IPTG) present to induce FFA overproduction, TY05 is expected to preferentially produce dodecanoic acid (C12:0), whereas NHL17 produces octanoic acid (C8:0).[16,17] The spatial location of each colony was determined using an ion image for a lipid common to both strains, phosphatidylglycerol (16:0/17:1), whereas the ion images corresponding dodecanoic acid and octanoic acid were localized to specific colonies, which readily distinguished the identities of each colony (figure 3.2A-B). Based on the expected results of the gene edits, we predicted that the colonies that co-localized with higher intensities of dodecanoic acid are the TY05 strain and those that co-localized with accumulation of octanoic acid are the NHL17 strain.[16,17]

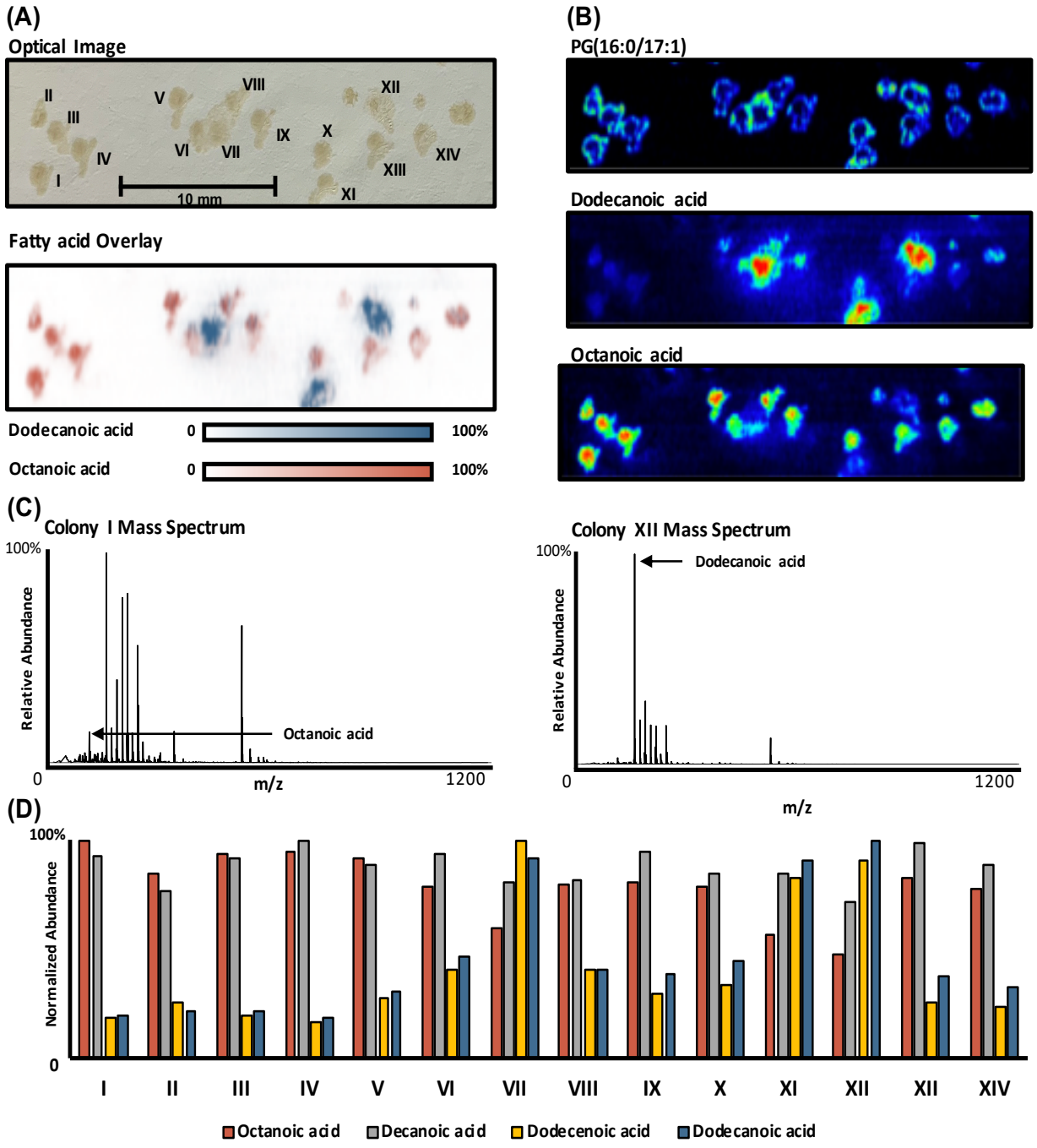

Figure 3.2. DESI-IMS data and results from a single IMS acquisition of the two engineered strains TY05 and NHL17. **(A)** Optical image labeled with colony numbers. Fatty acid overlay demonstrates the spatial localizations of primary biosynthetic products, that correlate with strain identities. **(B)** Spatial mapping of a lipid common to both strains, phosphatidylglycerol (16:0/17:1), which was used to define chemical boundaries of each colony for generation of mass spectra and fatty acid intensities. Ion images of dodecanoic acid and octanoic acid highlight the relative abundance of primary biosynthetic products individually. **(C)** Area integrated mass spectra highlight contributions of octanoic acid and dodecanoic acid to the measured metabolomes of TY05 and NHL17 strains. **(D)** Normalized fatty acid abundances for each colony.

In addition to differentiating these strains through biosynthetic products, we can further characterize NHL17 and TY05 through their measured metabolomes. To demonstrate this untargeted approach, we defined colony areas as regions of interest (ROI) and integrated the MS intensities associated with Colony I and XII to generate composite mass spectra representative of each strain (figure 3.2C). A comparison of these two integrated mass spectra reveals distinct metabolites associated with each strain. Of note, we observe an overall higher fatty acid production from colony XII (TY05 strain) and a predominant fatty acid peak corresponding to dodecanoic acid. In the composite mass spectrum obtained from colony I (NHL17), fatty acid abundances were lower than what was observed from colony XII, which may be due to the fact that under ambient conditions octanoic acid is in the liquid phase and thus subject to greater diffusive losses than the higher chain-length FFAs. It is important to note that while fatty acids dominate the representative mass spectra, higher mass analytes (such as the PG (16:0/17:1) lipid used for colony localization) also appear at lower abundances. As per the multiplexed nature of this analysis, an ion image can be projected for any metabolite observed in the sample, allowing each bacterial strain to be phenotyped based on the totality of chemical signatures present.

To determine fatty acid abundances, we normalized the signal intensities of acquired DESI-IMS data using an internal standard (pentadecanoic acid) introduced directly to the DESI ionization solvent. This provided a readout of fatty acid (FA) ionization at each image pixel. Next, colony areas were defined as ROIs using PG (16:0/17:1) ion image to determine each colony's chemical boundaries. Using these ROIs, total ion signals for discrete FFA mass measurements were integrated across each colony area to determine the FFA output of each colony (figure 3.2D). By comparing the FFA-specific output of each colony, we were able to determine that colony number XII and I are the highest producers of dodecanoic acid and octanoic acid, respectively (figure 3.2D).

These chemical comparisons are not limited to profiling two primary analytes. Using the same DESI-IMS data, we were able to perform a more comprehensive characterization of fatty acid biosynthesis by calculating the relative amounts of C8-C12 FFAs for each colony (figure 3.2D). As noted previously, dodecanoic acid is consistently present in greater relative

abundances than octanoic acid. For decanoic acid, we did not observe significant changes in the intensities from colony to colony. We also find that colonies producing the highest amounts of dodecanoic acid also seem to be producing the unsaturated fatty acid dodecenoic acid (C12:1) as well (figure 3.2D). This may be attributed to off-target production within the TY05 strain, which suggests an additional engineering strategy for TY05. More selective production may be achieved by knocking out the desaturase enzyme(s) responsible for the conversion of C12:0 to C12:1 to prevent the formation of the C12:1 byproduct. With this untargeted approach, we highlight both the relative amounts of biosynthetic products and specific information on the FFA chain lengths and degrees of unsaturation in off-target production. This chemical information has implications in the rational design of strains but is particularly applicable to randomly generated strains in directed evolution studies. By comprehensively characterizing biosynthesized products, the potential for discovering novel and favorable mutations is more feasible than profiling a specific product. Thus, our DESI-IMS platform can support the rapid development and discovery of strains with enhanced productivity.

3.3.2 *Untargeted molecular phenotyping via unsupervised segmentation* Whereas the FFAs were of immediate interest for this study, the vast majority of molecular species measured using untargeted DESI-IMS acquisitions are not free fatty acid products. These additional metabolites can provide further insights into biosynthetic processes such as product/precursor levels, product sinks, and off-target production, the latter of which has implications for discovering additional commercially relevant secondary products or wasteful byproduct pathways that reduce product yield. Furthermore, the effects of genetic edits on the growth and viability of the engineered organisms can be indicated by accumulation or depletion of metabolites outside of the primary biosynthesis pathways. This includes, but is not limited to, cellular redox through redox pairs, levels of amino acids and other central metabolites, and degrees of membrane lipid saturation. Comprehensive metabolic characterization (including biosynthetic products) of engineered organisms can identify future editing targets and strategies to enhance production without additional experiments. To facilitate the investigation of all measured molecular features within

these DESI-IMS experiments, we developed a spatially oriented untargeted metabolomics data analysis workflow using unsupervised segmentation.

Unsupervised segmentation is a computational process that groups IMS pixels into chemically similar regions using measured mass spectral similarities. The end result of this process is an image with spatially oriented groups (segments) that have discrete molecular signatures. The chemical fingerprints of each segment are calculated on the basis of a significance value determined by a t-test comparing the intensity of a feature within a segment area to the rest of the IMS image.[27,28] Thus, each feature associated with a segment is significantly upregulated within that region and also statistically absent from the remainder of the IMS image. There are many fundamental advantages to this untargeted analytics approach as the areas and even phenotypes of the microbial colonies are defined unbiasedly. This minimally-biased approach is advantageous in that it reduces the user input for analysis, removes error associated with manually defining colony areas and reduces overall analysis time. Moreover, the segments generated via discrete molecular profiles account for all of the measured features within a DESI-IMS experiment, which lead to a more robust assignment of phenotypes. This type of analysis includes any biomarkers that may be expressed by strains as a result of specific genetic edits. For instance, in our FFA-producing *E. coli* panel we may identify various lipid biomarkers as a result of the different alterations to fatty acid biosynthesis pathways. We compared unsupervised segmentation against other IMS data analysis methods such as ROI integration and MS profile averaging, and found no significant differences in the reproducibility and reported amounts of biosynthetic products (supplemental figure C.2). Thus, unsupervised segmentation provides untargeted metabolomic phenotyping across the measured metabolome while accurately and reproducibly characterizing biosynthetic products.

We applied our developed DESI-IMS and unsupervised segmentation workflow to a mixed culture comprised of the control strain TY06 strain and FFA-overproducing strains TY05, NHL17, and WTTesA that were collectively seeded on the microporous membrane scaffold.[16-18] This facilitated the formation of colonies for each strain that were distributed throughout the plate area randomly and unbeknownst to the experimenter. Unsupervised segmentation separated

the IMS image into 6 primary segments representing 6 distinct molecular profiles (figure 3.3). These 6 segments were subsequently classified into four segments representing colony areas, one segment representing the membrane scaffold, or background, and one representing the area surrounding each colony. While we anticipated only 5 segments (4 strains and 1 background), the additional segment discovered by the unsupervised method (colony margins) can provide additional insight into the growth and biosynthesis of these engineered strains. Unsupervised segmentation revealed accumulation of fatty acids in the area surrounding the colonies that were not expected based on the strain engineering strategy, namely nonadecenoic acid (C19:1), heptadecanoic acid (C17:0), and hexadecenoic acid (C16:1). We also found tetradecanoic acid (C14:0) and PG (16:0/15:1) to be in significant abundance within these boundary regions. This segment and the contributing metabolites may represent biomarkers of colony growth and expansion, byproducts stemming from lipid biosynthesis, or even diffusion of chemicals away from the colonies. More notably, this additional segment demonstrates the sensitivity of the DESI-IMS sampling method and the utility of unsupervised segmentation to discover unanticipated molecular signatures.

The four discrete molecular profiles associated with the bacterial colonies represent four unique metabolic phenotypes. To determine which strain these phenotypes corresponded to, we used t-statistic values and average mass spectrum for each segment (figure 3.3). With prior knowledge of the anticipated FFA production of each strain, we were able to infer strain identities using the measured FFA abundances. For instance, dodecanoic acid had the highest t-statistic value in the dark blue segment, which ultimately led to the associated colonies being assigned as the C12-producer TY05 (figure 3.3).[17] The highest average intensity of dodecanoic acid observed across all MS data was within this segment, which further supported this assignment. Additional analyses were required to distinguish the strains associated with octanoic acid. The WT-TesA strain overproduces a range of FFA chain-length distributions including C8:0, which is also the primary product of NHL17. [16,18] Due to the labile nature of octanoic acid yielding lower signal intensities in the DESI-IMS analysis, both the red and light blue segments had similar t-statistic values (figure 3.3). However, when we considered the average metabolite intensities for octanoic

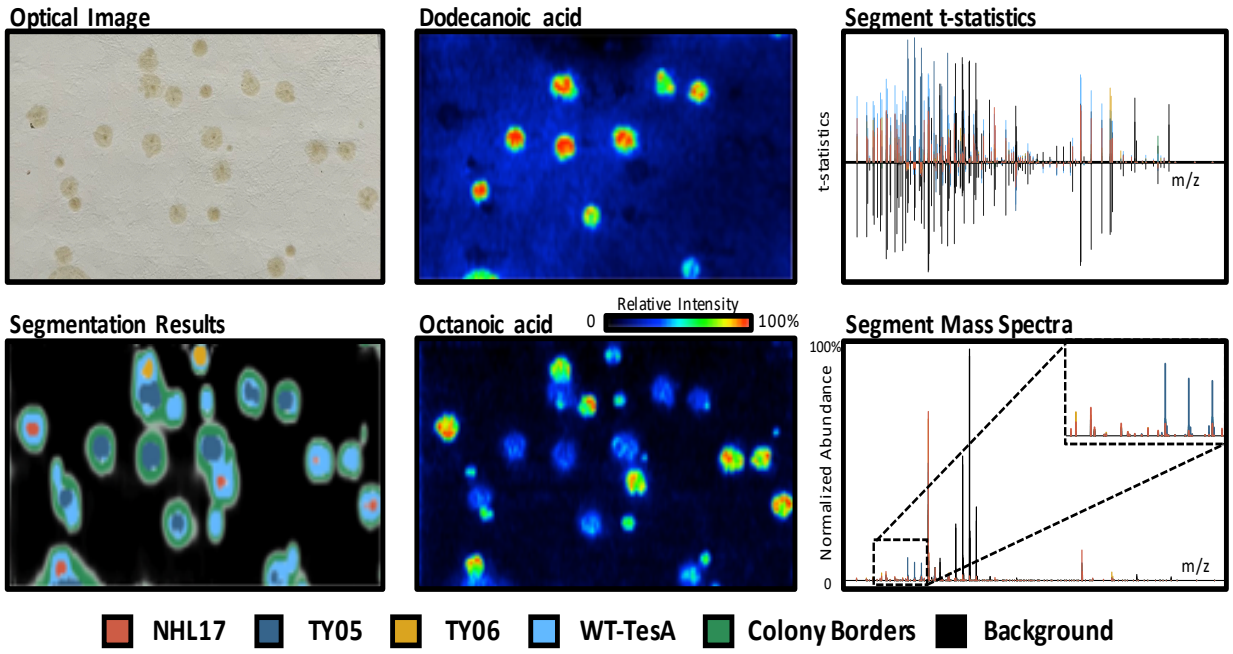

Figure 3.3. Unsupervised segmentation unbiasedly determines molecular phenotypes of engineered microorganisms on the basis of measured metabolomes. Segment statistics and mass spectra highlight the primary features contributing to each strain segments. The segmentation results show the unique phenotypes of the four strains analyzed in this experiment. The dark blue segment represents the dodecanoic acid producing TY05 strain and red corresponds to NHL17 engineered for octanoic acid production. The yellow and light blue segments represent the control TY06 strain and the broad FFA producing WT-TesA strain. We validated the identification on the basis of measured metabolomes with a PCR assay.

acid in the segments, we found that the red segment had nearly twice the amount of octanoic acid per pixel. This led us to tentatively assign the NHL17 strain to the red segment. To solidify our assignments, we characterized the abundances of fatty acids ranging from C8-C14 within the unassigned light blue and red segments (figure C.3). When comparing the segment fatty acid profiles, we found that the light blue segment exhibited broader FFA production, particularly we found elevated amounts of dodecanoic acid (C12:0), tetradecenoic acid (C14:1), and tetradecanoic acid (C14:0). Further, we observed higher accumulation of octanoic acid in the red segment (figure C.3). This confirmed our initial assignment of the NHL17 strain to the red segment and also designated the light blue segment as the WT-TesA strain. By process of elimination, the yellow segment was assigned as the TY06 strain. Additionally, the segment fatty acid profiles, t-statistics, and average metabolite abundances all indicated that this segment correlated to the minimal fatty acid production, supporting our identification. Importantly, all of these strain assignments were validated using a PCR assay (figure C.4). Thus, DESI-IMS and unsupervised segmentation corroborates established methods for identifying strains and effectively determines strain identities on the basis of the measured surface metabolome. Notably, this DESI-IMS phenotyping of specific gene edits is performed in a rapid, untargeted, and multiplexed manner.

3.3.3 *Unsupervised segmentation of DESI-IMS measurements elucidates the underlying biology of engineered microorganisms* To demonstrate the numerous features that are changing from segment to segment, we used traditional metabolomic statistical methods including principal component analysis (PCA) and volcano plot projections (figure 3.4). The mass spectral feature intensities associated with each strain segment were integrated to perform these statistical analyses in a spatially resolved manner. The PCA plot demonstrates that the sample replicates grouped together and partitioned from one another across two principal components (PC1 and PC2), indicating these molecular profiles were unique to each bacterial strain (figure 3.4A). Examination of the loadings plot corroborates the differences measured by segmentation between these sample types (figure C.5). Specifically, we observe that dodecanoic acid is one of the primary features in PC1, which explains the separation between TY05 and the remaining sample

types. We also found that octanoic acid was one of the distinguishing metabolites in PC2, which particularly differentiates NHL17 from WT-TesA and TY06 strains. The primary features associated with TY06 are amino acids, particularly glutamic acid, on the basis of accurate mass measurement. We also observe the unidentified features m/z 615.17 and 154.95 that contribute to the differences in TY06 and WT-TesA sample types, respectively. These and other unidentified features represent the potential for discovery using an untargeted metabolomics approach and may provide avenues for future engineering strategies for these strains.

While PCA can assess the broad scale molecular differences across different engineered strains, volcano plots highlight the specific compounds that contribute to these unique molecular profiles. The volcano plots shown in figure 3.4B demonstrate the statistical significance of the features within a segment as compared to the membrane background and further exhibit the number of features changing within each region. For instance, we found that NHL17 had 46 statistically upregulated features against the background compared to 59 of TY05. Further investigation of the most significant features (p-value $\geq$ 0.05, |fold change| $\geq$ 2) originating from NHL17 reveal that the most changing features correspond to varying ion species of octanoic acid. However, for TY05, we found that multiple fatty acids were significantly upregulated, particularly tetradecanoic acid (C14:0) and tetradecenoic acid (C14:1), which corroborates previous work characterizing TY05 FFA production.[17] We also observed this off-target production of TY05 in the segment fatty acid profiles that were used to distinguish WT-TesA and NHL17 (figure C.3). Within our DESI-IMS analyses, we find that dodecanoic acid (C12) represents 50% of TY05 fatty acid products within the C_8-C_{14} range followed by tetradecanoic acid (C14) at 38%. The remaining significant fatty acid products were unsaturated fatty acids, dodecenoic acid (C12:1) and tetradecenoic acid (C14:1), contributing 2% and 6%, respectively. Detailing the composition of these biosynthesized fatty acids has critical implications in screening both directed evolution studies and rationally designed strain libraries to tailor biosynthesis towards a specific product. Further, we observe higher specificity of CpFatB1 in NHL17 than BTE in TY05.

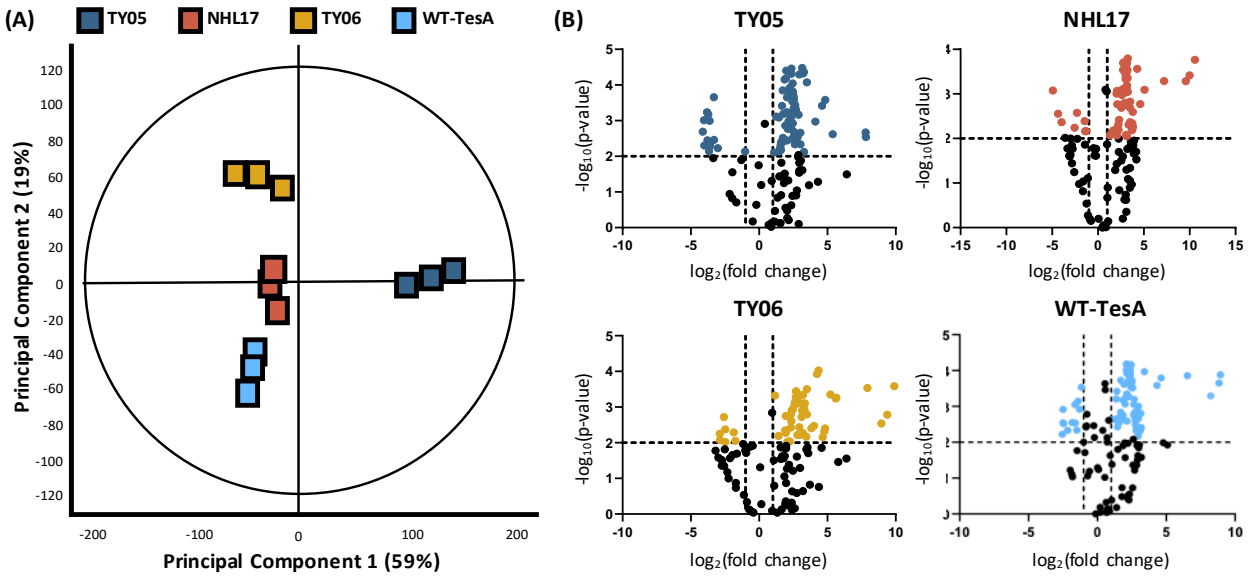

Figure 3.4. (A) PCA demonstrating the overall metabolic distinctions associated with the NHL17, TY05, TY06, and WT-TesA segments. **(B)** Volcano plots comparing observed features from each strain compared to the background segment. The highlighted points represent the significant (p-value ≥0.05, |fold change| ≥2) molecular features which contribute to each strain's unique phenotypes.

In additional targeted analyses, we were able to putatively identify 6 lipid species that were found to be significant within the unsupervised segmentation and volcano plots analysis. We identified these lipids by incorporating tandem mass spectrometry experiments in our DESI-IMS workflow (i.e., DESI-MS/MS) and corroborating the tentative identifications via accurate mass measurement with the fragmentation results (figure C.6). Of the lipids identified with DESI-MS/MS, unsaturated lipid species were found to be statistically significant in the TY05 segment compared to NHL17, WT-TesA, and TY06. In particular, we observed upregulation of phosphatidylglycerol (18:1/18:1), phosphatidylethanolamine (PE) (18:1/18:1), and PE (18:1/17:1). The increased amounts of these lipid species may contribute to membrane stress and affect the overall health and viability of the organism.[20] It has been previously shown that *E. coli* engineered for medium-chain-length free fatty acid production has reduced viability and a loss of inner membrane integrity.[20] The measured changes in lipid abundances via DESI-IMS that were revealed using unsupervised segmentation and volcano plots significance analysis specify downstream metabolic outcomes of genetic engineering that may be targeted to increase the overall growth and production of this particular strain.

3.4 Conclusions

In this chapter, we demonstrate the utility of the presented DESI-IMS and spatially-resolved metabolomic analytics to support synthetic biology approaches. Direct analysis of microbial colonies is facilitated using the microporous membrane scaffold method, which reduces sample handling to a single step procedure (scaffold transfer to the DESI slide). To demonstrate the utility of the untargeted approach, we successfully identify four bacterial strains in a mixed culture on the basis of their measured metabolomes using a novel unsupervised segmentation analytic approach. Additionally, by measuring the full complement of biosynthesized fatty acids produced by these strains, we provide information on the specificity of engineered production not typically acquired using endpoint analysis. The DESI-IMS results demonstrate that a single, untargeted IMS acquisition can provide analytical information regarding: (i) the highest producer of a specific biosynthetic product, (ii) any secondary and off-target production, and (iii) the

molecular profile of engineered organisms. This information has the promise to close the gap between genomic timescales and the analytical methods that assess them by providing various avenues for future engineering within a single multiplexed assay.

While we highlight the value of this DESI-IMS workflow for phenotyping engineered strains, we note that this approach is inherently a surface technique that measures excreted metabolites and molecules associated with the cell membranes. Thus, as implemented, DESI-IMS cannot readily provide readouts on intracellular metabolites as can be achieved from LC-MS and GC-MS, although including an extraction step prior to DESI analysis could provide intracellular metabolomic information. DESI-IMS is also a solid-phase screening method that can be used to select candidate strains to be further characterized in liquid culture, in which most characterizations of fermentation take place. The effects of solid-phase growth, fermentation, or co-culturing strains on biosynthetic production are not fully known. Although, co-culturing has been shown to bolster chemical production in *E. coli*, which could be examined using this method in future studies.[30]

The combination of DESI-IMS sampling and unsupervised segmentation have applications outside of the model system of FFA producing *E. coli*. DESI-IMS is amenable to a wide variety of small molecules (e.g., lipids, antibiotics, amino acids, etc.) many of which are not readily analyzed in vacuum-based ionization techniques. Further, DESI-IMS has been used to measure chemicals produced from a wide variety of microorganisms including gram-positive bacteria and fungi. [31-33] In sum, we developed a method that rapidly and comprehensively annotates the metabolome of engineered microorganisms with the potential to broadly accelerate synthetic biology workflows.

3.5 Acknowledgements

This work was supported by the U.S. Department of Energy, Office of Science, Biological and Environmental Research Division under award number DE-SC00019404. Financial support for aspects of this research was also provided by The National Institutes of Health (Grants NIH NIGMS R01GM092218, NIGMS R37GM067152, NCI R03CA222-452-01

and NCI 1F32GM128344-01), the U.S. Environmental Protection Agency under Assistance Agreement 83573601, and the U.S. Army Research Office and the Defense Advanced Research Projects Agency (DARPA) under Cooperative Agreement W911 NF-14-2-0022. This work has not been formally reviewed by the EPA. The views expressed in this document are solely those of the authors and do not necessarily reflect those of the funding agencies and organizations. EPA, DARPA, and the U.S. Government do not endorse any products or commercial services mentioned in this publication.

3.6 References

(1) Tong, S.; Zhao, H. *Synth. Syst. Biotechnol*., **2016**, 1, 258-264.

(2) National Research Council. 2015. Industrialization of Biology: A Roadmap to Accelerate the Advanced Manufacturing of Chemicals. Washington, DC: The National Academies Press. **2015**.

(3) Pfleger, B. F.; Gossing, M.; Nielsen, J. *Metab. Eng.,* **2019**, 29, 1-11.

(4) Sternberg, S. H.; Doudna, J. A. *Cell Press,* **2015**, 58 (4), 568-574.

(5) Garst, A. D.; Bassalo, M. C.; Pines, G.; Lynch, S. A.; Halweg-Edwards, A. L.; Liu, R.; Liang, L.; Wang, Z.; Zeitoun, R.; Alexander, W. G.; Gill, R. T. *Nat. Biotechnol.,* **2017**, 35, 48-55.

(6) Pfleger, B. F.; Prather, K. L. J. *Nat. Biotechnol*., **2015**, 33 (11), 1148-1149.

(7) Wehrs, M.; Beaumont-Felt, A.; Goranov, A.; Harrigan, P.; de Kok, A.; Lieder, S.; Vallandingham, J.; Tyner, K.. *J. Ind. Microbiol. Biotechnol.* **2020**, 47, 913-927.

(8) May, J.C.; McLean, J. A. *Ann. Rev. Anal. Chem*., **2016**, 9, 387-409.

(9) Wu, S.M.; Su, Y.; Liang, R. R.; Ai, X. X.; Qian, J.; Wang, C.; Chen, J. Q.; Yan, Z. Y. *RSC Adv.,* **2015**, 5, 79184-79191.

(10) Gajewski, J.; Pavlovic, R.; Fischer, M.; Boles, E.;Grininger, M. *Nat. Comm.*, **2017**, 8, 14650.

(11) Rigouin, C.; Gueroult, M.; Croux, C.; Dubois, G.; Borsenberger, V.; Barbe, S.; Bordes, F. *Microb. Cell Fact*., **2018**, 17 (1), 142.

(12) Xue, P.; Tong, S.; Mishra, S.; Zhang, L.; Choe, K.; Sweedler, J. V.; Zhao, H. *Biotechnol. Bioeng.* **2020**, 117 (7), 2131-2138.

(13) Fenselau, C.; Demirev, P. A. *Mass Spectrom. Rev.* **2001**, 20, 157-171.

(14) Yan, C.; Parmeggiani, F.; Jones, E. A.; Claude, E.; Hussain, S. A.; Turner, N. J.; Flitsch, S. L.; Barran, P.E. *Anal. Chem.* **2017**, 139 (4), 1408-1411.

(15) Ellis, B. M.; Fischer, C. N.; Martin, L. B.; Bachmann, B. O.; McLean, J. A. *Anal. Chem.* **2019**, 91 (21), 13703-13711.

(16) Lozada, N. J. H.; Lai, R.; Simmons, T. R.; Thomas, K. A.; Chowdhury, R.; Maranas, C. D.; Pfleger, B. F. *ACS Synth. Biol.* **2018**, 7 (9), 2205-2215.

(17) Lennen, R. M.; Politz, M. G.; Kruziki, M. A.; Pfleger, B. F. *J. Bacteriol.* **2012**, 195 (1), 135-144.

(18) Grisewood, M. J.; Hernandez Lozada, N. J.; Thoden, J. B.; Gifford, N. P.; Mendez-Perez, D.; Schoenberger, H. A.; Allan, M. F.; Floy, M. E.; Lai, R. Y.; Holden, H. M.; Pfleger, B. F.; Maranas, C. D. *ACS Catal.* **2017**, 7 (6), 3837-3849.

(19) J.-T. Youngquist, R.-M. Lennen, D.-R. Ranatunga, W.-H. Bothfeld, W.-D. Marner II, B.-F. Pfleger, Kinetic modeling of free fatty acid production in Escherichia coli based on continuous cultivation of a plasmid free strain. *Biotechnol. Bioeng.* 109 (6), 1518-1527 (2012).

(20) Lennen, R. M.; Kruziki, M. A.; Kumar, K.; Zinkel, R. A.; Burnum, K. E.; Lipton, M. S.; Hoover, S. W.; Ranatunga, D. R.; Wittkopp, T. M.; Marner II, W. D.; Pfleger, B. F. *Appl. Environ. Microbiol*. **2011**, 77 (22), 8114-8128.

(21) Tillner, J.; Wu, V.; Jones, E. A.; Pringle, S. D.; Karancsi, T.; Dannhorn, A.; Veselkov, K.; McKenzie, J. S.; Takats, Z. *J. Am. Soc. Mass Spectrom*. **2017**, 28 (10), 2090–2098.

(22) Bemis, K. D.; Harry, A.; Eberlin, L. S.; Ferreira, C. R.; van de Ven, S. M.; Mallick, P.; Stolowitz, M.; Vitek, O. *Mol. Cell. Proteomics,* **2016**, 15 (5), 1761–1772.

(23) Bemis, K. D.; Harry, A.; Eberlin, L. S.; Ferreira, C.; Van De Ven, S. M.; Mallick, P.; Stolowitz, M.; Vitek, O. *Bioinformatics*, **2015**, 31 (14), 2418-2420.

(24) Zhang, F.; Ouellet, M.; Batth, T. S.; Adams, P. D.; Petzold, C. J.; Mukhopadhyay, A.; Keasling, J. D. *Metab. Eng.* 14, 653–660 (2012).

(25) Lennen, R. M. Pfleger, B. F. *Trends Biotechnol.* **2012**, 30 (12), 659-667.

(26) Marella, E. R.; Holkenbrink, C.; Siewers, V.; Borodina, I. *Curr. Opin. Biotechnol.* **2018**, 50 39–46.

(27) Cobb, R. E.; Sun, N.; Zhao, H. *Methods.* **2013**, 60 81–90.

(28) Kizer, L.; Pitera, D. J.; Pfleger, B. F.; Keasling, J. D. *J. Appl. Environ. Microbiol.* **2008**, 74, 3229–3241.

(29) Heil, C. S.; Wehrheim, S. S.; Paithankar, K. S.; Grininger, K. M. *ChemBioChem* **2019**, 20, 2298–2321 (2019).

(30) Zhang, H.; Stephanopoulus, G. *Biotechnol J.*, **2016**, 11, 981-987.

(31) Tata, A.; Perez, C. J.; Ore, M. O.; Lostun, D.; Passas, A.; Morin, S.; Ifa, D. R. *RSC Adv.* **2015**, 5, 75458-75464.

(32) Song, Y.; Talaty, N.; Datsenko, K.; Wanner, B. L.; Cooks, R. G. *Analyst* **2009**, 134, 838-841.

(33) Zhang, J. I.; Talaty, N.; Costa, A. B.; Xia, Y.; Tao, W. A.; Bell, R.; Callahan, J. H.; Cooks, R. G. *Int. J. Mass Spectrom*. **2011**, 301 (1-3), 37-44.

CHAPTER 4

CHIRAL SEPARATION OF THE CYCLIC NONAPEPTIDES VASOPRESSIN AND DESMOPRESSIN BY UNIFORM FIELD ION MOBILITY MASS SPECTROMETRY

4.1 Introduction

Chiral recognition plays a significant role in determining the biochemical activity of pharmaceuticals and their protein targets.[1] For example, (R)-thalidomide was widely prescribed due to its therapeutic properties for alleviating the symptoms of morning sickness, while (S)-thalidomide was found to produce birth defects in newborns.[2] While most chiral molecules are separated and characterized by chromatographic methods, these assays can require substantial analysis time and sample derivatization.[3] Recognizing the significant impact of chirality on biological activity, discovering rapid and selective methods to separate and evaluate chiral compounds is imperative in quality control efforts related to pharmaceutical production.[4]

Ion mobility-mass spectrometry (IM-MS) is an integrated analytical technique that separates gas phase ions based on their size (collision cross section, CCS) and weight (mass-to-charge ratio, m/z).[5] These separations occur in the millisecond (IM) and microsecond (μs) time scales and hence provide a unique and rapid 2-dimensional analytical separation. IM-MS has previously been shown to effectively separate and characterize isomers spanning many biological classes including carbohydrates, lipids, and fatty acids.[6-8] Here, we utilize IM-MS to evaluate the stereochemistry of macromolecular diastereomers and explore the conformations of nonapeptides.

Nonapeptide hormones are a family of intrinsically disordered cyclic peptides whose structure consist of a nine amino acid chain comprised of a six-membered amino acid ring bridged by a cysteine-cysteine disulfide bond and a three amino acid side-chain, referred to as the tail (Fig. 1). The expression of nonapeptide hormones is conserved throughout both

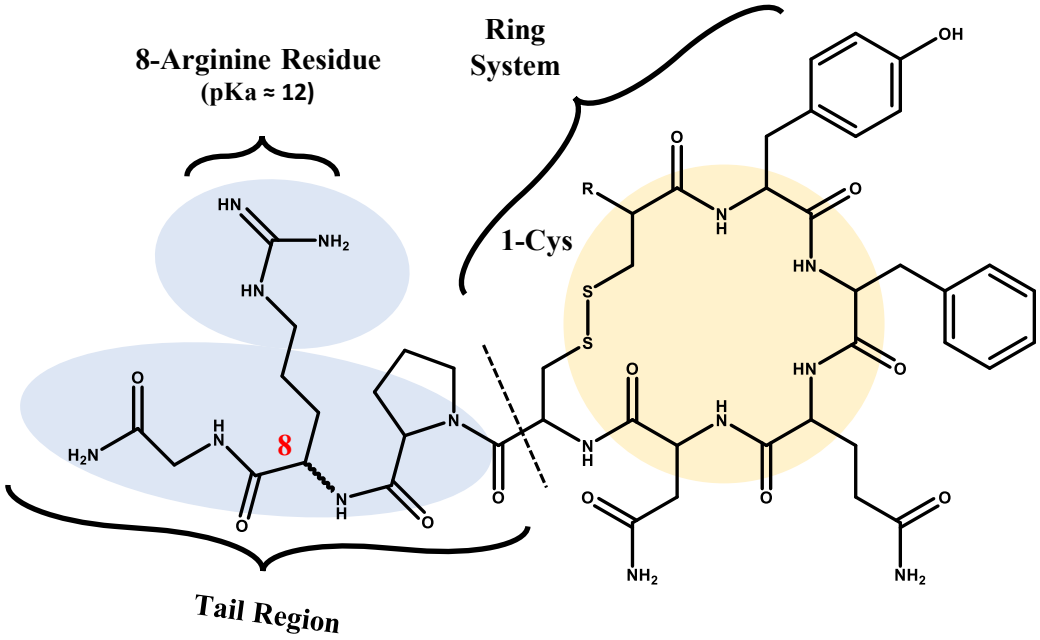

Figure 4.1 Chemical Scaffold of nonapeptide hormones desmopressin and vasopressin. The ring system is indicated in yellow and the tail region is highlighted in blue.

Table 4.1. Abbreviations and designations of chirality for diastereomers.

Nonapeptide	Abbreviation	Cysteine 1	Arginine 8
Vasopressin	8L-VP	-H	L
	8D-VP	-H	D
Desmopressin	8L-DP	$-NH_2$	L
	8D-Vp	$-NH_2$	D

vertebrates and invertebrates where they function in a variety of biochemical roles including vasoconstriction (vasopressin) and reproduction (oxytocin) among others.[9] Two of these nonapeptides are studied here and described in Table 4.1. Vasopressin (8L-arginine-vasopressin, 8L-VP) is a naturally-occurring hormone responsible for vasoconstriction and blood pressure control, and desmopressin (1-desamino-8D-arginine-vasopressin, 8D-DP), a synthetic derivative of vasopressin, has been used predominantly in the treatment of nocturnal enuresis.[10,11]

Desmopressin varies structurally from vasopressin in two locations in the peptide sequence: (1) the absence of an amine group at the 1-Cys residue of the amino acid ring, and (2) D-stereochemistry at the 8-Arg residue. Enantiomeric forms of these nonapeptides can also exist depending on whether the 8-Arg residue is expressed with D- or L- stereochemistry, resulting in four distinct nonapeptides: 8L-arginine-vasopressin (8L-VP), 8D-arginine-vasopressin (8D-VP), 1-desamino-8D-arginine-vasopressin (8D-DP), and 1-desamino-8L-arginine-vasopressin (8L-DP).

4.2 Experimental Methods

In this study, ion mobility separations for the diastereomers of vasopressin and desmopressin were facilitated using a commercial drift tube IM-MS (Agilent 6560) equipped with an electrospray ionization source operated in positive ion mode.[12] Samples of each diastereomer and 1:1 mixture of the diastereomeric pairs of vasopressin and desmopressin were prepared at a concentration of 10 μg/mL in ultra-pure water with 10 mM ammonium acetate added to provide a final solution with pH of ca. 6.5. To further investigate the conformational changes between Vasopressin and Desmopressin we employed molecular modeling. Each vasopressin and desmopressin diastereomer was subjected to simulated annealing calculations in Molecular Operating Environment (MOE) using the MM94ffx force field in order to generate 3,000 low energy conformations. These conformations were then used to calculate CCS values corresponding to helium drift gas using MOBCAL and the projection approximation algorithm.

4.3 Results and Discussion

Figure 4.2A depicts the ion mobility arrival time distribution of protonated $[M+H]^+$ adducts for the diasteromers of desmopressin [(L)-green trace and (D)-purple trace] along with the corresponding 1:1 mixture (grey dotted line). The IM spectra were obtained at an optimal separation drift field of 17 V/cm.[13] Protonation is expected to occur at the 8-arginine position as this amino acid has the highest pKa of all residues in each molecule. IM distributions for 8L-DP and 8D-DP produce a unique single CCS distribution for each diastereomer (CCS of 308 $Å^2$ and 314 $Å^2$, respectively). This difference in CCS (*ca.* 2%) is substantially larger than other studies of diastereomers observed in our laboratory (*ca.* 0.4% difference in CCS), which is enough to allow for separation of both molecules in a two component mixture (grey dotted trace).[14] The significant difference in CCS for the diasteromers of desmopressin in comparison to our previous small molecule studies is most likely attributed to significant differences in the gas-phase structures of these two isomers. Specifically, we hypothesize that 8L-DP can adopt a structure with a smaller cross section due to intermolecular folding of the tail with the ring system, whereas the 8D-DP diastereomer predominantly exists as an extended conformer with a larger (*ca*. 2%) CCS distribution. Previous IM studies have indicated that lasso peptides can exhibit multiple and complex conformations in the gas-phase.[15] Figure 4.2B contains the CCS distributions for the protonated $(M+H)^+$ adducts for the diasteromers of vasopressin [(L)-green trace and (D)-purple trace] along with the corresponding 1:1 mixture (grey). While the diasteromers of desmopressin each consist of single Gaussian arrival time distributions as noted in figure 4.2A, the spectra for the diasteromers of vasopressin (figure 4.2B) exhibit a single unique distribution for this 8D-VP, whereas two peaks with corresponding CCS of 303 $Å^2$ and 310 $Å^2$ (*ca.* 2% difference) are noted for 8L-VP. Interestingly, the larger conformer of 8L-vasopressin (CCS 310 $Å^2$) aligns with the cross section for the 8D-VP, suggesting a structural relationship between these two molecules.

To ensure the two distinct distributions of 8L-VP were not a result of impurities in the sample, mobility-resolved fragmentation experiments of the two peaks were conducted

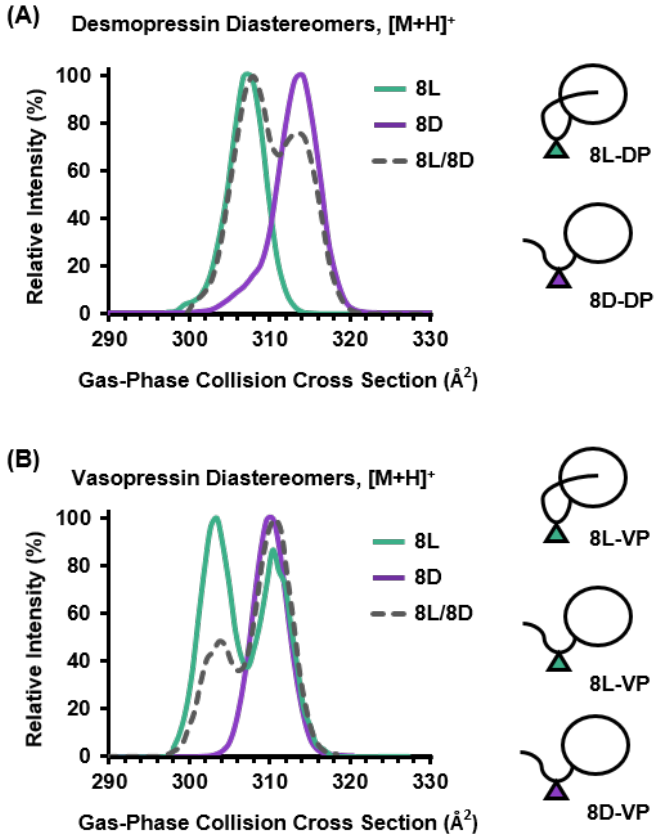

Figure 4.2 Ion mobility spectra of the protonated nonapeptides (desmopression **(A)** and vasopression **(B)**) with representative depictions of intermolecular folding (at right in each panel).

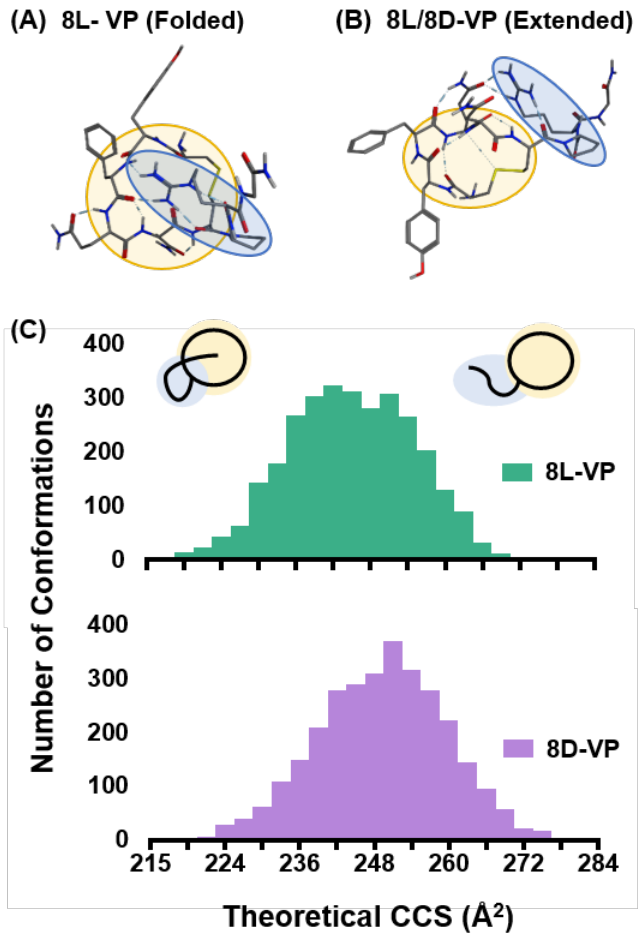

Figure 4.3 Structural representations and theoretical conformations contributing to CCS profiles of 8L-Vasopressin. **(A)** A compact CCS conformation observed as the tail arginine residue (blue) is stabilized within the ring (yellow). (**B)** An expanded conformer is observed wherein the tail and arginine residue interact on the periphery of the ring with glutamine. **(C)** Distribution of the number of theoretical conformations across calculated CCS values. The modelling results exhibit a broader ensemble of structures for 8L-VP extending to a lower CCS than is observed for 8D-VP. Note that molecular modelling was simulated in helium drift gas, as opposed the experimental work done in nitrogen.

(figure D.1). Mobility-aligned fragmentation spectra obtained at 60 V (laboratory frame) illustrate that both conformations contained identical fragmentation profiles and fragment relative abundances suggesting they are the same molecule, and not a contaminant. While the differences in stereochemistry for 8L-VP and 8D-VP do not produce different fragmentation spectra (figure D.2 and D.3), this information provides additional confidence that the two ion mobility distributions observed for 8L-VP originate from a molecule with the same chemical formula and not a degenerate artifact of the analyte, such as a multimeric species.

The sole structural distinction between the diastereomers of desmopressin and vasopressin are the changes in chirality at 8-Arg (colored triangles in Fig. 2A/B) and the corresponding deamination. This conversion in stereochemistry for the diastereomers of desmopressin under these conditions results in each molecule possessing a different experimentally observed cross sectional area which suggests a distinct three-dimensional gas phase structure is adopted for each. While similar behavior is observed for the diastereomers of vasopressin (*i.e.* a different cross section for each diastereomer), there is also the appearance of two peaks for 8L-VP suggesting that there are two unique conformations for this diastereomer.

A significant number of publications in the field of NMR and molecular modelling have been carried out on vasopressin and desmopressin and provide insight into the structural characteristics of these compounds. Of note, the tail-ring interactions (cartoon depicted in figures 4.2 and 4.3) and different ring folding conformations have been proposed to account for several different possible conformations for both desmopressin and vasopressin.[16] We hypothesized that these reported interactions were contributing to the two distinct conformations of 8L-VP observed in the ion mobility spectra and we used computational models to comprehensively investigate our experimental measurements. Although experimental CCS values obtained in nitrogen drift gas are reported in the main text, the separation is also conserved in helium (figure D.4) and these helium CCS measurements are subsequently compared to the theoretical CCS values obtained from the molecular modelling. The theoretical CCS density for vasopressin represented in figure 4.3C articulates the respective separations in that two conformational distributions are observed for 8L-VP and one primary distribution for 8D-VP. 8L-VP exhibits an

increased number of conformations at lower CCS values, which is indicative of the propensity 8L-VP to stabilize the basic arginine residue and tail moiety within the ring (figure 4.3A). This folded conformation appears to solely be present in the 8L-VP generated conformations, in addition to the more extended conformer wherein the tail system is interacting with glutamine on the outside of the ring (figure 4.3B) which is predominantly observed in 8D-VP. Furthermore, heavy atom root-mean-square-deviation (RMSD) hierarchical clustering reflected these analyses, wherein calculations for 8L-VP returned two distinct families of populations representing the folded and extended conformations which comprise 30% and 27% of the total generated conformations (N=3,000), respectively (figure D.5). RMSD calculations for 8D-VP and desmopressin diastereomers reflected one prominent family of the extended conformation representing ~40% of the structures with the remaining families representing sparse structural populations. The described computational models infer the chirality associated with the arginine residue gives rise to different low energy gas phase populations within the vasopressin and desmopressin systems (figure 4.3C and figure D.6). Specifically, a tail-ring conformer at lower CCS and an extended-tail conformer at higher CCS.

4.4 Conclusions

Because of the potential effect of chirality in biological systems as well as in the field of pharmaceuticals, there is a increasing need to discover new methods to rapidly evaluate chiral systems. In this capter we have illustrated the use of IM-MS to recoginize macromolecular structural differences between the diastereomers of desmopressin and vasopressin. Indeed, recent reports have demonstrated that chiral selectivity can be achieved in ion mobility for multimeric complexes such as analyte dimers, trimers, and tetramers.[17-19] The ability of IM-MS to recognize the presence of a mixture of diasteromers as well as conformations in these molecules suggests its application to more extensive areas, including the characterization of the chrial distribution of pharmaceuticals following synthesis and purification.[20]

4.5 Acknowledgements This work was supported in part using the resources of the Center for Innovative Technology atVanderbilt University. Financial support for this work was provided by the National Institutes of Health (NIH NIGMS R01GM092218 and NIH NCI 1R03CA222452-01) and the U.S. Environmental Protection Agency (EPA) under Assistance Agreement No. 83573601. This work has not been formally reviewed by the EPA and EPA does not endorse any products or commercial services mentioned in this document.

4.6 References

(1) Williams, K.; Lee, E. *Drugs*, **1985**, 30, 333-354.

(2) Lenz, W. *Teratology*, **1988**, 38, 203-215.

(3) Chan, S.; Lee, W.; Asmawi, M.; Tan, S. *J. Chromatogr. B. Analyt. Technol. Biomed. Life Sci.,* **2016**, 1025, 83-91.

(4) Ward, T.; Ward, K. *Anal. Chem.*, **2010**, 82, 4712-4712.

(5) Mairinger, T.; Causon, T.; Hann, S. *Curr. Opin. Chem. Biol.* 2017, 42, 9-15.

(6) Hofmann, J.; Hahm, H.; Seeberger, P.; Pagel, K. *Nature*, **2015**, 526, 241-244.

(7) Groessl, M.; Graf, S.; Knochenmuss, R. *Analyst*, **2015**, 140, 6904-6911.

(8) Kyle, J.; Zhang, X.; Weitz, K.; Monroe, M.; Ibrahim, Y.; Moore, R.; Cha, J.; Sun, X.; Lovelace, E.; Wagoner, J.; Polyak, S.; Metz, T.; Dey, S.; Smith, R.; Burnum-Johnson, K.; Baker, E. *Analyst*, **2016**, 141, 1649-1659.

(9) Archer, R.; Chauvet, J. *Front. Neuroendocrin.*, **1995**, 16, 237-289.

(10) F. Rotondo, H. Butz, L. Syro, G. Yousef, A. Di lvea, L. Restrepo, A. Quintanar-Stephano, I. Berczi and K. Kovacs, *Pituitary*, **2016**, 19, 345-355.

(11) A. Stenberg and G. Läckgren, *Pediatrics*, **1994**, 94, 841-846.

(12) May, J.; Goodwin, C.; Lareau, M.; Leaptrot, K.; Morris, C.; Kurulugama, R.; Mordehai, A.; Klein, C.; Barry, W.; Darland, E.; Overney, G.; Imatani, K.; Stafford, G.; Fjeldsted, J.; McLean, J. A. *Anal. Chem.*, **2014**, 86, 2107-2116.

(13) May, J.; Dodds, J.; Kurulugama, R.; Stafford, G.; Fjeldsted, J.; McLean, J. *Analyst*, **2015**, 140, 6824-6833.

(14) Dodds, J.; May, J.; McLean, J. *Anal. Chem.*, **2017**, 89, 952-959.

(15) Jeanne Dit Fouque, K.; Afonso, C.; Zirah, S.; Hegemann, J. D.; Zimmermann, M.; Marahiel, M. A.; Rebuffat, D.; Lavanant, H. *Anal. Chem.* **2015**, 87, 1166-1172.

(16) Haensele, E.; Saleh, N.; Read, C.; Banting, L.; Whitley, D.; Clark, T. *J. Chem. Inf. Model.,* **2016**, 56, 1798-1807.

(17) Jia, C.; Lietz, C.; Yu, Q.; Li, L. *Anal. Chem.,* **2014**, 86, 2972-2981.

(18) Chouinard, C.; Beekman, C.; Kemperman, R.; King, H.; Yost, R. *Int. J. Ion Mobil. Spec.*, **2017**, 20, 31-39.

(19) Yu, X.; Yao, Z. *Anal. Chim. Acta*, **2017**, 981, 62-70.

(20) Dwivedi, P.; Wu, C.; Matz, L. M.; Clowers, B. H.; Siems, W. F.; Hill, H. H. *Anal. Chem.* **2006**, 78, 8200-820.

CHAPTER 5

CONSPECTUS AND OUTLOOK

5.1 Conspectus

Desorption electrospray ionization-imaging mass spectrometry is a powerful tool to accelerate synthetic biology and natural product discovery workflows. As previously mentioned, the utility DESI-IMS measurements of molecules present in microbial biosynthesis provides a myriad of advantages. For example, directly sampling microbial colonies facilitates measurements of microbially produced chemicals without sample pretreatment. Furthermore, direct and ambient sampling also reduce error and increase throughput in sample preparation, which can accelerate both natural product discovery and synthetic biology workflows.

Unsupervised segmentation of DESI-IMS data provides unbiased definition of discrete spatiochemical phenotypes. This IMS analysis perfectly complements the minimalistic and rapid nature of DESI-IMS by reducing user input and error. Additionally, unsupervised segmentation utilizes all of the features changing across an IMS image, which facilitates a robust annotation of phenotypes and provides the opportunity for untargeted IMS experiments. In Chapter 2, we demonstrate the value of DESI-IMS and unsupervised segmentation in natural discovery workflows. Using the microporous membrane scaffold method, we report the ability to measure *in situ* spatiochemical annotations of microbial co-cultures. The robust and minimalistic sampling afforded by this technique not only facilitated repeatable metabolite localizations, but also unsupervised segmentation outputs. Unsupervised segmentation of IMS data defined the region of interaction between microorganisms in a co-culture experiment. Using this spatial annotation, we infer bioactivity of measured metabolites within this region. Importantly, this reduces the number of features considered for isolation from 4,000 measured features to 47 with inferred bioactivity. This can accelerate natural product discovery as isolating a compound is one of the primary challenges in these workflows. Isolation is the traditional means to determine bioactivity, whereas we can rapidly postulate bioactivity using the presented DESI-IMS

workflow incorporating spatial prioritization. The utility of DESI-IMS and unsupervised segmentation in natural product discovery workflows was demonstrated by linking the antibiotic myxovirescin and secondary metabolite DKxanthene-560 present to their known biological roles in *M. xanthus* and *E. coli* co-cultures.

The full advantages of DESI-IMS and unsupervised segmentation to accelerate synthetic biology workflows were described in Chapter 3. The combination of these techniques provides multiplexed untargeted metabolomic profiling of microorganisms engineered for chemical production. MMS DESI-IMS was demonstrated to increase throughput by reducing sample preparation to a single step and providing multiplexed sampling, which is not feasible using contemporary GC-MS, or LC-MS methods most commonly used in synthetic biology workflows. Furthermore, ambient analyses allowed for the direct analysis of labile analytes like octanoic acid, which require proxies in vacuum-based sampling modalities. Aside from sampling advantages, untargeted acquisitions can analytics accelerate synthetic biology workflows by providing multiple avenues for future engineering strategies within a single acquisition. Unsupervised segmentation was used to probe relative amounts of targeted biosynthetic products, off-target production, as well as the broader biology of engineered *E. coli* through lipidomic analyses. Obtaining this analytical information under the rapid and multiplexed sampling conditions of DESI-IMS has the potential to narrow the gap between the timescales associated with genetic editing and metabolic profiling. DESI-IMS and unsupervised segmentation can advance synthetic biology workflows and ultimately the commercial utility of microbial cell factories.

While we highlight the utility of DESI-IMS to rapidly profile microbial biosynthesis, additional measurements are possible within each acquisition. Incorporating ion mobility (IM) within DESI-IMS workflows has the potential to measure gas phase conformations of biomolecules using collision cross sections (CCS). In Chapter 4, we demonstrated the advantages of IM to probe molecular conformations, structure, and chirality by distinguishing nonapeptide diastereomers.

5.2 Outlook and Future Directions

In order to further advance DESI-IMS measurements of microbially produced chemicals, IM measurements can be incorporated. IM provides an orthogonal separation to that of spatial location and m/z measurements routinely performed in DESI-IMS analyses. To achieve this separation, ions are subjected to an electrostatic gradient against an inert buffer gas, which distinguishes ions on the basis of size and charge. IM has been shown to increase the selectivity and signal to noise ratio of measured metabolites.[1] Importantly, IM does not increase acquisitions times.[1] The milisecond separation using this technique nests perfectly within the measurement timescales of a typical IMS experiment (figure 6.1). Incorporating IM into DESI-IMS workflows probing microbial biosynthesis will not only increase metabolite annotations, but also accelerate synthetic biology and natural product discovery workflows.

5.2.1 *DESI-IM-IMS to enhance feature annotation* Ion mobility measurements have been shown to partition analytes from noise or interfering species, which would enhance DESI-IMS sampling when incorporated.[2] IM measurements separating isomeric and enantiomeric species like those in Chapter 4 have particular applications within IMS applications. An example of the ability of IM to separate isobaric species is shown in figure 5.2. Within this example, IM is not only able to separate two isobaric species at m/z 1039, it also highlights two unique localizations for tryptic peptides.[3] These two peptides would not be distinguished in typical peak processing or peak picking steps. Contemporary IMS data processing techniques output a localization for each unique measured m/z. In the case of tubulin and ubiquitin, the localization would be averaged between the two species. This would yield a confounded localization, which can affect the resulting IMS analyses and biological inferences.

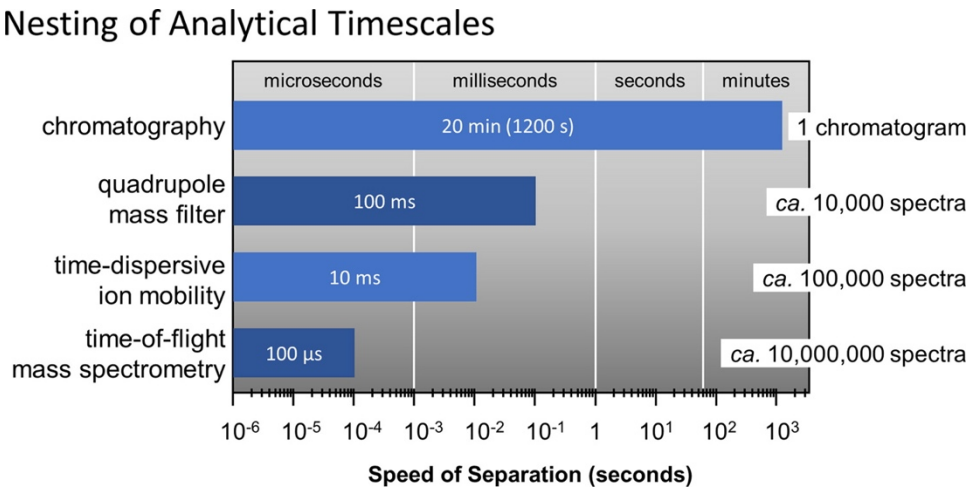

Figure 5.1. Nesting of analytical timescales based on speed of separation (left) and the total number of potential spectra generated (right). Adapted with permission from May, J.C.; McLean, J.A., "Ion Mobility-Mass Spectrometry: Time-Dispersive Instrumentation" *Anal. Chem*, **2015**, 87 (3), 1422-1436. https://pubs.acs.org/doi/10.1021/ac504720m.

A confounded localization would reduce the accuracy of unsupervised segmentation and other data analysis techniques to determine unique phenotypes, or even lead to incorrect segment assignments. This has specific implications in the application described in Chapter 2, in which we infer biological function and bioactivity on the basis of spatial location. A confounded localization may perturb the assignment of the primary bioactive components within a co-culture. It is important to note that while we did use IM in some of the acquisitions in Chapter 2, these were primarily used as a means to import data into metabolomic analysis programs for dereplication. The utility of metabolomics data, particularly IMS and IM-IMS data are limited by the depth and efficiency of data analytics platforms and programs. To maximize the utility of IMS and IM-IMS data, advanced data analytics platforms must be developed that can rapidly annotate spatial location, m/z, and IM drift times.

5.2.2 *IM-IMS to increase metabolite identification confidence* Adding IM drift times, and subsequently collision cross section into IMS data analytics workflows provides an additional avenue to improve DESI-IMS metabolite identifications. Putatively identifying metabolites in metabolomic workflows and thus being able to make biological inferences requires an additional analytical dimension outside of m/z.[4] Techniques for generating putative identifications are MS/MS and IM. Most IMS methods do not obtain enough signal to perform MS^e(fragmentation of all ions) and require additional targeted MS/MS experiments of a single ion of interest to putatively identify metabolites, which is described in Chapters 2 and 3.[4] Furthermore, most analytes investigated are small molecule metabolites that often have similar fragmentation patterns.[4] Given these factors and the ability of IM to generate CCS values for the majority of measured metabolites within the same timescales of traditional IMS acquisitions, IM is preferred.

Work in the McLean laboratory has been dedicated to using IM derived CCS values as a means to improve the confidence of small molecule identifications. Studies measuring libraries of metabolite standards and generating a unified CCS compendium have made this feasible.[6,7]

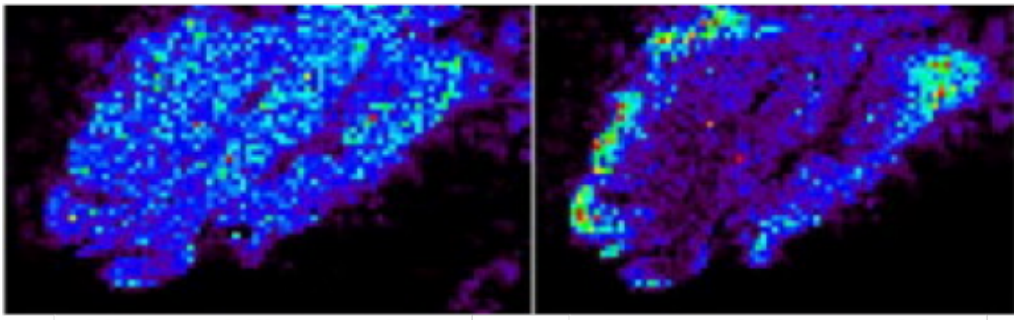

Figure 5.2. DESI-IM-IMS data highlighting separation of isobaric species of tryptic peptides and the unique localizations of each. Adapted with permission from Heeren, R. M. A.; Smith, D. F.; Stauber, J.; Kükrer-Kaletas, B.; MacAleese, L. "Imaging mass spectrometry: hype or hope?" *J. Am. Soc. Mass Spectrom.*, **2009**, 20 (6), 1006-1014. https://www.sciencedirect.com/science/article/pii/S1044030509000506

Integrating CCS values as a metabolite identifier into DESI-IM-IMS workflows would facilitate putative identifications for small molecule metabolites without additional experiments. This would further increase the throughput of DESI-IMS in synthetic biology workflows described in Chapter 4. Synthetic biologist and metabolic engineers use endogenous metabolite levels such as lipids and amino acids to determine metabolic bottlenecks, wasteful byproduct pathways that reduce product yield, and assess growth and viability of engineered organisms. Providing this information from a single experiment would further accelerate synthetic biology workflows by providing multiple avenues for future engineering strategies with high confidence.

5.2.3 *DESI-IM-IMS to Accelerate Natural Product Discovery* Significant work has been dedicated towards class specific CCS vs m/z trends.[1,2,6,8] Within these trends, biomolecular classes like carbohydrates, lipids, and peptides have distinct trendlines. CCS vs m/z trendlines have been used to distinguish between different lipid classes of isomeric species.[7] In natural product discovery workflows one of the primary steps in data analysis of generated data is dereplicating against known compounds. In Chapter 2, we describe dereplicating DESI-IM-IMS data against online repositories like KEGG and Chemspider, but only use m/z to do so. Using trendlines and CCS repositories like the Unified CCS Compendium, we can further dereplicate DESI-IM-IMS and prioritize unknown molecular species for natural product discovery (figure 6.3).[9] It is possible that natural products like non-ribosomal polyketides and macrolides may occupy a unique conformational space. If these trends are not annotated in future experiments, it is still possible to remove features that occupy lipid and carbohydrate trendlines. Lastly, bioactivity may be correlated with chemical rigidity or flexible conformations, which can also be discerned using IM. For instance, using DESI-IM-IMS analysis of the natural product DKxanthene-560 in Chapter 2 resulted in multiple conformations, which may be used as an additional means to prioritize secondary metabolite natural products for isolation. In sum, using the additional annotation of CCS provides a means to further dereplicate and prioritize novel chemical structures and scaffolds of natural products.

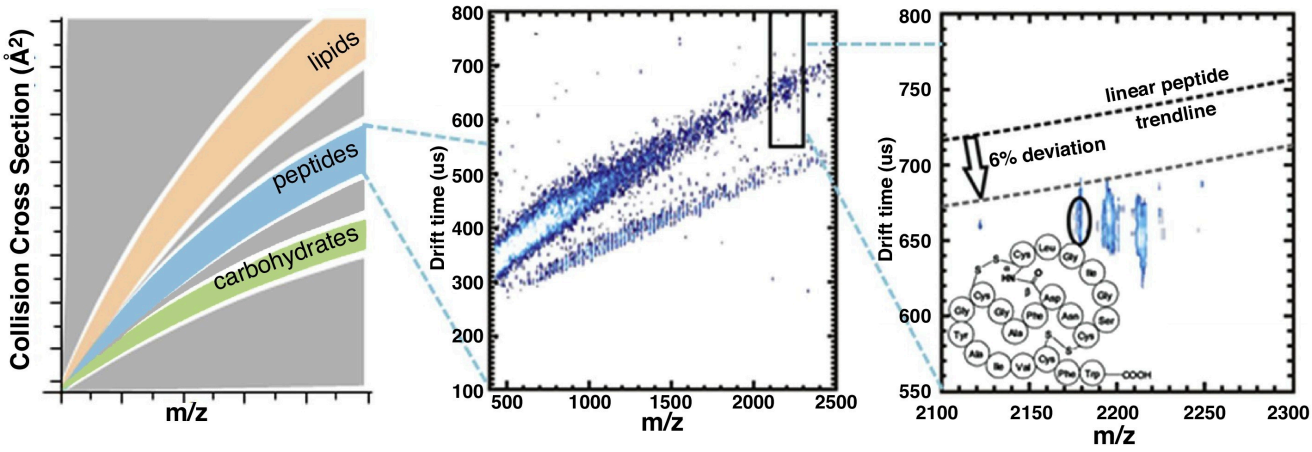

Figure 5.3. Ion mobility as a means for discovery and prioritization on the basis of molecular conformation. Adapted with permission from Schrimpe-Rutledge, A. C.; Sherrod, S. D.; McLean, J. A., "Improving the discovery of secondary metabolite natural products using ion mobility-mass spectrometry" *Curr. Opin. Chem. Biol.*, **2017**, 42, 160-166. https://www.sciencedirect.com/science/article/abs/pii/S1367593117301400?via%3Dihub

5.3 Concluding Remarks

DESI-IMS and DESI-IM-IMS are ideal analytical techniques for rapidly profiling biological tissues. While the work in this dissertation was primarily dedicated towards gram-negative bacteria, research has been extended to gram-positive bacteria, fungi, and eukaryotic systems ranging from human tumor tissue to rat brains.[10-13] Recent developments in the applications of DESI-IMS and DESI-IM-IMS have broadened the applications for this technology. Towers *et al.* described an adaptation of DESI to image proteins from the surface of tissue sections, which expanded the molecular breadth of DESI-IMS analyses.[14] Incorporating a heating element aided in the desolvation and analysis of protein species, but standardizing heated capillary inlets has the promise to greatly increase the signal levels and allow for additional analyses like MS^e. Furthermore, the development and commercialization of the new DESI-XS system by Waters (Manchester, UK) will accelerate the applications and utility of DESI-IMS in research and potentially clinical workflows. This newer model incorporated automated sample handling and preparation, which increases throughput. Finally, the DESI-XS system contains a stationary DESI sprayer that does not require optimization for sampling geometries, which increases the repeatability of the experiments and also greatly reduces the time dedicated towards geometry optimization of the DESI probe. The work using DESI-IMS to increase throughput in workflows described in Chapters 2 and 3 may act as a stepping stone for the future developments and applications of these new innovations. Additionally, integrating IM in these workflows has the potential to simultaneously distinguish conformers in an online fashion and achieve chiral separations as described in Chapter 4.

5.4 Acknowledgements

This work was supported by the U.S. Department of Energy, Office of Science, Biological and Environmental Research Division under award number DE-SC00019404. Financial support for aspects of this research was also provided by The National Institutes of Health (Grants NIH NIGMS R01GM092218, NIGMS R37GM067152, NCI R03CA222-452-01 and NCI 1F32GM128344-01), the U.S. Environmental Protection Agency under Assistance Agreement

83573601, and the U.S. Army Research Office and the Defense Advanced Research Projects Agency (DARPA) under Cooperative Agreement W911 NF-14-2-0022. This work has not been formally reviewed by the EPA. The views expressed in this document are solely those of the authors and do not necessarily reflect those of the funding agencies and organizations. EPA, DARPA, and the U.S. Government do not endorse any products or commercial services mentioned in this publication.

5.5 References

(1) May, J.C.; McLean, J.A. *Anal. Chem*, **2015**, 87 (3), 1422-1436.

(2) Stow, S. M.; Causon, T.J.; Zheng, X.; Kurulugama, R. T.; Mairinger, T. May, J. C.; Rennie, E. E.; Baker, E. S.; Smith, R. D.; McLean, J.A.; Hann, S. Fjeldsted, J. C. *Anal. Chem.*, **2017**, 89 (17), 9048-9055.

(3) Heeren, R. M. A.; Smith, D. F.; Stauber, J.; Kükrer-Kaletas, B.; MacAleese, L. *J. Am. Soc. Mass Spectrom.,* **2009**, 20 (6), 1006-1014.

(4) Schrimpe-Rutledge, A.C.; Codreanu, S. G.; Sherrod, S. D.; McLean, J.A. *J. Am. Soc. Mass Spectrom.*, **2016**, 27 (12), 1897-1905.

(5) Kind, T.; Fiehn, O. *Bioannal. Rev.,* **2010**, 2, 23-60.

(6) Nichols, C. M.; Dodds, J. N.; Rose, B. S.; Picache, J. A.; Morris, C. B.; Codreanu, S. G.; May, J. C.; Sherrod, S. D.; Mclean, J. A. *Anal. Chem.,* **2018**, 90 (24), 14484-14492.

(7) Picache, J. A.; Rose, B. S.; Ballinski, A.; Leaptrot, K. L.; Sherrod, S. D.; May, J. C.; Mclean, J. A. *Chem. Sci.,* **2019**, 10 (4), 983-993.

(8) Leaptrot, K. L.; May, J. C.; Dodds, J. N.; McLean, J. A. *Nature Comm.*, **2019**, 10 (1), 985.

(9) Schrimpe-Rutledge, A. C.; Sherrod, S. D.; McLean, J.A. *Curr. Opin. Chem. Biol.*, **2018**, 42, 160-166.

(10) Tata, A.; Perez, C. J.; Ore, M. O.; Lostun, D.; Passas, A.; Morin, S.; Ifa, D. R. *RSC Adv.* **2015**, 5, 75458-75464.

(11) Song, Y.; Talaty, N.; Datsenko, K.; Wanner, B. L.; Cooks, R. G. *Analyst* **2009**, 134, 838-841.

(12) Callargis, D.; Caragacianu, D.; Liu, X.; Norton, I.; Thompson, C. J.; Richardson, A. L.; Golshan, M. Easterling, M. L.; Santagrata, S.; Dillon, D. A.; Jolesz, F. A.; Agar, N. Y. R. *PNAS*, **2014**, 111 (42), 15184-15189.

(13) Fernandes, A. M. A. P.; Vendrammi, P. H.; Galaverna, R.; Schwab, N. V.; Alberici, L. C.; Augusti, R.; Castilho. R. F.; Eberlin, M. N. *J. Am. Soc. Mass Spectrom.*, **2016**, 27 (12), 1944-1951.

(14) Towers, M. W.; Karancsi, T.; Jones, E. A.; Pringle, S. D.; Claude, E. . *J. Am. Soc. Mass Spectrom.*, **2018**, 29, 2456-2466.

APPENDIX A

Reference of Adaption for Chapters

Chapter 1.

Ellis, B. M.; Fischer, C. N.; Martin, L. B. Bachmann, B. O.; McLean, J. A., "Spatiochemically Profiling Microbial Interactions with Membrane Scaffolded Desorption Electrospray Ionization-Ion Mobility-Imaging Mass Spectrometry and Unsupervised Segmentation" *Anal. Chem.* **2019**, 91 (21), 13703-13711.

Ellis, B. M.; Babele, P.; May, J. C.; Johnson, C. H.; Pfleger, B. F.; Young, J. D.; McLean, J.A. "Accelerating Strain Engineering Using Desorption Electrospray Ionization-Imaging Mass Spectrometry and Untargeted Molecular Analysis of Intact Microbial Colonies" *Biorxiv*, https://doi.org/10.1101/2021.04.01.438078.

Phlilips, S. T.; Dodds, J. N.; Ellis, B. M.; May, J. C.; McLean, J.A., "Chiral Separation of Diastereomers of the Cyclic Nonapeptides Vasopressin and Desmopressin by Uniform Field Ion Mobility Mass Spectrometry" *Chem Comm.* **2018**, 54 (68), 9398-9401.

May, J.C.; McLean, J.A., "Ion Mobility-Mass Spectometry: Time dispersive instrumentation" *Anal. Chem.* **2015**, 87 (3), 1422-1436.

Chapter 2.

Ellis, B. M.; Fischer, C. N.; Martin, L. B. Bachmann, B. O.; McLean, J. A., "Spatiochemically Profiling Microbial Interactions with Membrane Scaffolded Desorption Electrospray Ionization-Ion Mobility-Imaging Mass Spectrometry and Unsupervised Segmentation" *Anal. Chem.* **2019**, 91 (21), 13703-13711.

Chapter 3.

Ellis, B. M.; Babele, P.; May, J. C.; Johnson, C. H.; Pfleger, B. F.; Young, J. D.; McLean, J.A., "Accelerating Strain Engineering Using Desorption Electrospray Ionization-Imaging Mass Spectrometry and Untargeted Molecular Analysis of Intact Microbial Colonies" *Biorxiv*, https://doi.org/10.1101/2021.04.01.438078.

Chapter 4.

Phlilips, S. T.; Dodds, J. N.; Ellis, B. M.; May, J. C.; McLean, J.A., "Chiral Separation of Diastereomers of the Cyclic Nonapeptides Vasopressin and Desmopressin by Uniform Field Ion Mobility Mass Spectrometry" *Chem Comm.* **2018**, 54 (68), 9398-9401.

Chapter 5.

Schrimpe-Rutledge, A. C.; Sherrod, S. D.; McLean, J.A., "Improving the discovery of secondary metabolite natural products using ion mobility-mass spectrometry" *Curr. Opin. Chem. Bio.*, **2018**, 42, 160-166.

Heeren, R. M. A.; Smith, D. F.; Stauber, J.; Kükrer-Kaletas, B.; MacAleese, L. "Imaging mass spectrometry: hype or hope?" *J. Am. Soc. Mass Spectrom.*, **2009**, 20 (6), 1006-1014.

APPENDIX B

SUPPLEMENTARY MATERIALS FOR CHAPTER 2

Spatiochemically Profiling Microbial Interactions with Membrane Scaffolded Desorption Electrospray Ionization-Ion Mobility-Imaging Mass Spectrometry and Unsupervised Segmentation.

Berkley M. Ellis[1-5], Caleb N. Fischer[1,3,4], Leroy B. Martin[6], Brian O. Bachmann[1,3,4], John A. McLean*[1-5]

[1]Department of Chemistry, Vanderbilt University, Nashville, TN USA; [2]Center for Innovative Technology, Vanderbilt University, Nashville, TN USA; [3]Institute of Chemical Biology, Vanderbilt University, Nashville, TN USA; [4]Institute for Integrative Biosystems Research and Education, Vanderbilt University, Nashville, TN USA; [5]Vanderbilt-Ingram Cancer Center, Vanderbilt University, Nashville, TN USA; [6]Waters Corporation, 34 Maple Street, Milford, MA USA

Abstract

Imaging the inventory of microbial small molecule interactions provides important insights into microbial chemical ecology with applications in human medicine from manipulating microbiomes therapeutically to antibiotic discovery. Herein we demonstrate a new method for enhanced detection and analysis of metabolites present in interspecies interactions of microorganisms on surfaces. We demonstrate that desorption electrospray ionization-imaging mass spectrometry (DESI-IMS) using microporous membrane scaffolds enable enhanced detection of molecular features associated with intermicrobial interactions. Membrane scaffolded DESI-IMS has inherent advantages compared to matrix-assisted laser desorption ionization (MALDI), liquid extraction surface analysis (LESA), and other IMS methods through direct IMS analyses of microbial chemistry *in situ*. This minimalistic method yields sensitive MS

measurements with orthogonal detection capabilities to reverse phase liquid chromatography-electrospray ionization-mass spectrometry (RPLC-ESI-MS). Unsupervised segmentation imaging analysis of acquired DESI-IMS data reveals distinct chemical regions corresponding to intermicrobial phenomenon such as predation. We validate the method by linking myxovirescin and dkxanthene560 to their known biological roles of predation and phase variation, respectively. In addition to providing the topographic locations of known natural products, we prioritize 47 other features without database matches within the predation region. Thus, unsupervised segmentation recapitulates the known biology of myxobacteria and points to the exploration of uncharacterized metabolites. In other words, microporous membrane scaffolded DESI-IMS and unsupervised segmentation provides insights into the roles of metabolites in chemical communication between organisms.

B.1.1 Supplemental Tables

Table B.1: Calculated values annotating sampling efficiency (n=3).

Sample	Dried Agar	Imprinting	Nylon Membrane
Average TIC	4.30×10^9	9.84×10^9	1.75×10^9
Significant Features (S/N >3)	193	340	355
Average Intensity*	$27 \times 10^3 \pm 14 \times 10^3$	$57 \times 10^3 \pm 25 \times 10^3$	$27 \times 10^3 \pm 5 \times 10^3$
Percent Covariance*	54.60%	44.10%	20.20%
Average S/N*	15.5 ± 10.6	110.3 ± 49.65	77.1 ± 15.0

* Calculated using dkxanthene534, dkxanthene560, myxovirescin, lyso-PE 16:1, and PG 16:0/18:1

Table B.2: Measured features and their corresponding segmentation region (defined in figure B.4), segmentation statistics, and tentative metabolite identifications on the basis of accurate mass measurement.

m/z	Segmentation region	Tstatistic	Tstatistic Standard Deviation	Identification*	Molecular formula	Adduct	Mass Accuracy (ppm)	Normalized Abundance
76.97	x	0	0	n/a	n/a	n/a	n/a	3517
78.96	Green	69.36	9.21	Phosphoric acid	H3O4P	M-H2O-H	-0.87	8343
79.96	Purple	14	6.56	n/a	n/a	n/a	n/a	609363
80.97	Blue	5.33	1.53	n/a	n/a	n/a	n/a	710846
93.03	x	0	0	n/a	n/a	n/a	n/a	24282
95.01	x	0	0	n/a	n/a	n/a	n/a	4897
96.96	Green	64.25	31.03	n/a	n/a	n/a	n/a	724849
98.02	Green	43.33	20.74	N-Formyl-beta-alanine	C4H7NO3	M-H2O-H	-8.47	4086
98.96	Green	17.33	8.39	n/a	n/a	n/a	n/a	645959
102.06	Purple	63.25	10.08	n/a	n/a	n/a	n/a	6876
108.02	x	0	0	n/a	n/a	n/a	n/a	118416
111.04	x	0	0	n/a	n/a	n/a	n/a	16664
114.94	x	0	0	n/a	n/a	n/a	n/a	14843
115.04	x	0	0	1-Deoxypent-2-ulose	C5H10O4	M-H2O-H	5.48	12040
116.07	Purple	23.46	3.3	n/a	n/a	n/a	n/a	697946
116.93	x	0	0	n/a	n/a	n/a	n/a	13886
118.03	x	0	0	S-acetylcysteamine	C4H9NOS	M-H	2.67	22973
118.94	Blue	61.17	18.47	n/a	n/a	n/a	n/a	167409
119.05	x	0	0	n/a	n/a	n/a	n/a	93894
120.94	x	0	0	n/a	n/a	n/a	n/a	14474
121.03	x	0	0	methoxyresorcinol	C7H8O3	M-H2O-H	-8.85	154803
123.08	x	0	0	n/a	n/a	n/a	n/a	7077
125.1	Orange	16.71	14.01	(Z)-5-Octene-1,3-diol	C8H16O2	M-H2O-H	-9.96	24280
126.03	x	0	0	n/a	n/a	n/a	n/a	21578
126.9	x	0	0	n/a	n/a	n/a	n/a	745878
126.99	x	0	0	n/a	n/a	n/a	n/a	11321
128.03	Purple	71.33	6.03	n/a	n/a	n/a	n/a	154503
129.04	Purple	22.33	9.45	n/a	n/a	n/a	n/a	527846
130.09	Green	35.67	4.04	n/a	n/a	n/a	n/a	186683
131.04	Cyan	34	2.65	n/a	n/a	n/a	n/a	1559737
132.04	x	0	0	n/a	n/a	n/a	n/a	56302
134.92	Green	45.62	25.05	n/a	n/a	n/a	n/a	36239
135.04	x	0	0	n/a	n/a	n/a	n/a	149165
136.94	Green	20.71	13.22	n/a	n/a	n/a	n/a	78548
137.1	x	0	0	3-Methyl-1-hexanol	C7H16O	M+Na-2H	3.54	7495
138.02	x	0	0	n/a	n/a	n/a	n/a	320273
141.04	x	0	0	n/a	n/a	n/a	n/a	176900
142.01	x	0	0	N-formylmaleamic acid	C5H5NO4	M-H	-8.7	26567

143.04	Green	53.89	4.81	n/a	n/a	n/a	n/a	489745
143.11	x	0	0	1,3,7-Octanetriol	C8H18O3	M-H2O-H, M-H	-7.7	79912
144.04	Cyan	60.22	7.65	(3E)-4-(pyridin-3-yl)but-3-enoic acid	C9H9NO2	M-H2O-H	-8.46	2855362
145.1	x	0	0	n/a	n/a	n/a	n/a	123986
146.05	Purple	88.87	19.99	n/a	n/a	n/a	n/a	6802644
146.98	x	0	0	monoethyl phosphate	C2H7O4P	M+Na-2H	1.26	9914
147.05	Purple	45.71	11.35	n/a	n/a	n/a	n/a	812527
148.04	Green	12.37	1.42	n/a	n/a	n/a	n/a	464213
149.03	Green	13	2.65	(4Z)-4-Heptenoic acid	C7H12O2	M+Na-2H	6.54	103029
150.01	Yellow	17.99	4.45	n/a	n/a	n/a	n/a	897264
151.03	Green	55.26	5.31	n/a	n/a	n/a	n/a	71052
151.11	x	0	0	3-Methyl-1-heptanol	C8H18O	M+Na-2H	-1.55	13194
152.01	x	0	0	n/a	n/a	n/a	n/a	424051
154.06	Green	95.38	1.46	n/a	n/a	n/a	n/a	785886
154.9	x	0	0	n/a	n/a	n/a	n/a	18154
154.95	Green	60.28	18.02	n/a	n/a	n/a	n/a	42513
155.11	x	0	0	n/a	n/a	n/a	n/a	55481
155.95	Green	23.48	6.04	n/a	n/a	n/a	n/a	543296
156.9	x	0	0	Phosphenic acid, ion(1-)	O3P-	M-, 2M-H	-5.64	19720
156.94	x	0	0	n/a	n/a	n/a	n/a	13050
157.08	x	0	0	n/a	n/a	n/a	n/a	244263
157.12	x	0	0	1,2,3-Triethoxypropane	C9H20O3	M-H2O-H	-9.69	380174
158.91	x	0	0	n/a	n/a	n/a	n/a	7296
159.07	Green	34.93	3.77	n/a	n/a	n/a	n/a	384797
160.06	Purple	21.67	10.69	n/a	n/a	n/a	n/a	636991
160.84	x	0	0	n/a	n/a	n/a	n/a	2312
160.91	x	0	0	n/a	n/a	n/a	n/a	8202
161.05	Purple	15.67	8.5	n/a	n/a	n/a	n/a	533954
162.02	x	0	0	n/a	n/a	n/a	n/a	66896
162.49	x	0	0	n/a	n/a	n/a	n/a	1995
162.84	x	0	0	n/a	n/a	n/a	n/a	2106
162.96	Purple	13.42	9.89	n/a	n/a	n/a	n/a	17738
163.11	x	0	0	n/a	n/a	n/a	n/a	13897
164.07	Green	81.36	2.92	n/a	n/a	n/a	n/a	5753
165.13	x	0	0	5-Ethyl-2-heptanol	C9H20O	M+Na-2H	2.58	72588
166.05	x	0	0	n/a	n/a	n/a	n/a	375108
167.02	Blue	62.45	2.6	n/a	n/a	n/a	n/a	1420
167.11	x	0	0	2,3-Octanediol	C8H18O2	M+Na-2H	3.53	53267
168.03	Blue	23.21	5.81	n/a	n/a	n/a	n/a	454034
168.83	x	0	0	n/a	n/a	n/a	n/a	11968
169	Green	38.19	2.85	n/a	n/a	n/a	n/a	561255
169.96	x	0	0	n/a	n/a	n/a	n/a	9955

170.01	x	0	0	n/a	n/a	n/a	n/a	148654
170.83	x	0	0	n/a	n/a	n/a	n/a	20709
171.1	x	0	0	7-Methyl-6-oxooctanoic acid	C9H16O3	M-H	-9.83	523380
171.14	Black	30.58	4.41	1,2,7-Trimethoxyheptane	C10H22O3	M-H2O-H, M-H	-9.02	717208
172.1	Purple	14.16	1.13	n/a	n/a	n/a	n/a	1400794
172.96	Purple	44.99	14.36	n/a	n/a	n/a	n/a	17041
174.05	x	0	0	1-Ethyl-6-hydroxy-4-methyltetrahydro-2(1H)-pyrimidinethione	C7H14N2OS	M-H2O-H, M-	-4.18	1098867
174.83	x	0	0	n/a	n/a	n/a	n/a	8542
176.93	x	0	0	n/a	n/a	n/a	n/a	19601
177.09	x	0	0	n/a	n/a	n/a	n/a	201851
179.06	Blue	68.1	17.1	n/a	n/a	n/a	n/a	394675
179.14	x	0	0	Isoamyl Ether	C10H22O	M+Na-2H	-3.33	18943
180.99	x	0	0	2,4-Dihydroxypyrimidine-5,6-dicarboxylic acid	C6H4N2O6	M-H2O-H	-6.76	58311
181.08	Cyan	36.38	0.35	n/a	n/a	n/a	n/a	611078
181.12	x	0	0	n/a	n/a	n/a	n/a	43337
183.01	x	0	0	4-(5-Amino-1,3,4-thiadiazol-2-yl)-1,2,5-oxadiazol-3-amine	C4H4N6OS	M-H, M+K-2H	-2.5	2012438
183.11	Green	132.33	2.42	n/a	n/a	n/a	n/a	1480493
184.5	x	0	0	n/a	n/a	n/a	n/a	16148
184.98	x	0	0	2-Phosphoglyceric acid	C3H7O7P	M-H	-8.48	118588
185.02	x	0	0	Phenylpyruvic acid	C9H8O3	M+Na-2H	1.17	321855
185.15	Cyan	34.82	7.5	1,2,3-Undecanetriol	C11H24O3	M-H2O-H	-9.67	375999
187.1	x	0	0	1-(Carbamoylamino)-3,5-dimethylpyridinium	C8H12N3O+	M-H, M+Na-2H	-5.42	520305
188.06	Purple	83.33	9.87	n/a	n/a	n/a	n/a	1158955
188.94	Green	51.85	10.9	n/a	n/a	n/a	n/a	266509
189.07	x	0	0	n/a	n/a	n/a	n/a	491038
190.05	x	0	0	n/a	n/a	n/a	n/a	126794
191.02	Green	86.82	15.48	n/a	n/a	n/a	n/a	51161
191.11	x	0	0	n/a	n/a	n/a	n/a	110003
192.03	x	0	0	n/a	n/a	n/a	n/a	125772
193.01	x	0	0	n/a	n/a	n/a	n/a	172810
193.16	x	0	0	Undecanol	C11H24O	M+Na-2H	-0.19	50045
194.08	x	0	0	n/a	n/a	n/a	n/a	87070
194.94	Green	20.67	10.07	n/a	n/a	n/a	n/a	99046
195.17	x	0	0	(~2~H_5_)Aniline	C6H[2]5H[1]2N	2M-H	5.75	58284
196.06	x	0	0	n/a	n/a	n/a	n/a	357759
196.98	x	0	0	n/a	n/a	n/a	n/a	23552
197.03	x	0	0	1,4-Naphthalenedicarboxylic acid	C12H8O4	M-H2O-H	9.91	300500
197.12	Orange	50.86	10.56	n/a	n/a	n/a	n/a	170577
198.9	x	0	0	n/a	n/a	n/a	n/a	42204

199.13	Orange	70.79	20.91	(1S)-1-[(2R,3aS,6S,6aR)-6-(Hydroxymethyl)hexahydro-2H-cyclopenta[b]furan-2-yl]-1-propanol	C11H20O3	M-H	-8.77	4082788
200.14	Orange	65.62	22.76	n/a	n/a	n/a	n/a	4513136
201.14	Blue	14.77	6.05	n/a	n/a	n/a	n/a	1019683
201.95	x	0	0	n/a	n/a	n/a	n/a	22586
202.08	Green	9.45	11.26	n/a	n/a	n/a	n/a	389714
202.12	x	0	0	n,n-diethylcinnamamide	C13H17NO	M-H	5.04	10528
203.08	Purple	34.9	19.5	n/a	n/a	n/a	n/a	496173
203.14	x	0	0	n/a	n/a	n/a	n/a	21681
203.93	x	0	0	n/a	n/a	n/a	n/a	5614
204.01	Green	11.44	9.92	n/a	n/a	n/a	n/a	419236
204.36	x	0	0	n/a	n/a	n/a	n/a	110609
204.91	Green	37.81	15.18	n/a	n/a	n/a	n/a	552276
204.99	x	0	0	2-Hydroxy-3-oxobutyl phosphate	C4H9O6P	M+Na-2H	-2.68	8913
205.89	x	0	0	n/a	n/a	n/a	n/a	5661
205.94	x	0	0	n/a	n/a	n/a	n/a	94969
206.05	Purple	4.75	1.49	n/a	n/a	n/a	n/a	392516
206.42	x	0	0	n/a	n/a	n/a	n/a	20133
206.85	x	0	0	n/a	n/a	n/a	n/a	11274
206.96	Green	35.19	17.58	n/a	n/a	n/a	n/a	389714
207.14	x	0	0	n/a	n/a	n/a	n/a	413477
207.59	x	0	0	n/a	n/a	n/a	n/a	4248
208.06	Blue	80.61	15.26	Methyl 3-[(isopropylideneamino)oxy]-1-propanesulfonate	C7H15NO4S	M-H	1.77	110888092
208.13	x	0	0	N-(2-Hydroxyethyl)octanamide	C10H21NO2	M+Na-2H	3	5618582
208.24	x	0	0	n/a	n/a	n/a	n/a	6302041
208.85	x	0	0	n/a	n/a	n/a	n/a	10512
209.07	Blue	73.94	13.77	n/a	n/a	n/a	n/a	9339062
209.42	x	0	0	n/a	n/a	n/a	n/a	302699
209.46	x	0	0	n/a	n/a	n/a	n/a	118152
209.59	x	0	0	n/a	n/a	n/a	n/a	5029
209.95	x	0	0	n/a	n/a	n/a	n/a	240262
210.02	x	0	0	Kynurenic acid	C10H7NO3	M+Na-2H	-5.53	6332
210.06	Purple	73.66	19.87	Melithiazol A	C20H26N2O4S2	M-2H	9.9	11131
210.32	x	0	0	n/a	n/a	n/a	n/a	172284
210.85	x	0	0	n/a	n/a	n/a	n/a	3818
211.13	x	0	0	1,2-Decanediol	C10H22O2	M+Na-2H, M+K-2H	6.35	250593
211.17	Orange	70.17	22.99	2-Hydroxytridecanoic acid	C13H26O3	M-H2O-H	-8.34	259706
211.2	x	0	0	n/a	n/a	n/a	n/a	216389
212.07	Purple	6.65	5.92	n/a	n/a	n/a	n/a	599673
213.03	x	0	0	n/a	n/a	n/a	n/a	391911
213.19	Orange	85.81	17.75	2-Nonanyl butyrate	C13H26O2	M-H	-9.24	3646993

213.31	x	0	0	n/a	n/a	n/a	n/a	62253
213.51	x	0	0	n/a	n/a	n/a	n/a	9407
213.96	x	0	0	n/a	n/a	n/a	n/a	75245
214.19	Orange	57.02	15.13	n/a	n/a	n/a	n/a	7187273
215.08	x	0	0	n/a	n/a	n/a	n/a	1590427
215.13	Orange	77.41	28.82	Dimethyl 4-methyloctanedioate	C11H20O4	M-H	-1.25	4019
215.34	x	0	0	n/a	n/a	n/a	n/a	4033
215.68	x	0	0	n/a	n/a	n/a	n/a	2202
215.84	x	0	0	n/a	n/a	n/a	n/a	17686
216.08	x	0	0	n/a	n/a	n/a	n/a	206758
216.13	Orange	46.71	21.94	n/a	n/a	n/a	n/a	2062909
216.91	Green	38.14	15.18	n/a	n/a	n/a	n/a	167878
217.01	x	0	0	n/a	n/a	n/a	n/a	229922
217.1	x	0	0	n/a	n/a	n/a	n/a	196337
217.83	x	0	0	n/a	n/a	n/a	n/a	7759
218.1	Green	25.78	1.6	n/a	n/a	n/a	n/a	130303
218.9	Green	10.5	2.13	n/a	n/a	n/a	n/a	30307
219.05	x	0	0	2-Methyl 1-phenyl 4-(4-chlorophenyl)-3-(4-morpholinyl)-1H-pyrrole-1,2-dicarboxylate	C23H21ClN2O5	M-2H	-2.08	29814
219.17	x	0	0	n/a	n/a	n/a	n/a	147691
220.05	Green	6.84	5.46	n/a	n/a	n/a	n/a	180863
220.14	x	0	0	n/a	n/a	n/a	n/a	41631
220.55	x	0	0	n/a	n/a	n/a	n/a	2793
220.89	Green	26.6	5.91	n/a	n/a	n/a	n/a	437590
221.08	x	0	0	n/a	n/a	n/a	n/a	21551
222.04	Cyan	7.98	9.37	Methyl 3-(4-acetoxyphenyl)propanoate	C12H14O4	M-H	-5.24	522372
222.11	Green	8.36	0.38	n/a	n/a	n/a	n/a	59374
223.03	x	0	0	Corallorazine C	C12H17NO3	M-H	2.8	1402764
223.08	Cyan	53.91	21.08	n/a	n/a	n/a	n/a	543296
223.12	x	0	0	n/a	n/a	n/a	n/a	3550
223.6	x	0	0	n/a	n/a	n/a	n/a	129670
224.12	Cyan	24.98	17.57	n/a	n/a	n/a	n/a	488667
224.8	x	0	0	n/a	n/a	n/a	n/a	43024
225.01	x	0	0	n/a	n/a	n/a	n/a	10507
225.18	Cyan	87.15	14.73	1-Phenyl-3-formyl-4-hydroxypyrazole	C10H8N2O2	M+K-2H	3.31	103062
225.31	x	0	0	n/a	n/a	n/a	n/a	51714
226.09	x	0	0	n/a	n/a	n/a	n/a	92452
226.19	Cyan	57.95	9.76	n/a	n/a	n/a	n/a	4737085
226.8	x	0	0	n/a	n/a	n/a	n/a	31138
227.03	Cyan	91.29	24.77	n/a	n/a	n/a	n/a	120617
227.2	x	0	0	4-Methyltridecanoic acid	C14H28O2	M-H	-6.96	19827179
227.33	x	0	0	n/a	n/a	n/a	n/a	571206

227.56	x	0	0	Sorazolon B	C14H15N1O2	M-H	6.18	5214
228.17	x	0	0	Methyl 5,5-dimethyl-9-oxodecanoate	C13H24O3	M-H2O-H, M-	-9.25	196445
228.2	Cyan	79.79	21.85	n/a	n/a	n/a	n/a	355641
228.93	Green	46.11	35.1	n/a	n/a	n/a	n/a	17869
228.99	x	0	0	2,3-Dihydroxypropyl 2,6-dioxo-1,2,3,6-tetrahydro-4-pyrimidinecarboxylate	C8H10N2O6	M-H	-9.98	459817
229.2	Cyan	25.83	6.95	n/a	n/a	n/a	n/a	739147
229.6	x	0	0	n/a	n/a	n/a	n/a	10288
229.99	x	0	0	n/a	n/a	n/a	n/a	4050
230.11	Purple	5.08	4.74	n/a	n/a	n/a	n/a	455579
230.98	x	0	0	n/a	n/a	n/a	n/a	597639
231.03	Green	10.41	6.56	2-(1,3-Benzothiazol-2-ylamino)-1H-imidazol-5-ol	C10H8N4OS	M-H	-0.55	346583
231.11	Green	12.07	7.83	n/a	n/a	n/a	n/a	336492
232.11	x	0	0	n/a	n/a	n/a	n/a	116605
232.92	Cyan	20.15	1.91	n/a	n/a	n/a	n/a	213508
233.15	x	0	0	n/a	n/a	n/a	n/a	840509
233.53	Black	29.62	18.69	n/a	n/a	n/a	n/a	3980
234.06	x	0	0	n/a	n/a	n/a	n/a	136728
235.1	Black	9.45	13.26	n/a	n/a	n/a	n/a	550121
235.18	x	0	0	n/a	n/a	n/a	n/a	94393
236.06	Black	14.74	7.62	n/a	n/a	n/a	n/a	21171
236.1	x	0	0	D-4-PHOSPHOERYTHRONIC ACID	C4H9O8P	M+Na-2H	-1.37	5203
237.08	x	0	0	1-Tridecanol	C13H28O	M+Na-2H, M+K-2H	-7.35	772696
237.19	Orange	52.2	8.66	3-Methyl-1-[1-(3-methylbutoxy)propoxy]butane	C13H28O2	M+Na-2H	0.37	41858
237.6	x	0	0	n/a	n/a	n/a	n/a	7812
238.04	x	0	0	n/a	n/a	n/a	n/a	628394
238.19	Cyan	37.33	20.85	n/a	n/a	n/a	n/a	1077424
238.88	x	0	0	n/a	n/a	n/a	n/a	297812
239.2	Orange	99.24	7.25	n/a	n/a	n/a	n/a	9015331
239.61	x	0	0	n/a	n/a	n/a	n/a	11254
240.13	x	0	0	n/a	n/a	n/a	n/a	66804
240.2	Orange	88.29	8.28	n/a	n/a	n/a	n/a	21136084
240.57	x	0	0	n/a	n/a	n/a	n/a	14691
241.07	x	0	0	n/a	n/a	n/a	n/a	681049
241.22	Orange	104.25	6.22	1,2,15-Pentadecanetriol	C15H32O3	M-H2O-H	0.26	80678281
241.41	x	0	0	n/a	n/a	n/a	n/a	4190433
241.95	x	0	0	n/a	n/a	n/a	n/a	1923716
242.22	Orange	97.07	4.87	n/a	n/a	n/a	n/a	304778
242.67	x	0	0	n/a	n/a	n/a	n/a	340948
243.06	x	0	0	n/a	n/a	n/a	n/a	459716
243.22	Orange	74.65	7.34	n/a	n/a	n/a	n/a	54216
243.52	x	0	0	n/a	n/a	n/a	n/a	33005

244.13	Purple	46.95	5.56	n/a	n/a	n/a	n/a	842570
244.91	x	0	0	n/a	n/a	n/a	n/a	124291
245.04	x	0	0	(2E)-1-(2-Naphthyl)-3-(2-thienyl)-2-propen-1-one	C17H12OS	M-H2O-H	-5.24	235624
245.11	Green	92.04	67.12	n/a	n/a	n/a	n/a	334466
246.06	x	0	0	n/a	n/a	n/a	n/a	3182
246.12	Green	61.52	37.54	n/a	n/a	n/a	n/a	102001
247.08	Black	23.81	5.51	n/a	n/a	n/a	n/a	383222
247.17	x	0	0	n/a	n/a	n/a	n/a	130049
248.08	Black	107.86	30.78	n/a	n/a	n/a	n/a	3846914
248.21	x	0	0	n/a	n/a	n/a	n/a	81317
248.58	Black	82.18	36.58	n/a	n/a	n/a	n/a	8136778
248.9	x	0	0	n/a	n/a	n/a	n/a	69015
248.97	x	0	0	n/a	n/a	n/a	n/a	412424
249.15	Blue	19.65	9.43	n/a	n/a	n/a	n/a	5045985
250.04	Blue	6.92	9.11	n/a	n/a	n/a	n/a	387554
250.19	x	0	0	n/a	n/a	n/a	n/a	57509
250.62	x	0	0	n/a	n/a	n/a	n/a	14901
250.89	x	0	0	n/a	n/a	n/a	n/a	77059
251.02	x	0	0	{[(3-Methyl-2,6-dioxo-2,3,6,7-tetrahydro-1H-purin-8-yl)methyl]sulfanyl}acetic acid	C9H10N4O4S	M-H2O-H	1.29	135187
251.2	Cyan	81.83	14.45	(9Z,12E)-9,12-TETRADECADIEN-1-YL ACETATE	C16H28O2	M-H, M+K-2H	-7.83	11501509
251.33	x	0	0	n/a	n/a	n/a	n/a	198537
252.2	Cyan	67.12	9.85	n/a	n/a	n/a	n/a	8244724
252.89	x	0	0	n/a	n/a	n/a	n/a	40699
253.08	x	0	0	n/a	n/a	n/a	n/a	276369
253.22	Yellow	111.59	27.9	Methyl 3-methoxytetradecanoate	C16H32O3	M-H2O-H	-6.25	24539435
253.42	x	0	0	n/a	n/a	n/a	n/a	150426
254.05	x	0	0	n/a	n/a	n/a	n/a	2046
254.22	Yellow	108.92	26.77	n/a	n/a	n/a	n/a	28387024
254.61	x	0	0	n/a	n/a	n/a	n/a	9460
254.84	x	0	0	n/a	n/a	n/a	n/a	4076
254.98	x	0	0	2-O-Sulfo-L-idopyranuronic acid	C6H10O10S	M-H2O-H	6.67	17466
255.23	Black	146.59	11.72	n/a	n/a	n/a	n/a	50021010
255.31	x	0	0	n/a	n/a	n/a	n/a	1082600
255.44	x	0	0	n/a	n/a	n/a	n/a	544665
255.68	x	0	0	n/a	n/a	n/a	n/a	72381
256.14	x	0	0		C30H42O7	M-2H	-2.28	8635
256.24	Black	141.05	13.27	n/a	n/a	n/a	n/a	28017499
257.23	Black	79.12	27.62	n/a	n/a	n/a	n/a	3314480
258.03	x	0	0	n/a	n/a	n/a	n/a	657252
258.23	Black	7.35	9.31	n/a	n/a	n/a	n/a	579569
258.9	x	0	0	n/a	n/a	n/a	n/a	69983

259.19	Green	27.82	6.9	n/a	n/a	n/a	n/a	322360
260.09	Green	38.77	25.36	n/a	n/a	n/a	n/a	150554
260.87	Blue	54.2	24.69	n/a	n/a	n/a	n/a	288992
261.13	Orange	21.16	18.34	10-Undecenyl acrylate	C14H24O2	M-H, M+K-2H	-9.96	746904
262.1	Black	22.45	3.87	n/a	n/a	n/a	n/a	108554
262.47	x	0	0	n/a	n/a	n/a	n/a	5990
262.77	x	0	0	n/a	n/a	n/a	n/a	3342
262.97	x	0	0	2,2'-(1,2,4-Thiadiazole-3,5-diyldisulfanediyl)diacetamide	C6H8N4O2S3	M-H	-0.74	44180
263.06	x	0	0	N-(5-sec-Butyl-4-ethyl-1,3-thiazol-2-yl)acetamide	C11H18N2OS	M+K-2H	-4.84	251731
263.13	Black	75.23	25.65	n/a	n/a	n/a	n/a	612880
263.2	x	0	0	4-Acetoxytridecane	C15H30O2	M+Na-2H	-1.25	86694
264.14	Black	14.59	16.19	n/a	n/a	n/a	n/a	7346
264.77	x	0	0	n/a	n/a	n/a	n/a	2318
265.07	x	0	0	n/a	n/a	n/a	n/a	1031074
265.15	Black	126.55	27.82	1-S-Heptyl-1-thiopentitol	C12H26O4S	M-H	-4.22	20522550
265.22	x	0	0	16-Oxoheptadecanoic acid	C17H32O3	M-H2O-H	-6.33	8747081
265.6	x	0	0	n/a	n/a	n/a	n/a	22672
266.15	Black	114.74	18.55	n/a	n/a	n/a	n/a	11941697
267.1	x	0	0	4,4'-Dimethoxychalcone	C17H16O3	M-H	7.49	9240
267.23	Yellow	141.69	11.34	(12S)-12-Hydroxyheptadecanoic acid	C17H34O3	M-H2O-H	-6.78	14475554
267.37	x	0	0	n/a	n/a	n/a	n/a	366528
268.1	x	0	0	n/a	n/a	n/a	n/a	19387
268.24	Yellow	135.16	12.02	n/a	n/a	n/a	n/a	28312240
268.98	x	0	0	Xylitol 5-phosphate	C5H13O8P	M+K-2H	-8.48	11000
269.12	x	0	0	3,3,6,6-Tetramethyl-3a-p-tolyl-tetrahydro-furo[3,2-b]furan-2,5-dione	C17H20O4	M-H2O-H	8.47	298796
269.25	Orange	85.31	11.69	Margaric acid	C17H34O2	M-H	-8.05	14817979
269.32	x	0	0	n/a	n/a	n/a	n/a	223636
270.25	Orange	73.76	10.18	n/a	n/a	n/a	n/a	651135
270.94	x	0	0	n/a	n/a	n/a	n/a	62829
271.23	Black	86.57	33.93	n/a	n/a	n/a	n/a	15997
271.97	x	0	0	n/a	n/a	n/a	n/a	56411
272.09	Green	109	8.2	n/a	n/a	n/a	n/a	1714221
273.21	Yellow	52.13	23.96	n/a	n/a	n/a	n/a	1493943
273.61	x	0	0	n/a	n/a	n/a	n/a	7555
273.91	x	0	0	n/a	n/a	n/a	n/a	71787
274.21	Green	4.14	4.42	n/a	n/a	n/a	n/a	631251
274.6	x	0	0	n/a	n/a	n/a	n/a	39412
274.98	x	0	0	pyromellitic acid	C10H6O8	M+Na-2H	1.42	8825
275.11	Green	20.89	14.79	n/a	n/a	n/a	n/a	154524
275.18	x	0	0	9-Dodecyn-1-yl methoxyacetate	C15H26O3	M-H2O-H, M+Na-2H	-5.03	290518
276.06	Blue	26.17	32.23	n/a	n/a	n/a	n/a	5268

276.62	x	0	0	n/a	n/a	n/a	n/a	186921
276.85	Purple	41.22	7.36	n/a	n/a	n/a	n/a	85984
276.99	x	0	0	1,2,3,4,7(5H)-Phenazinepentone	C12H4N2O5	M+Na-2H	-1.94	85766
277.14	x	0	0	Methyl 8-[5-(2-methoxy-2-oxoethyl)-2-furyl]octanoate	C16H24O5	M-H2O-H	-4.59	34735
277.21	x	0	0	2-Acetoxytetradecane	C16H32O2	M+Na-2H	-9.7	939246
278.86	x	0	0	n/a	n/a	n/a	n/a	131398
279.07	x	0	0	2-(5,7-Dimethyl-[1,2,4]triazolo[4,3-a]pyrimidin-3-ylsulfanyl)-1-phenyl-ethanone	C15H14N4OS	M-H2O-H	5.54	873079
279.16	Black	83	58.28	10-Undecen-1-yl methoxyacetate	C14H26O3	M-H2O-H, M+K-2H	-7.83	5939633
279.23	x	0	0	Cetyl glycol	C16H34O2	M+Na-2H	0.27	4266169
280.17	Black	63.55	46.38	n/a	n/a	n/a	n/a	8856
280.98	x	0	0	2-Deoxy-D-glucose 6-phosphate	C6H13O8P	M+K-2H	-9.64	1220229
281.12	x	0	0	4-Pentyloxyxanthen-9-one	C18H18O3	M-H	1.93	6147
281.25	Purple	54.53	32.23	15-Hydroxyoctadecanoic acid	C18H36O3	M-H2O-H	-8.67	7601541
281.39	x	0	0	n/a	n/a	n/a	n/a	140413
282.25	Purple	53.06	32.17	n/a	n/a	n/a	n/a	20524566
282.63	x	0	0	n/a	n/a	n/a	n/a	120925
283.13	x	0	0	4-(6-Isopropyl-5-methyl-1-naphthyl)-4-oxobutanoic acid	C18H20O3	M-H	-0.73	874679
283.26	Black	141.96	3.13	Ethyl palmitate	C18H36O2	M-H	-7.16	27476127
283.34	x	0	0	n/a	n/a	n/a	n/a	447176
283.4	x	0	0	n/a	n/a	n/a	n/a	755576
283.73	x	0	0	n/a	n/a	n/a	n/a	28311
284.08	x	0	0	n/a	n/a	n/a	n/a	465940
284.27	Black	132.94	4.39	n/a	n/a	n/a	n/a	16225591
284.81	x	0	0	n/a	n/a	n/a	n/a	19211
285.17	x	0	0	1-O-(Hydroxy{[(6Z,10E,14E)-3,7,11,15,19-pentamethyl-6,10,14,18-icosatetraen-1-yl]oxy}phosphoryl)-beta-D-xylopyranose	C30H53O8P	M-2H	-1.16	83488
285.21	Purple	34.33	9.17	n/a	n/a	n/a	n/a	969741
286.18	x	0	0	2-(Heptylaminomethylene)-5,5-dimethyl-1,3-cyclohexanedione	C16H27NO2	M+Na-2H	1.06	6698
286.21	Purple	7.69	2.33	n/a	n/a	n/a	n/a	467809
287.04	x	0	0	1,1'-MONOGLYCERIDE CITRATE	C9H14O9	M+Na-2H	-2.18	63165
287.22	Purple	124.62	31.27	15,16-Dihydroxyhexadecanoic acid	C16H32O4	M-H	-9.72	1971103
287.92	x	0	0	n/a	n/a	n/a	n/a	41832
288.22	Purple	101.12	32.24	n/a	n/a	n/a	n/a	2782812
288.35	x	0	0	n/a	n/a	n/a	n/a	3874
288.96	x	0	0	n/a	n/a	n/a	n/a	175658
289.23	Purple	47.97	16.21	n/a	n/a	n/a	n/a	676439
290.07	Green	7.63	3.39	n/a	n/a	n/a	n/a	55092
290.91	x	0	0	n/a	n/a	n/a	n/a	127971
291.02	x	0	0	n/a	n/a	n/a	n/a	3336

291.16	Blue	34.06	7.59	(6E)-6-Hexadecenoic acid	C16H30O2	M+K-2H	3.54	963239
292.02	x	0	0	n/a	n/a	n/a	n/a	1503
292.98	x	0	0	2-Deoxy-1-O-[hydroxy(phosphonooxy)phosphoryl]-D-erythro-pentofuranose	C5H12O10P2	M-H	-7.77	59862
293.04	x	0	0	Ethyl 2-[(2-amino-2-oxoethanethioyl)amino]-4,5,6,7-tetrahydro-1-benzothiophene-3-carboxylate	C13H16N2O3S2	M-H2O-H	-2.95	2436624
293.18	Black	106.75	10.29	Myristyl sulfate	C14H30O4S	M-H, M+Na-2H	-6.12	14024222
294.18	Black	78.64	9.99	n/a	n/a	n/a	n/a	95007
294.84	x	0	0	n/a	n/a	n/a	n/a	83706
295.18	x	0	0	4-Hydroxy-5-methylhexanal, diphenylhydrazone	C19H24N2O	M-H	5.87	13292
295.26	Yellow	120.89	19.1	Methyl 9-nonyloxynonanoate	C19H38O3	M-H2O-H	-8.66	1226038
295.41	x	0	0	n/a	n/a	n/a	n/a	15828
296.27	Yellow	107.51	18.41	n/a	n/a	n/a	n/a	11351687
296.61	x	0	0	n/a	n/a	n/a	n/a	12203
297.15	Black	110	39.87	4-[(6E)-3-Hydroxy-7-phenyl-6-hepten-1-yl]-1,2-benzenediol	C19H22O3	M-H	6.6	34539033
297.38	x	0	0	n/a	n/a	n/a	n/a	260134
297.52	x	0	0	n/a	n/a	n/a	n/a	16459
298.16	Black	85.64	40.22	n/a	n/a	n/a	n/a	17528
298.38	x	0	0	n/a	n/a	n/a	n/a	5497
298.92	x	0	0	n/a	n/a	n/a	n/a	94020
299.04	x	0	0	N-{3-[(2-Phenylethyl)sulfanyl]-1H-1,2,4-triazol-5-yl}acetamide	C12H14N4OS	M+K-2H	-0.17	462113
299.26	Black	88.16	44.27	n/a	n/a	n/a	n/a	3155239
299.87	x	0	0	n/a	n/a	n/a	n/a	9786
300.02	x	0	0	n/a	n/a	n/a	n/a	3625
300.15	x	0	0	n/a	n/a	n/a	n/a	68708
300.26	Black	56	18.7	n/a	n/a	n/a	n/a	841855
300.78	x	0	0	n/a	n/a	n/a	n/a	4355
301.03	x	0	0	n/a	n/a	n/a	n/a	290205
301.22	Cyan	48.12	32.52	Octadecadienoic acid	C18H32O2	M+Na-2H	0.34	1068217
301.93	x	0	0	n/a	n/a	n/a	n/a	111883
302.17	x	0	0	S-[2-(Diethylamino)ethyl] O-(3-methylcyclohexyl) ethylphosphonothioate	C15H32NO2PS	M-H2O-H	-5.38	719801
302.22	Cyan	27.52	8.11	n/a	n/a	n/a	n/a	1221546
302.76	x	0	0	n/a	n/a	n/a	n/a	3041
303.11	x	0	0	1,4,5-Tri-O-acetyl-2,6-anhydro-3-O-methyl-L-mannitol	C13H20O8	M-H	4.23	35130
303.23	Cyan	46.32	34.44	n/a	n/a	n/a	n/a	3212489
303.62	x	0	0	n/a	n/a	n/a	n/a	6591
304.19	x	0	0	Heptyl N-(4-methylbenzoyl)alaninate	C18H27NO3	M-H	1.46	50846
304.23	Cyan	22.17	15.62	N-Heptyl-N-octylmethanesulfonamide	C16H35NO2S	M-H	0.78	13964
305.11	x	0	0	n/a	n/a	n/a	n/a	80683

306.08	Green	142.45	8.93	Ethyl 4-[(4-hydroxybenzoyl)amino]benzoate	C16H15NO4	M+Na-2H	-0.34	2739159
306.14	x	0	0	n/a	n/a	n/a	n/a	174357
306.69	x	0	0	n/a	n/a	n/a	n/a	50506
306.87	x	0	0	n/a	n/a	n/a	n/a	23875
307.08	Green	112	6.13	n/a	n/a	n/a	n/a	1491466
307.19	x	0	0	Soraphen O	C18H28O4	M-H	1.83	3068966
307.26	x	0	0	1,1-Dimethoxyhexadecane	C18H38O2	M+Na-2H	-4.32	53389
308.07	Green	86.49	5.55	n/a	n/a	n/a	n/a	865451
309.1	x	0	0	Pyrronazol C	C15H19Cl1N2O3	M-H	2.14	671420
309.17	Black	91.16	12.82	n/a	n/a	n/a	n/a	4635667
309.62	x	0	0	n/a	n/a	n/a	n/a	7963
310.05	x	0	0	n/a	n/a	n/a	n/a	1201402
310.17	Black	42.79	9.25	n/a	n/a	n/a	n/a	2928880
310.88	x	0	0	n/a	n/a	n/a	n/a	156294
311.17	Black	128.77	23.34	(1S,3S,3aR,7aS)-3-(3-Hydroxy-4-methoxybenzyl)-7-methylene-1-vinyloctahydro-4H-inden-4-one	C20H24O3	M-H	7.47	88684637
311.32	x	0	0	n/a	n/a	n/a	n/a	3469740
311.66	x	0	0	n/a	n/a	n/a	n/a	130304
312.17	Black	116.06	31.52	n/a	n/a	n/a	n/a	27603464
312.97	x	0	0	6-O-Phosphonohexonic acid	C6H13O10P	M+K-2H	3.64	3546
313.24	Purple	38.96	18.83	2,2-Dimethylpropyl undecyl oxalate	C18H34O4	M-H	-9.57	819871
314.11	x	0	0	n/a	n/a	n/a	n/a	146173
314.24	Purple	13.21	6.35	n/a	n/a	n/a	n/a	524253
315.18	Blue	29.12	17.41	n/a	n/a	n/a	n/a	622887
316.18	Blue	6.83	5.78	n/a	n/a	n/a	n/a	613670
317.12	x	0	0	4-(Benzyloxy)phenyl phenylacetate	C21H18O3	M-H	-0.95	74034
317.22	Yellow	8.78	6.29	(5S,8Z,11Z,13E,15R)-5,15-Dihydroxy-6,8,11,13-icosatetraenoic acid	C20H32O4	M-H2O-H	-9.51	454149
317.83	x	0	0	n/a	n/a	n/a	n/a	3125
318.16	Black	12.75	9.73	Haliamide	C19H25N1O1	M+Cl	3.62	279343
318.98	x	0	0	4-(2-Iodoethyl)-1-naphthol	C12H11IO	M-H, M+Na-2H	-6.69	38865
319.22	Blue	20.4	2.1	4-(Diisopropylamino)-2,2-diphenylbutanamide	C22H30N2O	M-H2O-H	1.74	786810
320.08	Blue	38.5	4.86	n/a	n/a	n/a	n/a	847219
320.2	x	0	0	2',2'-dihydroxy-2-oxospirilloxanthin	C42H58O5	M-2H	-6.35	80447
321.11	x	0	0	2,3,5,6-Tetrahydroxy-4-methoxy-N'-phenylhexanehydrazide	C13H20N2O6	M+Na-2H	3.37	201632
321.21	Black	80.14	10.14	8-Methylhexadecanedioic acid	C17H32O4	M+Na-2H	-8.43	2994708
321.87	x	0	0	n/a	n/a	n/a	n/a	110155
322.05	Green	76.32	14.46	n/a	n/a	n/a	n/a	4149
323.03	Green	85.6	9.53	n/a	n/a	n/a	n/a	13084
323.17	x	0	0	2-(4-Morpholin-4-yl-4-oxo-butyl)-isoindole-1,3-dione	C16H18N2O4	M-H, M+Na-2H	-3.71	3481732
323.26	x	0	0	n/a	n/a	n/a	n/a	322221
324.16	x	0	0	n/a	n/a	n/a	n/a	139299

325.18	Black	108.88	21.22	n/a	n/a	n/a	n/a	87298227
325.27	x	0	0	N,N-Dimethyl-N'-(1,3,4a-trimethyl-2,3,4,4a,9,9a-hexahydro-1H-xanthen-2-ylmethyl)-propane-1,3-diamine	C22H36N2O	M-H2O-H	2.89	2034954
325.41	x	0	0	n/a	n/a	n/a	n/a	849630
325.69	x	0	0	n/a	n/a	n/a	n/a	80127
326.19	Black	104.14	24.64	n/a	n/a	n/a	n/a	91101
326.83	x	0	0	n/a	n/a	n/a	n/a	64777
327.18	Black	90.52	30.2	n/a	n/a	n/a	n/a	32664173
327.61	x	0	0	n/a	n/a	n/a	n/a	5598
328.01	Blue	66.63	19.72	2-Benzoyl-5H-[1,3,4]thiadiazolo[3,2-a]quinazolin-5-one	C16H9N3O2S	M+Na-2H	-9.08	2037180
328.05	x	0	0	n/a	n/a	n/a	n/a	476061
328.98	x	0	0	5-Diphosphomevalonic acid	C6H14O10P2	M+Na-2H, M+K-2H	0.49	93029
329.02	Blue	13.84	6.69	Inosinic acid	C10H13N4O8P	M-H2O-H	-1.08	52747
330.01	Blue	19.91	10.28	n/a	n/a	n/a	n/a	634839
330.98	x	0	0	Ribulose 1,5-diphosphate	C5H12O11P2	M-H, M+Na-2H	-7.3	1310864
331.19	x	0	0	2-(2-Methoxyethyl)hexyl propyl phthalate	C20H30O5	M-H2O-H	-3.66	18090
331.25	Yellow	21.53	20.73	n/a	n/a	n/a	n/a	681816
332.17	Black	60.45	31.59	n/a	n/a	n/a	n/a	726144
332.94	x	0	0	n/a	n/a	n/a	n/a	55894
333.13	x	0	0	Ethyl (2E)-4-[2-(diphenylacetyl)hydrazino]-4-oxo-2-butenoate	C20H20N2O4	M-H2O-H	3.34	235060
333.18	Black	16.18	4.73	n/a	n/a	n/a	n/a	460351
334.72	x	0	0	n/a	n/a	n/a	n/a	84950
334.9	x	0	0	n/a	n/a	n/a	n/a	319988
335.15	x	0	0	n/a	n/a	n/a	n/a	22632
335.16	x	0	0	Ethyl (2E)-4-[(N-{[(2-methyl-2-propanyl)oxy]carbonyl}alanyl)amino]-2-pentenoate	C15H26N2O5	M+Na-2H	-6.6	230438
335.21	Yellow	23.67	6.83	n/a	n/a	n/a	n/a	579210
335.64	x	0	0	n/a	n/a	n/a	n/a	22827
337.05	x	0	0	n/a	n/a	n/a	n/a	860523
337.2	Black	85.46	2.99	N'-(5-Nitro-2-oxo-2H-indol-3-yl)-3-phenylpropanehydrazide	C17H14N4O4	M-H2O-H, M-H	5.4	4150380
337.68	x	0	0	n/a	n/a	n/a	n/a	27423
338.2	Black	32.6	6.24	n/a	n/a	n/a	n/a	1997998
339.2	Black	127.93	22.07	4-Ethoxyphenyl 4-heptylbenzoate	C22H28O3	M-H, M+K-2H	4.42	63463626
339.35	x	0	0	N,N-Diheptyloctanamide	C22H45NO	M-	9.8	1528446
339.44	x	0	0	n/a	n/a	n/a	n/a	307020
340.2	Black	116.08	23.37	n/a	n/a	n/a	n/a	777602
341.11	Blue	151.72	7.23	beta-Maltose	C12H22O11	M-H	-6.39	1000078
341.27	x	0	0	n/a	n/a	n/a	n/a	710100
342.11	Blue	107.9	14.66	N-[(Benzyloxy)carbonyl]alanyl-N-ethylalaninamide	C16H23N3O4	M+Na-2H	-6.9	29008

342.65	x	0	0	n/a	n/a	n/a	n/a	49740
343.13	x	0	0	N-[2-(2-Amino-4,5-dihydro-1H-imidazol-5-yl)ethyl]-9H-beta-carboline-3-carboxamide	C17H18N6O	M+Na-2H	-0.6	75103
343.21	Black	17.9	14.95	n/a	n/a	n/a	n/a	3005924
344.03	Green	67.01	38.07	n/a	n/a	n/a	n/a	205937
344.68	x	0	0	n/a	n/a	n/a	n/a	25210
345.01	Green	23.12	7.73	n/a	n/a	n/a	n/a	376389
345.11	x	0	0	6-Isopropenyl-3-methyl-3-cyclohexen-1-yl 3,5-dinitrobenzoate	C17H18N2O6	M-H, M+Na-2H	-4.7	74411
345.67	x	0	0	n/a	n/a	n/a	n/a	170748
346.05	Green	106.58	9.97	n/a	n/a	n/a	n/a	840782
347.06	x	0	0	Pyrronazol C2	C15H19Cl1N2O3	M+K-2H	0.41	410597
347.13	x	0	0	Ethyl N-(4-{[(benzyloxy)carbonyl]amino}-2-hydrazino-4-oxobutanoyl)glycinate	C16H22N4O6	M-H2O-H	-6.66	125786
347.23	Black	54.28	9.56	n/a	n/a	n/a	n/a	890825
348.23	Black	44	43.41	n/a	n/a	n/a	n/a	72303
349.18	x	0	0	n/a	n/a	n/a	n/a	134808
349.53	x	0	0	n/a	n/a	n/a	n/a	3773
350	Blue	61.41	12.61	n/a	n/a	n/a	n/a	515189
351.15	x	0	0	1-(2,3-Diacetoxypropoxy)-2-(2-acetoxypropyl)benzene	C18H24O7	M-H	0.86	137221
351.22	Black	87.35	20.29	n/a	n/a	n/a	n/a	8096311
352.22	Black	54.83	14.76	n/a	n/a	n/a	n/a	1453584
352.86	x	0	0	n/a	n/a	n/a	n/a	76774
353.05	x	0	0	2-(2-Isopropylsulfanyl-benzothiazol-6-yl)-isoindole-1,3-dione	C18H14N2O2S2	M-H	8	27566
353.21	Black	84.19	4.39	Bengamide F	C18H32N2O6	M-H2O-H	2.73	14879
354.21	Black	25.99	6.86	n/a	n/a	n/a	n/a	1701793
355.05	x	0	0	2-Methyl-4,6,9-trioxo-6,9-dihydro-4H-benzo[g]chromene-5,8-diyl diacetate	C18H12O8	M-H	0.79	22286
355.18	Blue	2.93	1.88	n/a	n/a	n/a	n/a	3316218
355.92	x	0	0	n/a	n/a	n/a	n/a	103368
356.28	Yellow	32.25	3.71	n/a	n/a	n/a	n/a	661380
356.66	x	0	0	n/a	n/a	n/a	n/a	71203
357.23	Blue	9.49	5.99	n/a	n/a	n/a	n/a	884751
359	Blue	24.26	7.13	(2-Oxido-1,2,5-oxadiazole-3,4-diyl)bis[(4-methyl-5-oxido-1,2,5-oxadiazol-3-yl)methanone]	C10H6N6O8	M+Na-2H	-1.86	31430
359.43	x	0	0	n/a	n/a	n/a	n/a	3075
360.1	Green	10.17	2.6	n/a	n/a	n/a	n/a	26750
360.28	x	0	0	n/a	n/a	n/a	n/a	130377
360.68	x	0	0	n/a	n/a	n/a	n/a	19242
360.83	x	0	0	n/a	n/a	n/a	n/a	43477
361.15	Blue	11.45	3.46	n/a	n/a	n/a	n/a	3188759
361.76	x	0	0	n/a	n/a	n/a	n/a	6903
362.25	x	0	0	n/a	n/a	n/a	n/a	10599

363.09	Blue	61.96	5.5	n/a	n/a	n/a	n/a	875284
363.17	x	0	0	(2E,2'E)-2,2'-[(1E,2E)-1,2-Ethanediylidene]bis[N'-(4-methoxyphenyl)hydrazinecarboximidamide]	C18H22N8O2	M-H2O-H	-0.44	176639
363.67	x	0	0	n/a	n/a	n/a	n/a	71795
364.05	Green	7.98	2.21	n/a	n/a	n/a	n/a	437590
365.06	Green	47.21	45.16	n/a	n/a	n/a	n/a	16731
365.22	x	0	0	2,3-Bis(4-morpholinylmethyl)-4a,5,6,7,8,8a-hexahydroquinoxaline 1,4-dioxide	C18H30N4O4	M-H	-2.62	1479158
365.97	Black	34.67	15.54	n/a	n/a	n/a	n/a	924403
366.69	x	0	0	n/a	n/a	n/a	n/a	22070
367.22	Black	28.17	14.29	n/a	n/a	n/a	n/a	4068607
367.69	x	0	0	n/a	n/a	n/a	n/a	116721
368.22	Black	7.29	4.85	n/a	n/a	n/a	n/a	5714258
368.85	x	0	0	n/a	n/a	n/a	n/a	56571
369.14	x	0	0	3-(2,2-Dimethyltetrahydrofuro[3,4-d][1,3]dioxol-4-yl)-1-phenyl-1H-pyrazolo[3,4-b]quinoxaline	C22H20N4O3	M-H2O-H	3.2	474787
369.3	Black	69.98	6.64	Methyl 9,12,13-trimethoxyoctadecanoate	C22H44O5	M-H2O-H	-7.98	4201
369.67	x	0	0	n/a	n/a	n/a	n/a	79848
369.82	x	0	0	n/a	n/a	n/a	n/a	57809
370.07	Purple	0	0	n/a	n/a	n/a	n/a	106150
371.17	x	0	0	3,3,12,12-Tetramethyl-1,5,10,14-tetraoxacyclooctadecane-6,9,15,18-tetrone	C18H28O8	M-H	-2.72	16803
371.24	Black	15.77	13.57	n/a	n/a	n/a	n/a	518798
371.54	x	0	0	n/a	n/a	n/a	n/a	13318
372.25	Black	12.57	5.28	n/a	n/a	n/a	n/a	956536
373.16	x	0	0	n/a	n/a	n/a	n/a	483452
374.15	x	0	0	Gaudichaudysolin	C37H50O16	M-2H	0.01	11103
374.76	x	0	0	n/a	n/a	n/a	n/a	61604
376.1	Blue	9.67	9.87	n/a	n/a	n/a	n/a	85268
376.23	x	0	0	n/a	n/a	n/a	n/a	1043868
376.77	x	0	0	n/a	n/a	n/a	n/a	98119
377.09	Blue	142.62	11.56	Carbenicillin	C17H18N2O6S	M-H	0.71	1061141
377.19	x	0	0	1-[(2-Methyl-2-propanyl)amino]-3-{4-[(1E)-N-phenoxyethanimidoyl]phenoxy}-2-propanol	C21H28N2O3	M+Na-2H	4.17	37605
378.09	Blue	87.93	7.48	n/a	n/a	n/a	n/a	64946
378.17	x	0	0	Phenoxal	C23H25NO4	M-H	0.16	584596
379.08	Blue	122.24	14.29	tetracenomycin F1 methyl ester	C21H16O7	M-H	-0.39	379185
379.21	x	0	0	S-[8-(Dibutoxyphosphoryl)octyl] ethanethioate	C18H37O4PS	M-H	-1.64	1180761
380.09	Blue	42.1	27.31	n/a	n/a	n/a	n/a	546888
381.07	x	0	0	triciribine phosphate	C13H17N6O7P	M-H2O-H	2.6	8814
381.23	Black	55.92	4.55	n/a	n/a	n/a	n/a	4095967
381.36	x	0	0	n/a	n/a	n/a	n/a	193630
381.95	Purple	39.69	6.05	n/a	n/a	n/a	n/a	434711

383.06	x	0	0	Pyrronazol B	C17H17Cl1N2O4	M+Cl	1.95	361981
383.31	Black	55.7	4.4	n/a	n/a	n/a	n/a	1055635
383.68	x	0	0	n/a	n/a	n/a	n/a	56585
384.31	Black	14.94	10.05	n/a	n/a	n/a	n/a	1672769
385.19	Blue	2.33	2.08	n/a	n/a	n/a	n/a	1664904
385.97	Blue	7	6.08	n/a	n/a	n/a	n/a	82288
386.84	x	0	0	n/a	n/a	n/a	n/a	107251
387.11	Green	20	34.64	n/a	n/a	n/a	n/a	437590
387.74	x	0	0	n/a	n/a	n/a	n/a	30656
388.14	Yellow	3.32	3.64	n/a	n/a	n/a	n/a	1511445
388.28	x	0	0	n/a	n/a	n/a	n/a	633601
389.18	Yellow	17.2	6.59	n/a	n/a	n/a	n/a	51609
389.97	x	0	0	n/a	n/a	n/a	n/a	351339
390.8	x	0	0	n/a	n/a	n/a	n/a	7063
391.25	Black	7.25	1.95	n/a	n/a	n/a	n/a	613311
391.81	x	0	0	n/a	n/a	n/a	n/a	3277
392.25	Black	13.32	21.92	n/a	n/a	n/a	n/a	2134394
393.07	x	0	0	5-O-methylcelebixanthone	C20H20O6	M+K-2H	-5.48	75939
393.16	x	0	0	N,N'-Bis(4-ethylphenyl)terephthalamide	C24H24N2O2	M+Na-2H	0.95	13969
393.54	Green	72.99	6.77	n/a	n/a	n/a	n/a	137977
393.67	x	0	0	n/a	n/a	n/a	n/a	101228
394.04	Green	43.74	7.2	n/a	n/a	n/a	n/a	428594
394.88	x	0	0	n/a	n/a	n/a	n/a	5273
395.08	x	0	0	n/a	n/a	n/a	n/a	46751
395.18	x	0	0	(4Z,8Z)-4,8,14a-Trimethyl-12-methylene-11-oxo-1a,2,3,6,7,9a,11,12,12a,13,14,14a-dodecahydrooxireno[5,6]cyclotetradeca[1,2-b]furan-14-yl acetate	C22H30O5	M+Na-2H	0.66	47044
395.22	Cyan	47.37	13.59	n/a	n/a	n/a	n/a	4341763
396.14	x	0	0	11-Acetoxy-O~3~-acetylcephalotaxine	C22H25NO7	M-H2O-H	-3.39	158449
396.78	x	0	0	n/a	n/a	n/a	n/a	123411
397.19	x	0	0	1-Benzyl-6-hydroxy-7-methoxy-N-(1-phenylethyl)-3,4-dihydro-2(1H)-isoquinolinecarboxamide	C26H28N2O3	M-H2O-H	3.38	34980
397.33	Black	51.9	39.92	6,6-Bis(hexylsulfanyl)-1,2,3,4,5-hexanepentol	C18H38O5S2	M-H2O-H, M-H	3.28	878227
398.23	x	0	0	Aurachin D	C35H33NO	M+Cl	3.26	884751
399.08	Blue	45.94	4.26	n/a	n/a	n/a	n/a	653132
399.17	x	0	0	N'-[(E)-(3,4-Dimethoxyphenyl)methylene]-2,2-diphenylcyclopropanecarbohydrazide	C25H24N2O3	M-H	-0.47	46867
399.21	x	0	0	n/a	n/a	n/a	n/a	59866
400.28	x	0	0		C25H39NO3	M-H	-9.18	62074
401.13	Blue	18.88	15.61	2-Methyl-2-propanyl (3-{[1-(1-benzothiophen-2-yl)cyclohexyl]amino}-3-oxopropyl)carbamate	C22H30N2O3S	M-H	4.76	66894
401.55	x	0	0	n/a	n/a	n/a	n/a	48548

402.06	Blue	2.8	2.46	n/a	n/a	n/a	n/a	490464
402.83	x	0	0	n/a	n/a	n/a	n/a	196077
403.01	Green	71.1	11.2	n/a	n/a	n/a	n/a	556227
403.19	x	0	0	1-Naphthyl octyl phthalate	C26H28O4	M-H	5.75	288712
404.09	x	0	0	N-Acetyl-6-O-L-fucosyl-D-glucosamine	C14H25NO10	M+K-2H	-6.98	30657
404.11	Blue	102.97	15.45	n/a	n/a	n/a	n/a	326655
404.81	x	0	0	n/a	n/a	n/a	n/a	16345
405.29	Yellow	43.27	9.02	n/a	n/a	n/a	n/a	1259213
405.96	Green	4.33	2.02	n/a	n/a	n/a	n/a	444427
406.21	x	0	0	n/a	n/a	n/a	n/a	46229
406.92	x	0	0	n/a	n/a	n/a	n/a	253146
407.24	Black	20.8	18.56	n/a	n/a	n/a	n/a	2958711
407.31	x	0	0	n/a	n/a	n/a	n/a	304250
407.95	Blue	10.01	9.54	n/a	n/a	n/a	n/a	494060
408.19	x	0	0	n/a	n/a	n/a	n/a	39301
409.26	Black	36.73	24.83	n/a	n/a	n/a	n/a	801436
409.4	x	0	0	(3E)-3-(Dimethylhydrazono)cholestane	C29H52N2	M-H2O-H	4.37	31033
411.08	x	0	0	2'-Hydroxy-3,4,4',5,6'-pentamethoxychalcone	C20H22O7	M+K-2H	-2.21	14577
411.24	Black	24.98	34.71	PG(18:0/22:5(4Z,7Z,10Z,13Z,16Z))	C46H81O10P	M-2H	-2.06	107823
411.89	x	0	0	n/a	n/a	n/a	n/a	48928
412.17	Cyan	41.33	19.4	n/a	n/a	n/a	n/a	1165359
412.77	x	0	0	n/a	n/a	n/a	n/a	17513
412.99	x	0	0	n/a	n/a	n/a	n/a	69046
413.18	Cyan	7.33	6.43	n/a	n/a	n/a	n/a	40086
414.3	x	0	0	Myxalamid A	C26H41NO3	M-H	5.47	475362
414.54	x	0	0	n/a	n/a	n/a	n/a	19806
415.14	x	0	0	(2E,5R)-5-Hydroxy-5-[(2R,3S)-4-hydroxy-7-methoxy-2,3,8-trimethyl-6,9-dioxo-2,3,6,9-tetrahydronaphtho[1,2-b]furan-3-yl]-2-methyl-2-pentenoic acid	C22H24O8	M-H	-1.38	34777
415.22	x	0	0	n/a	n/a	n/a	n/a	847980
415.29	Cyan	20.67	1.53	n/a	n/a	n/a	n/a	433577
415.83	x	0	0	n/a	n/a	n/a	n/a	160387
416.14	x	0	0	Myxocoumarin A	C20H29NO6	M+K-2H	9.93	306838
416.28	Cyan	2	3.46	n/a	n/a	n/a	n/a	121934
417.21	Black	83.04	6.63	15-(1-Anthryl)-2,5,8,11-tetraoxapentadecane	C25H32O4	M+Na-2H	6.98	1145522
418.21	Black	36.81	4.88	n/a	n/a	n/a	n/a	334968
418.97	x	0	0	n/a	n/a	n/a	n/a	52878
419.16	x	0	0	n/a	n/a	n/a	n/a	810183
419.31	Yellow	65.96	15.25	Hexadecyl hexyl oxalate	C24H46O4	M+Na-2H	-4.07	1014870
420.22	x	0	0	n/a	n/a	n/a	n/a	147170
421.23	Black	63.15	7.9	n/a	n/a	n/a	n/a	7182982
421.79	x	0	0	n/a	n/a	n/a	n/a	10430

422.24	Black	9.57	15.98	n/a	n/a	n/a	n/a	1528617
422.81	x	0	0	n/a	n/a	n/a	n/a	64216
423.18	x	0	0	n/a	n/a	n/a	n/a	27333
423.22	Cyan	38.54	3.94	n/a	n/a	n/a	n/a	138517
423.41	x	0	0	n/a	n/a	n/a	n/a	36919
424.24	Cyan	25.1	21.81	n/a	n/a	n/a	n/a	937258
424.73	x	0	0	n/a	n/a	n/a	n/a	64863
425.2	x	0	0	myristicyclin A	C25H30O6	M-H	-1.23	22439
425.36	x	0	0	N-[2-(1H-Indol-3-yl)ethyl]octadecanamide	C28H46N2O	M-H	5.86	624617
426.02	Green	76.34	9.09	n/a	n/a	n/a	n/a	507361
426.12	x	0	0	N-{4-[2-(2-Amino-4-oxo-4,7-dihydro-1H-pyrrolo[2,3-d]pyrimidin-5-yl)ethyl]benzoyl}-D-glutamic acid	C20H21N5O6	M-H	-3.69	437617
426.55	x	0	0	n/a	n/a	n/a	n/a	134519
427.18	Cyan	30.98	8.9	n/a	n/a	n/a	n/a	836849
428.12	Purple	6.24	1.19	n/a	n/a	n/a	n/a	1796529
428.22	x	0	0	n/a	n/a	n/a	n/a	41501
428.31	x	0	0	3,6-Anhydro-1-O-[(9E)-9-octadecenoyl]hexitol	C24H44O6	M-	-6.06	11154
428.83	x	0	0	n/a	n/a	n/a	n/a	124756
428.97	x	0	0	N-(2-Iodophenyl)-3-(2-oxo-1,3-benzoxazol-3(2H)-yl)propanamide	C16H13IN2O3	M+Na-2H, M+K-2H	7.9	145712
429.29	Cyan	19.52	10.45	Ethyl (1,2,3,10-tetramethoxy-9-oxo-5,6,7,9-tetrahydrobenzo[a]heptalen-7-yl)carbamate	C23H27NO7	M-H2O-H, M-	-3.99	1460260
429.9	x	0	0	n/a	n/a	n/a	n/a	32158
430.29	x	0	0	Pellasoren B	C26H41N1O4	M-H	4.74	34377
431.14	Blue	83.76	23.35	n/a	n/a	n/a	n/a	1308217
431.21	x	0	0	n/a	n/a	n/a	n/a	49169
432.28	Black	3.4	5.9	Dioctyl 4-cyclohexene-1,2-dicarboxylate	C24H42O4	M+K-2H	-1.49	1220819
433.15	x	0	0	Microsclerodermins	C40H49N8O12Cl	M-2H	0.83	430393
433.3	Black	31.01	16.23	n/a	n/a	n/a	n/a	1118025
434.22	x	0	0	n/a	n/a	n/a	n/a	28007
434.3	Black	10.61	7.75	n/a	n/a	n/a	n/a	446226
434.54	x	0	0	n/a	n/a	n/a	n/a	80174
435.21	Blue	55.47	34.22	n/a	n/a	n/a	n/a	168607
435.95	x	0	0	n/a	n/a	n/a	n/a	51615
436.25	Orange	21.99	8.78	n/a	n/a	n/a	n/a	998225
436.83	x	0	0	n/a	n/a	n/a	n/a	40791
437.24	Cyan	18.69	12.07	n/a	n/a	n/a	n/a	815746
437.53	x	0	0	n/a	n/a	n/a	n/a	15348
438.26	Cyan	82.61	69.12	LysoPE(15:0)	C20H42NO7P	M-H	-8.13	5032906
439.1	Blue	113.76	20.53	S-{(2Z)-2-Amino-2-[({3-[4-(methylsulfanyl)phenyl]adamantan-1-yl}methyl)imino]ethyl} hydrogen sulfurothioate	C20H28N2O3S3	M-H	-6.74	15146910
439.65	x	0	0	n/a	n/a	n/a	n/a	63861

440.12	Blue	39.4	25.04	n/a	n/a	n/a	n/a	564488
440.54	x	0	0	n/a	n/a	n/a	n/a	24948
440.85	x	0	0	n/a	n/a	n/a	n/a	68716
441.11	Blue	36.63	14.94	n/a	n/a	n/a	n/a	24121
441.27	x	0	0	n/a	n/a	n/a	n/a	2710881
442	Green	23.19	5.34	n/a	n/a	n/a	n/a	413117
442.24	x	0	0	n/a	n/a	n/a	n/a	43532
442.53	x	0	0	n/a	n/a	n/a	n/a	39693
442.65	x	0	0	n/a	n/a	n/a	n/a	10564
442.97	x	0	0	n/a	n/a	n/a	n/a	6712
443.17	Cyan	6.67	11.55	n/a	n/a	n/a	n/a	335655
443.24	x	0	0	n/a	n/a	n/a	n/a	132124
444.16	x	0	0	n/a	n/a	n/a	n/a	39315
444.53	x	0	0	n/a	n/a	n/a	n/a	17083
445.13	x	0	0	3,4-Dihydro-2(1H)-isoquinolinyl[3-(3-ethoxyphenyl)-4-quinolinyl]methanone	C27H24N2O2	M+K-2H	2.39	30974
445.69	x	0	0	n/a	n/a	n/a	n/a	71177
446.55	x	0	0	n/a	n/a	n/a	n/a	105655
446.97	x	0	0	n/a	n/a	n/a	n/a	58744
447.13	Black	30.72	13.28	(3,4,5,6-Tetraacetoxy-1-cyclohexen-1-yl)methyl benzoate	C22H24O10	M-H	3.57	1978228
447.2	x	0	0	n/a	n/a	n/a	n/a	479678
447.98	Green	58.07	4.27	n/a	n/a	n/a	n/a	787424
448.22	x	0	0	n/a	n/a	n/a	n/a	761651
448.74	x	0	0	n/a	n/a	n/a	n/a	20546
449.28	Yellow	19.3	12.91	n/a	n/a	n/a	n/a	142164
450.26	Orange	53.63	3.94	LysoPE(16:1)	C21H42NO7P	M-H	1.07	5921522
451.02	x	0	0	n/a	n/a	n/a	n/a	140289
451.32	x	0	0	n/a	n/a	n/a	n/a	21750
452.13	x	0	0	n/a	n/a	n/a	n/a	633740
452.25	Cyan	56.14	9.87	n/a	n/a	n/a	n/a	4278243
452.53	x	0	0	n/a	n/a	n/a	n/a	25991
453.25	Cyan	20.37	12.45	n/a	n/a	n/a	n/a	804298
453.7	x	0	0	n/a	n/a	n/a	n/a	52399
454.19	Purple	45.9	3.39	n/a	n/a	n/a	n/a	439749
454.54	x	0	0	n/a	n/a	n/a	n/a	85262
455.09	Purple	87.72	10.08	1-(8-ethoxy-4,4-dimethyl-1-thioxo-1H-[1,2]dithiolo[3,4-c]quinolin-5(4H)-yl)-2-(piperidin-1-yl)ethanone	C21H26N2O2S3	M+Na-2H	0.24	2540000
455.35	x	0	0	4a,6a-Dimethyl-1,2,3,4,4a,4b,5,6,6a,7,14,14a,14b,15,16,16a-hexadecahydrobenzo[e]naphtho[2',1':4,5]indeno[1,2-b]indol-2-yl acetate	C31H37NO2	M-H2O-H, M-	-6.76	6435076
455.53	x	0	0	n/a	n/a	n/a	n/a	27016

456.1	Purple	40.5	4.78	n/a	n/a	n/a	n/a	485790
456.25	x	0	0	n/a	n/a	n/a	n/a	134883
456.52	x	0	0	n/a	n/a	n/a	n/a	14135
456.76	x	0	0	n/a	n/a	n/a	n/a	37963
456.81	x	0	0	n/a	n/a	n/a	n/a	94282
457.09	Purple	45.94	5.57	5a,11a-Dehydrooxytetracycline	C22H22N2O9	M-H	-2.54	211835
458.04	x	0	0	n/a	n/a	n/a	n/a	11106
458.16	x	0	0	(4-hydroxyphenethyl)acrylamide	C27H27NO7	M-H2O-H	-4.08	26674
458.19	Blue	23	7	n/a	n/a	n/a	n/a	22280
458.2	x	0	0	n/a	n/a	n/a	n/a	95463
459.3	Blue	7.64	6.63	2-phytyl-1,4-dihydroxynaphthalene	C30H46O2	M+Na-2H	-6.21	81458
459.52	x	0	0	n/a	n/a	n/a	n/a	39942
460.22	x	0	0	(Benzylimino)di-2,1-ethanediyl bis[(3-methylphenyl)carbamate]	C27H31N3O4	M-H	-1.64	957332
460.86	x	0	0	n/a	n/a	n/a	n/a	59966
461.06	Blue	134.98	9.01	n/a	n/a	n/a	n/a	341510
462.06	Blue	59.67	11.93	n/a	n/a	n/a	n/a	424995
462.19	x	0	0	Apicularen A	C25H32NO6	M+Na-H	8.45	360900
462.52	x	0	0	n/a	n/a	n/a	n/a	44378
464.26	Cyan	42.52	8.48	n/a	n/a	n/a	n/a	2492121
464.53	x	0	0	n/a	n/a	n/a	n/a	28680
465.27	Cyan	17.67	2.89	1-arachidoyl-sn-glycero-3-phosphate	C23H47O7P	M-H	5.35	505585
466.26	Cyan	102.17	21.82	(2R)-3-{[(2-Aminoethoxy)(hydroxy)phosphoryl]oxy}-2-(octanoyloxy)propyl octanoate	C21H42NO8P	M-H	-5.42	19880622
466.54	x	0	0	n/a	n/a	n/a	n/a	37967
466.96	x	0	0	n/a	n/a	n/a	n/a	20493
467.26	Cyan	76.2	43.72	n/a	n/a	n/a	n/a	5007850
467.53	x	0	0	n/a	n/a	n/a	n/a	28777
467.78	x	0	0	n/a	n/a	n/a	n/a	6336
468.26	Cyan	43.75	26.74	n/a	n/a	n/a	n/a	1326317
468.97	x	0	0	n/a	n/a	n/a	n/a	41458
469.26	Cyan	90.44	67.03	n/a	n/a	n/a	n/a	7161976
469.56	x	0	0	n/a	n/a	n/a	n/a	9217
469.94	x	0	0	2-(1,3-Dioxo-2,3-dihydro-1H-inden-2-yl)-6,8-quinolinedisulfonic acid	C18H11NO8S2	M+K-2H	-5.05	469799
470.15	Blue	32.05	37.36	n/a	n/a	n/a	n/a	977673
470.27	x	0	0	n/a	n/a	n/a	n/a	25660
470.51	x	0	0	n/a	n/a	n/a	n/a	28510
470.72	x	0	0	n/a	n/a	n/a	n/a	254624
470.82	x	0	0	n/a	n/a	n/a	n/a	30482
471.27	Cyan	30.14	5.09	15,24-Dimethyl-1,4,7,10,18,21-hexaoxa-15,24-diazacyclooctacosane-11,14,25,28-tetrone	C22H38N2O10	M-H2O-H	1.19	130299

472.21	Blue	39.79	14.81	n/a	n/a	n/a	n/a	69975
472.52	x	0	0	n/a	n/a	n/a	n/a	42356
473.28	Black	12.38	8.39	(3S)-2-{(2R,3R)-3-Hydroxy-2-[(methoxyacetyl)amino]-4-methylpentanoyl}-N-[(2S,3S)-3-hydroxy-1-phenyl-2-pentanyl]hexahydro-3-pyridazinecarboxamide	C25H40N4O6	M-H2O-H	3.46	938980
474.15	x	0	0	n/a	n/a	n/a	n/a	38366
475.52	x	0	0	n/a	n/a	n/a	n/a	14857
476.17	x	0	0	n/a	n/a	n/a	n/a	50378
476.51	x	0	0	n/a	n/a	n/a	n/a	10546
477.03	Blue	97.12	17.33	n/a	n/a	n/a	n/a	59063
478.28	Yellow	26.99	2.71	n/a	n/a	n/a	n/a	1136180
479.12	x	0	0	(2R,3R)-5,7-Dihydroxy-2-(4-hydroxyphenyl)-6-methoxy-4-oxo-3,4-dihydro-2H-chromen-3-yl beta-D-threo-hexopyranoside	C22H24O12	M-H	-6.46	182432
479.28	x	0	0	didecanoylphosphatidic acid	C23H45O8P	M-H	3.85	85497
479.53	x	0	0	n/a	n/a	n/a	n/a	105968
480.25	x	0	0	n/a	n/a	n/a	n/a	5330021
481.09	x	0	0	4-Acetoxy-6',7-dimethyl-5',8'-dimethoxy-1,2'-binaphthalene-1',4',5,8-tetrone	C26H20O8	M+Na-2H	7.43	165822
481.26	Cyan	27.09	21.9	n/a	n/a	n/a	n/a	4544751
481.53	x	0	0	n/a	n/a	n/a	n/a	22464
482.26	Cyan	27.78	12.12	Noricumazole A	C28H39NO7	M-H2O-H	9.44	1114820
482.76	x	0	0	n/a	n/a	n/a	n/a	14611
483.27	Purple	98.82	26.81	n/a	n/a	n/a	n/a	2700622
483.37	x	0	0	n/a	n/a	n/a	n/a	90829
484.27	Purple	63.28	11.37	n/a	n/a	n/a	n/a	731267
484.98	x	0	0	n/a	n/a	n/a	n/a	27261
485.17	x	0	0	Nocardicin C	C23H26N4O8	M-H	-3.27	8624
485.3	x	0	0	n/a	n/a	n/a	n/a	1979672
485.92	Purple	17.31	2.37	n/a	n/a	n/a	n/a	136588
486.23	x	0	0	S-(2-{Bis[5-(cyclopentyloxy)pentyl]amino}ethyl) hydrogen sulfurothioate	C22H43NO5S2	M+Na-2H	-1.15	146364
486.52	x	0	0	n/a	n/a	n/a	n/a	10567
486.73	x	0	0	n/a	n/a	n/a	n/a	57533
487.28	Blue	3.67	6.35	Hyafurone B	C32H42O5	M-H2O-H	5.42	3026017
487.52	x	0	0	n/a	n/a	n/a	n/a	84716
487.91	x	0	0	n/a	n/a	n/a	n/a	78434
488.16	Blue	68.68	7.72	n/a	n/a	n/a	n/a	551917
488.75	x	0	0	n/a	n/a	n/a	n/a	35286
488.99	x	0	0	n/a	n/a	n/a	n/a	12286
489.17	Blue	7	12.12	n/a	n/a	n/a	n/a	124977
489.39	x	0	0	4-acetoxy-plakinamine B	C33H52N2O2	M-H2O-H	0.83	45669
490.23	x	0	0	n/a	n/a	n/a	n/a	438080

490.54	x	0	0	n/a	n/a	n/a	n/a	8510
491.23	x	0	0	Benzyl 2,3,4-tri-O-benzylpentopyranoside	C33H34O5	M-H2O-H	5.63	51537
492.28	Purple	27.33	17.62	n/a	n/a	n/a	n/a	820294
492.84	x	0	0	n/a	n/a	n/a	n/a	67770
493.27	Cyan	39.93	38.1	Cytochromone A	C28H42O5	M+Cl	6.69	51273
494.25	Cyan	83.47	34.24	2(3H)-Furanone, 3-cyclohexylidene-5-(4-hexadecanoyloxyphenyl)-	C32H46O4	M-H2O-H, M-	-5.65	12841324
494.65	x	0	0	n/a	n/a	n/a	n/a	11033
494.97	x	0	0	n/a	n/a	n/a	n/a	116806
495.26	Cyan	63.27	23.84	n/a	n/a	n/a	n/a	7677584
495.41	x	0	0	n/a	n/a	n/a	n/a	269275
496.27	Cyan	39.68	8.7	n/a	n/a	n/a	n/a	1599675
496.52	x	0	0	n/a	n/a	n/a	n/a	32521
497.17	x	0	0	2-Acetyl-1-(3,4-diacetoxybenzyl)-1,2,3,4-tetrahydroisoquinoline-6,7-diyl diacetate	C26H27NO9	M-	-2.34	2189552
497.27	Cyan	112.7	20.22	n/a	n/a	n/a	n/a	4858800
498.27	Cyan	83.57	12.13	n/a	n/a	n/a	n/a	1670298
498.86	x	0	0	n/a	n/a	n/a	n/a	6358
499.25	x	0	0	n/a	n/a	n/a	n/a	334479
499.36	Black	14.22	12.71	n/a	n/a	n/a	n/a	2760281
499.53	x	0	0	n/a	n/a	n/a	n/a	74768
500.36	x	0	0	Plakinamine I	C32H56N2O2	M-H2O-H, M-	-3.26	610770
500.76	x	0	0	n/a	n/a	n/a	n/a	64716
501.01	Blue	3.33	2.95	n/a	n/a	n/a	n/a	150396
501.25	x	0	0	n/a	n/a	n/a	n/a	129574
501.9	Purple	26.94	6.05	n/a	n/a	n/a	n/a	392595
502.64	x	0	0	n/a	n/a	n/a	n/a	13552
502.71	x	0	0	n/a	n/a	n/a	n/a	11044
503.04	x	0	0	N-adenylylanthranilic acid	C17H19N6O8P	M+K-2H	-9.03	32237
503.24	x	0	0	Carolacton	C25H40O8	M+Cl	1.08	385033
503.5	x	0	0	n/a	n/a	n/a	n/a	15732
504.27	Cyan	37.48	11.35	n/a	n/a	n/a	n/a	2037445
504.51	x	0	0	n/a	n/a	n/a	n/a	19020
505.28	Cyan	5.72	9.9	n/a	n/a	n/a	n/a	171884
505.42	x	0	0	Methyl 2,4-dimethoxyheptacosanoate	C30H60O4	M+Na-2H	-9.14	603236
506.19	Blue	9	3.61	n/a	n/a	n/a	n/a	333874
507.24	Yellow	19.33	13.65	3,4,15-Triacetoxy-12,13-epoxytrichothec-9-en-8-yl 3-methylbutanoate	C26H36O10	M-H	-5.25	281583
507.52	x	0	0	Tetratriacontanoic acid	C34H68O2	M-H	7.56	59301
508.11	x	0	0	n/a	n/a	n/a	n/a	47213
508.26	Cyan	31.21	19.66	Corallopyronin A2	C30H41N1O7	M-H2O-H	9.66	153012
509.01	x	0	0	n/a	n/a	n/a	n/a	21577
509.29	Purple	116.29	24.72	n/a	n/a	n/a	n/a	122678

510.27	Purple	61.68	22.94	n/a	n/a	n/a	n/a	884036
510.99	x	0	0	3-({3,4-Dihydroxy-5-[(3,4,5-trihydroxybenzoyl)oxy]benzoyl}oxy)-4,5-dihydroxybenzoic acid	C21H14O13	M+K-2H	-5.63	6473
511.28	Purple	17.81	14.34	n/a	n/a	n/a	n/a	33374
512.51	x	0	0	n/a	n/a	n/a	n/a	27345
513.29	x	0	0	Stigmatellin	C30H42O7	M-H	-0.56	114716
513.38	Cyan	33.26	15.24	n/a	n/a	n/a	n/a	2672841
514.13	Green	13.61	5.86	n/a	n/a	n/a	n/a	336397
514.22	x	0	0	n/a	n/a	n/a	n/a	447226
514.26	x	0	0	n/a	n/a	n/a	n/a	225362
515.15	Green	36.29	17.6	n/a	n/a	n/a	n/a	397996
515.23	Yellow	54	20	DKXanthene-534	C29H34N4O6	M-H2O-H	4.4	637709
515.4	x	0	0	n/a	n/a	n/a	n/a	105188
515.51	x	0	0	n/a	n/a	n/a	n/a	39052
516.21	x	0	0	n/a	n/a	n/a	n/a	46248
516.95	x	0	0	n/a	n/a	n/a	n/a	116219
517.25	Yellow	64.8	28.69	Dkxanthene-518	C29H34N4O5	M-H	1.7	2929017
517.42	x	0	0	n/a	n/a	n/a	n/a	235114
518.28	Yellow	50	26.46	n/a	n/a	n/a	n/a	1777160
518.67	x	0	0	n/a	n/a	n/a	n/a	44878
519.03	Blue	21.95	17.29	n/a	n/a	n/a	n/a	506642
519.15	x	0	0	1-[3-(3-{[(1S,2R)-1-Carboxy-2-hydroxypropyl]carbamoyl}-6-hydroxy-9H-beta-carbolin-1-yl)propanoyl]-L-proline	C24H26N4O8	M+Na-2H	7.46	540139
519.29	Cyan	24.89	10.05	Crocacin A	C31H42N2O6	M-H2O-H	1.96	720162
519.37	x	0	0	2,3-Bis(octanoyloxy)propyl decanoate	C29H54O6	M+Na-2H	-2.62	320456
520.27	Cyan	26.6	19.59	n/a	n/a	n/a	n/a	44646
520.51	x	0	0	n/a	n/a	n/a	n/a	11112
522.26	x	0	0	Calcimycin	C29H37N3O6	M-H	5.54	69448
522.85	x	0	0	n/a	n/a	n/a	n/a	25980
523.3	Purple	49	38.77	1'-(N-Hydroxy-2-methylalanyl-5-phenyl-D-norvalyl)-1-(methylsulfonyl)-1,2-dihydrospiro[indole-3,4'-piperidine]	C28H38N4O5S	M-H2O-H	4.77	138561
523.5	x	0	0	n/a	n/a	n/a	n/a	47586
524.09	x	0	0	n/a	n/a	n/a	n/a	413124
524.28	Purple	8.85	6.08	n/a	n/a	n/a	n/a	421036
524.35	x	0	0	n/a	n/a	n/a	n/a	93769
525.25	x	0	0	Nebramycin IV	C19H38N6O11	M-H	0.93	30980
525.38	x	0	0	24-Methyl-2-oxooxacyclotetracosan-3-yl beta-D-mannopyranoside	C30H56O8	M-H2O-H	1.89	617262
525.72	x	0	0	n/a	n/a	n/a	n/a	43342
526.24	Yellow	23.4	16.81	Antalid	C28H37N3O5S	M-H	0.51	593930
527.38	x	0	0	Cholestane-3,22,27-triyl triacetate	C33H54O6	M-H2O-H	4.05	646125

527.95	Green	69.32	39.87	n/a	n/a	n/a	n/a	483992
528.27	x	0	0	n/a	n/a	n/a	n/a	73276
528.97	x	0	0	n/a	n/a	n/a	n/a	32023
529.25	Cyan	27.41	7.74	(2E)-5-[(2R)-2-{(1R,2R,3S,4aS,6R,8R,8aS)-3,6-Dihydroxy-1-[(2Z)-3-hydroxy-2-propenoyl]-1,3,6,8-tetramethyl-4-oxodecahydro-2-naphthalenyl}butoxy]-3-methyl-5-oxo-2-pentenoic acid	C27H40O9	M+Na-2H	-2.64	675005
529.41	x	0	0	all-trans-6-methoxy-2-hexaprenylhydroquinone	C37H56O3	M-H2O-H	5.43	153764
530.28	Cyan	19.13	10.06	n/a	n/a	n/a	n/a	2045704
531.26	Cyan	4.4	1.56	1-(2,6-Dihydroxyphenyl)-9-(4-hydroxy-3-{[2-(4-methyl-3-cyclohexen-1-yl)-2-propanyl]oxy}phenyl)-1-nonanone	C31H42O5	M+K-2H	-0.56	357929
532.51	x	0	0	n/a	n/a	n/a	n/a	50227
533.04	x	0	0	n/a	n/a	n/a	n/a	166618
533.24	Yellow	129.21	17.28	DKXanthene-534	C29H34N4O6	M-H	0.4	16449149
533.43	x	0	0	(2R,3R)-3-Hydroxy-2-tetradecyloctadecanoic acid	C32H64O3	M+K-2H	-4.63	202031
533.74	x	0	0	n/a	n/a	n/a	n/a	67396
534.25	Yellow	108.69	18.01	n/a	n/a	n/a	n/a	4685458
535.26	Yellow	60.24	10.87	n/a	n/a	n/a	n/a	107005
536.28	Cyan	45.12	26.23	n/a	n/a	n/a	n/a	1025745
537.12	Green	39.99	1.74	n/a	n/a	n/a	n/a	394395
537.28	x	0	0	Roimatacene	C30H44O7	M+Na-H	4.87	64472
538.25	Cyan	50.98	7.15	Chondrochloren B	C28H42NO7Cl	M-H	5.86	865451
538.51	x	0	0	n/a	n/a	n/a	n/a	24998
539.26	Cyan	23.67	13.2	n/a	n/a	n/a	n/a	41377
539.37	x	0	0	n/a	n/a	n/a	n/a	9912
540.05	Green	128.17	15.74	n/a	n/a	n/a	n/a	218365
540.23	x	0	0	n/a	n/a	n/a	n/a	21505
540.5	x	0	0	n/a	n/a	n/a	n/a	59335
540.77	x	0	0	n/a	n/a	n/a	n/a	65534
541.05	Green	64.72	10.47	n/a	n/a	n/a	n/a	476441
541.24	x	0	0		C31H36N4O6	M-H2O-H	-7.92	167255
541.74	x	0	0	n/a	n/a	n/a	n/a	54718
542.08	Green	28.74	5.93	n/a	n/a	n/a	n/a	467090
542.23	x	0	0	n/a	n/a	n/a	n/a	121104
542.52	x	0	0	n/a	n/a	n/a	n/a	27961
543.05	x	0	0	n/a	n/a	n/a	n/a	348842
543.26	Cyan	14.15	4.17	(3beta,5alpha,16beta,20S)-20-Methyl-6,21-dioxo-16,21-epoxypregnan-3-yl D-allopyranoside	C28H42O9	M+Na-2H	0.77	844553
543.28	x	0	0	n/a	n/a	n/a	n/a	2062391
544.28	Cyan	12.57	4.66	Phenalamide C	C32H45NO4	M+K-2H	2.38	668551
544.42	x	0	0	n/a	n/a	n/a	n/a	364017

544.76	x	0	0	n/a	n/a	n/a	n/a	77298
545.11	x	0	0	S-Benzyl-N-[(benzyloxy)carbonyl]cysteinyltyrosine	C27H28N2O6S	M+K-2H	-3.97	161196
545.27	Cyan	2.37	1.2	n/a	n/a	n/a	n/a	483992
546.29	Cyan	6.67	11.55	n/a	n/a	n/a	n/a	506282
546.52	x	0	0	n/a	n/a	n/a	n/a	21207
546.78	x	0	0	n/a	n/a	n/a	n/a	74791
547.26	Yellow	68.74	21.54	fischerindoline	C29H38N2O6	M+Na-2H, M+K-2H	4.22	1686336
547.41	x	0	0	n/a	n/a	n/a	n/a	277344
548.27	Yellow	25.99	7.53	Corallopyronin A2	C30H41N1O7	M+Na-H	9.18	752397
548.5	x	0	0	n/a	n/a	n/a	n/a	49095
549.38	x	0	0	n/a	n/a	n/a	n/a	133378
549.83	x	0	0	n/a	n/a	n/a	n/a	181884
550.18	Blue	151.57	3.22	6-Deoxy-alpha-L-galactopyranosyl-(1->2)-beta-D-galactopyranosyl-(1->3)-2-acetamido-2-deoxy-D-galactose	C20H35NO15	M+Na-2H	6.56	7602346
550.26	x	0	0	n/a	n/a	n/a	n/a	1141981
550.38	x	0	0	N,N'-Bis(3-{[2-(dimethylamino)ethyl](methyl)amino}propyl)-1,9-phenazinedicarboxamide	C30H46N8O2	M-	6.59	123881
550.48	x	0	0	n/a	n/a	n/a	n/a	26549
551.18	Blue	135.39	7.36	n/a	n/a	n/a	n/a	1662181
551.27	x	0	0	Roimatacene	C30H44O7	M+Cl	8.8	843643
551.88	x	0	0	n/a	n/a	n/a	n/a	93850
552.18	Blue	115.23	10.63	n/a	n/a	n/a	n/a	17602
552.28	x	0	0	n/a	n/a	n/a	n/a	2364685
552.51	x	0	0	n/a	n/a	n/a	n/a	56056
553.19	Blue	34.73	23.1	n/a	n/a	n/a	n/a	386113
554.24	x	0	0	2-Methyl-2-propanyl 4-({2-[(2-ethoxy-2-oxoethyl)amino]-4-phenyl-6-quinazolinyl}carbamoyl)-1-piperidinecarboxylate	C29H35N5O5	M+Na-2H	2.46	145297
554.26	x	0	0	Leu-enkephalin	C28H37N5O7	M-H	-3.2	204096243
554.56	x	0	0	n/a	n/a	n/a	n/a	2080847
554.92	x	0	0	n/a	n/a	n/a	n/a	99987
555.26	x	0	0	n/a	n/a	n/a	n/a	2685698
555.76	x	0	0	n/a	n/a	n/a	n/a	119031
556.27	x	0	0	n/a	n/a	n/a	n/a	759558
556.49	x	0	0	n/a	n/a	n/a	n/a	35939
557.27	Cyan	26.33	30.44	n/a	n/a	n/a	n/a	1362857
557.48	Orange	41.67	38.42	n/a	n/a	n/a	n/a	7554418
557.74	x	0	0	n/a	n/a	n/a	n/a	119482
558.44	x	0	0	n/a	n/a	n/a	n/a	745190
558.77	x	0	0	n/a	n/a	n/a	n/a	212904
559.06	x	0	0	n/a	n/a	n/a	n/a	1328657

559.26	Yellow	95.23	11.59	DKxanthene560	C31H36N4O6	M-H	-3.66	5431436
559.38	x	0	0	n/a	n/a	n/a	n/a	165381
559.45	x	0	0	N,N-Dicyclohexyl-2-(2-{[2-(dicyclohexylamino)-2-oxoethoxy]methyl}-2-methylbutoxy)acetamide	C34H60N2O4	M-H	5.07	39670
560.27	Yellow	75.97	3.5	n/a	n/a	n/a	n/a	4394592
560.5	x	0	0	n/a	n/a	n/a	n/a	42128
561.27	x	0	0	n/a	n/a	n/a	n/a	556687
562.04	Green	85.74	8.44	n/a	n/a	n/a	n/a	475362
562.28	x	0	0	n/a	n/a	n/a	n/a	654902
563.06	Green	29.72	5.65	n/a	n/a	n/a	n/a	399436
563.28	x	0	0	n/a	n/a	n/a	n/a	435905
564.29	Cyan	80.99	29.66	n/a	n/a	n/a	n/a	107603
565.28	Cyan	53.68	18.91	n/a	n/a	n/a	n/a	870098
566.27	Cyan	64.59	28.37	n/a	n/a	n/a	n/a	132338
567.28	Cyan	46.64	22.34	Maltepolid D	C30H44O8	M+Cl	9.96	903687
567.75	x	0	0	n/a	n/a	n/a	n/a	36278
567.89	x	0	0	n/a	n/a	n/a	n/a	345665
568.28	Cyan	24.67	15.82	n/a	n/a	n/a	n/a	753471
568.48	x	0	0	n/a	n/a	n/a	n/a	33608
568.96	x	0	0	n/a	n/a	n/a	n/a	24443
569.27	x	0	0	dinoflagellate luciferin	C33H40N4O6	M-H2O-H	-8.43	62673
569.48	Orange	53.78	15.55	n/a	n/a	n/a	n/a	5686928
570.48	Orange	20.67	8.5	n/a	n/a	n/a	n/a	2287288
571.31	x	0	0	n/a	n/a	n/a	n/a	4757635
571.8	x	0	0	n/a	n/a	n/a	n/a	134043
572.16	Blue	43.68	14.96	n/a	n/a	n/a	n/a	418516
572.45	x	0	0	n/a	n/a	n/a	n/a	1233334
572.77	x	0	0	n/a	n/a	n/a	n/a	20863
573.27	Yellow	57.24	6.32	Crocacin A	C31H42N2O6	M+Cl	0.56	675600
574.16	x	0	0	n/a	n/a	n/a	n/a	26473
575.05	Purple	25.29	7.16	n/a	n/a	n/a	n/a	988860
575.8	x	0	0	n/a	n/a	n/a	n/a	48657
576.24	x	0	0	Leu-enkephalin	C28H37N5O7	M+Na-2H	-4.83	16057915
576.25	x	0	0	n/a	n/a	n/a	n/a	97611
577.26	Green	43.66	17.06	Omadacycline	C29H40N4O7	M+Na-2H	-6.24	59298
577.58	x	0	0	n/a	n/a	n/a	n/a	7940
578.29	Cyan	37.84	22.57	n/a	n/a	n/a	n/a	90582
578.49	x	0	0	n/a	n/a	n/a	n/a	19136
579.28	x	0	0	n/a	n/a	n/a	n/a	124491
580.29	x	0	0	n/a	n/a	n/a	n/a	161825
581	Blue	62.47	21.24	n/a	n/a	n/a	n/a	110737
581.77	x	0	0	n/a	n/a	n/a	n/a	58426

582.29	Cyan	27.39	14.4	Maltepoild C	C31H46O8	M+Cl	3.43	7763640
582.49	x	0	0	n/a	n/a	n/a	n/a	12867
582.53	x	0	0	n/a	n/a	n/a	n/a	82028
583.49	Yellow	39.55	31.17	n/a	n/a	n/a	n/a	3453765
583.85	x	0	0	n/a	n/a	n/a	n/a	123716
585.27	Cyan	38.76	10.91	Saframycin MX1	C33H38N4O6	M-H	3.91	243430
585.31	x	0	0	n/a	n/a	n/a	n/a	88989
586.48	Blue	52.46	39.84	n/a	n/a	n/a	n/a	2410889
587.32	x	0	0	n/a	n/a	n/a	n/a	483060
588.36	Black	20.18	17.74	n/a	n/a	n/a	n/a	2754012
588.96	x	0	0	n/a	n/a	n/a	n/a	23123
589.25	x	0	0	Phenylalanyl-N-{1-[4-amino-6-(dimethylamino)-1,3,5-triazin-2-yl]-2-phenylethyl}phenylalaninamide	C31H36N8O2	M+K-2H	2.05	61645
590.34	Cyan	40.63	9.84	n/a	n/a	n/a	n/a	653490
591.24	x	0	0	(1S,6S,7S)-7-(Hydroxymethyl)-4-[(L-idopyranosyloxy)methyl]-6-{[(2E)-3-phenyl-2-propenoyl]oxy}-1,4a,5,6,7,7a-hexahydrocyclopenta[c]pyran-1-yl 3-methylbutanoate	C30H40O12	M-H	-4.81	173912
591.25	Yellow	11.33	4.16	1,4-Piperazinediylbis(2-pyridinylmethanone)	C16H16N4O2	2M-H	1.44	505263
591.85	x	0	0	n/a	n/a	n/a	n/a	300291
592.22	Green	30.86	11.48	n/a	n/a	n/a	n/a	4948868
593.13	Black	43.79	31	n/a	n/a	n/a	n/a	1475029
594.3	Cyan	56.67	13.2	(3R)-1,7-Bis(4-hydroxyphenyl)-3-heptanyl 3-O-alpha-D-glucopyranosyl-beta-D-xylopyranoside	C30H42O12	M-H	-1.32	523984
594.31	x	0	0	n/a	n/a	n/a	n/a	3943701
594.33	x	0	0	n/a	n/a	n/a	n/a	54056
595.66	Green	73.79	3.32	UDP-N-acetylmuramoyl-L-alanyl-gamma-D-glutamyl-meso-2,6-diaminopimeloyl-D-alanyl-D-alanine	C41H65N9O28P2	M-2H	-3.59	187705
596.16	Green	55.66	8.32	n/a	n/a	n/a	n/a	365943
596.47	Yellow	65.67	9.07	n/a	n/a	n/a	n/a	1764808
596.81	x	0	0	n/a	n/a	n/a	n/a	24110
597	Blue	42.33	26.65	Adenosine diphosphate ribose	C15H24N5O14P2+	M+K-2H	5.15	147326
597.31	x	0	0	Chondramide C	C35H44N4O6	M-H2O-H	2.11	504845
597.4	x	0	0	n/a	n/a	n/a	n/a	1154284
598.23	Green	55.83	20.41	n/a	n/a	n/a	n/a	8198570
599.23	Green	40.79	16.52	(3S,3aS,4S,5S,6aS)-5-[(1R,4aR,6R,8S,8aR)-8-Acetoxy-8a-(acetoxymethyl)-5,6-dimethyloctahydro-2H-spiro[naphthalene-1,2'-oxiran]-5-yl]-4-hydroxy-3a,6a-dimethylhexahydrofuro[2,3-b]furan-3-yl benzoate	C33H44O10	M-H	-7.86	55400
599.29	x	0	0	n/a	n/a	n/a	n/a	331447
599.4	x	0	0	n/a	n/a	n/a	n/a	2265928

600.36	Cyan	36.33	17.62	n/a	n/a	n/a	n/a	1176032
600.82	x	0	0	n/a	n/a	n/a	n/a	64405
601.28	x	0	0	n/a	n/a	n/a	n/a	443829
602.36	x	0	0	(2R)-1-{[(2-Aminoethoxy)(hydroxy)phosphoryl]oxy}-3-hydroxy-2-propanyl tetracosanoate	C29H60NO7P	M+K-2H	-0.62	1596231
602.99	Green	39.33	8.33	n/a	n/a	n/a	n/a	454860
603.27	x	0	0	6-2-Butanyl-7,15-dihydroxy-5',6,10,14,16-pentamethyl-5',6'-dihydro-3H-spiro[2,20-dioxatricycloricosa-4,6,8,10,12,16-hexaene-21,2'-pyran]-3,4'(3'H)-dione	C34H46O7	M+K-2H	-0.3	14352
604.25	x	0	0	n/a	n/a	n/a	n/a	590825
604.36	Cyan	41.33	18.45	n/a	n/a	n/a	n/a	2018686
604.42	Yellow	95.33	11.15	Myxovirscin A	C35H61NO8	M-H2O-H	2.15	282315
604.83	x	0	0	n/a	n/a	n/a	n/a	30116
605.26	x	0	0	n/a	n/a	n/a	n/a	419203
605.85	x	0	0	n/a	n/a	n/a	n/a	385378
606.21	x	0	0	n/a	n/a	n/a	n/a	43824
606.36	x	0	0	3-(Benzyloxy)-17-methyl-7,8-didehydro-4,5-epoxymorphinan-6-yl myristate	C38H51NO4	M+Na-2H	-2.13	2280043
606.65	Green	73	6.93	n/a	n/a	n/a	n/a	143994
607.26	x	0	0	6-({5-Acetoxy-6-[acetoxy(methoxy)methyl]-3,4-dimethoxytetrahydro-2H-pyran-2-yl}methoxy)-2,3,4-trimethoxy-1,5-hexanediyl diacetate	C27H46O16	M-H2O-H, M-	-1.11	361487
608.33	Cyan	38.97	17.04	n/a	n/a	n/a	n/a	397683
608.45	x	0	0	2,2'-{[2-(2-Pyridinylmethyl)-1,3-propanediyl]bis(oxy)}bis(N,N-dicyclohexylacetamide)	C37H59N3O4	M-H	3.11	4488293
608.81	x	0	0	n/a	n/a	n/a	n/a	148824
609.33	Purple	30.67	8.5	(2R,2'R,3S,3'S)-2,2',3,3'-Tetrahydroxy-beta,beta-carotene-4,4'-dione	C40H52O6	M-H2O-H	-8.82	168801
610.23	x	0	0	n/a	n/a	n/a	n/a	137241
610.32	Cyan	13.67	15.89	n/a	n/a	n/a	n/a	529283
611.3	Cyan	39.02	45.13	cytochalasin B2	C34H44O10	M-H	2.35	5914100
611.85	x	0	0	n/a	n/a	n/a	n/a	202162
612.3	Cyan	20.58	8.56	n/a	n/a	n/a	n/a	560178
612.95	x	0	0	n/a	n/a	n/a	n/a	70833
613.33	x	0	0	n/a	n/a	n/a	n/a	239869
613.48	x	0	0	n/a	n/a	n/a	n/a	1297795
614.2	Green	21	10.82	n/a	n/a	n/a	n/a	3012500
614.64	Green	44.44	5.58	n/a	n/a	n/a	n/a	475362
614.95	x	0	0	n/a	n/a	n/a	n/a	130201
615.14	x	0	0	n/a	n/a	n/a	n/a	34740
615.2	Green	12.13	3.7	n/a	n/a	n/a	n/a	435071
615.83	x	0	0	n/a	n/a	n/a	n/a	145512

616.38	Cyan	22.91	3.4	D-Isoleucyl-L-prolyl-L-tyrosyl-D-isoleucyl-L-leucine	C32H51N5O7	M-H	9.51	1158606
616.72	x	0	0	n/a	n/a	n/a	n/a	42795
616.97	x	0	0	n/a	n/a	n/a	n/a	35684
617.19	x	0	0	n/a	n/a	n/a	n/a	91539
618.14	x	0	0	Hyalachelin A	C29H31N3O10	M+K-2H	7.77	324995
618.37	Cyan	88.09	11.8	n/a	n/a	n/a	n/a	3112906
618.71	x	0	0	n/a	n/a	n/a	n/a	51520
618.97	Blue	65.1	9.59	n/a	n/a	n/a	n/a	14009
619.38	x	0	0	Bengamide A	C31H56N2O8	M+Cl	9.45	973667
620.2	x	0	0	n/a	n/a	n/a	n/a	3526825
620.21	Green	39.33	15.37	n/a	n/a	n/a	n/a	646317
620.38	x	0	0	Methyl N-decanoylglycylprolyltryptophylleucinate	C35H53N5O6	M-H2O-H	1.76	2699088
621.04	x	0	0	n/a	n/a	n/a	n/a	88837
621.2	x	0	0	n/a	n/a	n/a	n/a	75626
621.27	x	0	0	n/a	n/a	n/a	n/a	129818
622.29	x	0	0	n/a	n/a	n/a	n/a	435405
622.43	Yellow	102	8.72	Myxovirescin A	C35H61NO8	M-H	3.59	5815828
623.29	x	0	0	9-[(2E)-3,7-Dimethyl-2,6-octadien-1-yl]-8,10-dihydroxy-3,3,5'-trimethyl-11-(3-methyl-2-buten-1-yl)-4,6a-dihydro-3H-spiro[furo[3,4-d]xanthene-1,2'-pyran]-6',7(3'H,3aH)-dione	C37H46O7	M+Na-2H	-7.85	37468
623.36	Cyan	36	16.52	n/a	n/a	n/a	n/a	934402
623.72	x	0	0	n/a	n/a	n/a	n/a	6568
623.97	x	0	0	n/a	n/a	n/a	n/a	3897
624.28	x	0	0	n/a	n/a	n/a	n/a	210181
624.36	Cyan	18.33	9.61	n/a	n/a	n/a	n/a	540062
625.32	Cyan	26.41	7.35	n/a	n/a	n/a	n/a	163397
625.63	Green	30	10	n/a	n/a	n/a	n/a	635565
626.1	x	0	0	n/a	n/a	n/a	n/a	40553
626.31	x	0	0	Cruentaren	C33H51NO8	M+K-2H	1.67	486509
627.22	x	0	0	n/a	n/a	n/a	n/a	87962
627.39	Black	16	6.08	n/a	n/a	n/a	n/a	68385
627.47	x	0	0	VEPE	C35H69NO7P	M-H2O-H	5.66	529283
628.18	x	0	0	n/a	n/a	n/a	n/a	187233
628.35	x	0	0	n/a	n/a	n/a	n/a	1873867
628.49	Orange	10.65	4.47	n/a	n/a	n/a	n/a	269373
629.5	Orange	9.84	2.55	n/a	n/a	n/a	n/a	700813
630.39	x	0	0	13-(Methoxymethoxy)-6,10-dimethyl-5-{1-[3-(3-methyl-2-butanyl)-2-oxiranyl]ethyl}-18-phenyl-16,18,20-triazahexacyclo[13.5.2.0~1,9~.0~2,6~.0~10,15~.0~16,20~]docos-21-ene-17,19-dione	C38H53N3O5	M-H	1.31	1383577
630.96	x	0	0	n/a	n/a	n/a	n/a	79408

631.82	x	0	0	n/a	n/a	n/a	n/a	3108
632.13	x	0	0	n/a	n/a	n/a	n/a	15529
632.28	x	0	0	n/a	n/a	n/a	n/a	144282
632.39	Cyan	28.01	13.89	n/a	n/a	n/a	n/a	1967702
632.47	x	0	0	n/a	n/a	n/a	n/a	24344
633.38	Cyan	18.15	8.88	Bengamide I	C32H58N2O8	M+Cl	8.76	569515
633.62	x	0	0	n/a	n/a	n/a	n/a	19064
633.85	x	0	0	n/a	n/a	n/a	n/a	95231
634.2	x	0	0	(10Z)-4,9,13-Triacetoxy-3,6,6,10,14-pentamethyl-2-oxo-16-oxatetracyclo[10.3.1.0~1,12~.0~5,7~]hexadec-10-en-8-yl nicotinate	C32H39NO10	M+K-2H	-8.44	615602
634.38	Cyan	53.41	36.18	Methyl 1-(2-acetoxypentanoyl)prolylisoleucyl-N-methylvalyl-N-methylalanyl-beta-alaninate	C32H55N5O9	M-H2O-H	-0.2	2798986
634.47	x	0	0	n/a	n/a	n/a	n/a	8021
635.82	x	0	0	n/a	n/a	n/a	n/a	375185
636.37	Cyan	60.67	34.43	n/a	n/a	n/a	n/a	6351441
636.48	x	0	0	n/a	n/a	n/a	n/a	113480
637.31	x	0	0	Grahamine B	C35H46N2O9	M-H	-0.74	350907
637.38	Purple	60.64	30.2	n/a	n/a	n/a	n/a	2743291
637.44	x	0	0	n/a	n/a	n/a	n/a	43428
637.72	x	0	0	n/a	n/a	n/a	n/a	101012
637.97	x	0	0	n/a	n/a	n/a	n/a	81802
638.38	Purple	33.99	16.28	n/a	n/a	n/a	n/a	1049986
638.96	x	0	0	n/a	n/a	n/a	n/a	27572
639.24	x	0	0	(4S)-4-Amino-5-{[1-(2-amino-4-{[(2S)-2-amino-4-carboxybutanoyl]oxy}-5-methyl-5,8-dihydro-6-pteridinyl)-1-{[(2S)-2-amino-4-carboxybutanoyl]oxy}-2-propanyl]oxy}-5-oxopentanoic acid	C25H36N8O12	M-H	-0.32	1269970
639.36	Purple	17.51	10.92	n/a	n/a	n/a	n/a	622999
639.76	x	0	0	n/a	n/a	n/a	n/a	306312
639.83	x	0	0	n/a	n/a	n/a	n/a	5363
640.02	x	0	0	n/a	n/a	n/a	n/a	3469
640.23	x	0	0	n/a	n/a	n/a	n/a	5075
640.42	x	0	0	n/a	n/a	n/a	n/a	5268545
640.49	Yellow	24.08	14.44	n/a	n/a	n/a	n/a	1000068
641.41	Black	37.33	17.01	n/a	n/a	n/a	n/a	2081843
642.19	x	0	0	n/a	n/a	n/a	n/a	2002828
642.42	Yellow	62.67	4.73	n/a	n/a	n/a	n/a	9402
642.51	Yellow	53.32	17.93	n/a	n/a	n/a	n/a	1191921
642.66	x	0	0	n/a	n/a	n/a	n/a	67921
643.51	Yellow	38.13	30.63	n/a	n/a	n/a	n/a	1082767
644.41	Yellow	45.39	19.68	n/a	n/a	n/a	n/a	16316289

644.64	x	0	0	n/a	n/a	n/a	n/a	78385
644.72	x	0	0	n/a	n/a	n/a	n/a	8579
644.97	x	0	0	n/a	n/a	n/a	n/a	4886
645.32	x	0	0	21',24'-Dihydroxy-6-isopropyl-5,11',13',22'-tetramethyl-12'-(phenylsulfanyl)-3,4,5,6-tetrahydro-2'H-spiro[pyran-2,6'-[3,7,19]trioxatetracyclo[15.6.1.1~4,8~.0~20,24~]pentacosa[10,14,16,22]tetraen]-2'-one	C39H52O7S	M-H2O-H	-3.38	281564
646.43	Cyan	27.25	9.82	n/a	n/a	n/a	n/a	819324
647.18	x	0	0	n/a	n/a	n/a	n/a	48070
647.41	x	0	0	n/a	n/a	n/a	n/a	170890
648.19	x	0	0	4-[2-(([5-(Dimethylamino)-1-naphthyl]sulfonyl)amino)-1-hydroxyethyl]-2-methoxyphenyl 5-(dimethylamino)-1-naphthalenesulfonate	C33H35N3O7S2	M-H	4.43	476885
648.4	Cyan	87.17	9.43	n/a	n/a	n/a	n/a	52225
648.46	x	0	0	n/a	n/a	n/a	n/a	74330
648.67	x	0	0	n/a	n/a	n/a	n/a	120665
649.86	x	0	0	n/a	n/a	n/a	n/a	168303
650.37	x	0	0	Pretubulysin D	C36H55N5O5S1	M-H2O-H	6.27	1656533
651.19	x	0	0	n/a	n/a	n/a	n/a	245275
651.38	Cyan	95.86	5.49	n/a	n/a	n/a	n/a	5959582
651.86	x	0	0	n/a	n/a	n/a	n/a	114116
652.05	x	0	0	n/a	n/a	n/a	n/a	70171
652.22	x	0	0	n/a	n/a	n/a	n/a	3283059
653.18	x	0	0	Methyl 2,3-di-O-benzyl-4,6-bis-O-(4-nitrobenzoyl)hexopyranoside	C35H32N2O12	M-H2O-H	8.3	33282
653.3	x	0	0	(12beta,22R)-12,21-Dihydroxy-1,26-dioxo-22,26-epoxyergosta-2,5,24-trien-27-yl beta-D-threo-hexopyranoside	C34H48O11	M-H, M+Na-2H	-0.88	406680
653.37	Cyan	40.68	3.22	n/a	n/a	n/a	n/a	980803
653.4	x	0	0	n/a	n/a	n/a	n/a	57325
654.51	Yellow	80.16	18.84	n/a	n/a	n/a	n/a	399852
655.51	Yellow	28.69	16.04	n/a	n/a	n/a	n/a	939044
655.9	x	0	0	n/a	n/a	n/a	n/a	20822
656.32	x	0	0	n/a	n/a	n/a	n/a	47887
656.42	x	0	0	n/a	n/a	n/a	n/a	5076881
656.52	Yellow	34	3.99	n/a	n/a	n/a	n/a	2543279
656.94	x	0	0	n/a	n/a	n/a	n/a	496445
657.53	Orange	111.64	139.76	n/a	n/a	n/a	n/a	1295437
658.38	x	0	0	1,2-Dilauroyl-sn-glycero-3-phosphocholine	C32H64NO8P	M+K-2H	-1.83	8028816
658.42	Yellow	38	20.07	n/a	n/a	n/a	n/a	1250686
658.51	Orange	14.67	4.93	n/a	n/a	n/a	n/a	818966
658.62	x	0	0	n/a	n/a	n/a	n/a	29111

659.17	x	0	0	n/a	n/a	n/a	n/a	150369
659.34	x	0	0	n/a	n/a	n/a	n/a	513739
659.42	Yellow	28.67	4.93	n/a	n/a	n/a	n/a	156146
660.42	Cyan	46.77	12.79	O-{[2,3-Bis(tetradecanoyloxy)propoxy](hydroxy)phosphoryl}-L-serine	C34H66NO10P	M-H2O-H	-9.22	7464180
661.03	x	0	0	n/a	n/a	n/a	n/a	7146
662.19	x	0	0	n/a	n/a	n/a	n/a	479592
662.46	Cyan	102.53	3.79	n/a	n/a	n/a	n/a	8809444
662.69	x	0	0	n/a	n/a	n/a	n/a	46654
664.06	x	0	0	n/a	n/a	n/a	n/a	184522
664.39	Cyan	66	26	n/a	n/a	n/a	n/a	8753625
665.42	Purple	57.09	9.96	n/a	n/a	n/a	n/a	2344563
666.06	x	0	0	n/a	n/a	n/a	n/a	3973508
666.42	Green	46	3.61	n/a	n/a	n/a	n/a	736282
667.39	Cyan	51.67	26.86	n/a	n/a	n/a	n/a	1384842
667.44	x	0	0	n/a	n/a	n/a	n/a	55958
668.16	x	0	0	n/a	n/a	n/a	n/a	11797
668.3	x	0	0	thuggacin B	C35H53NO7S	M+K-2H	-8.27	29793
668.38	x	0	0	Pretubulysin D	C36H55N5O5S1	M-H	1.01	823258
668.49	Yellow	86.33	8.02	n/a	n/a	n/a	n/a	2654796
668.52	Yellow	93.78	4.53	n/a	n/a	n/a	n/a	593946
668.95	x	0	0	n/a	n/a	n/a	n/a	8634
669.16	x	0	0	n/a	n/a	n/a	n/a	95176
669.41	x	0	0	n/a	n/a	n/a	n/a	3207135
670.52	Yellow	39.65	11	n/a	n/a	n/a	n/a	1573170
671.16	x	0	0	3-Hydroxy-5-methoxy-4-oxo-2-{4-[(2,3,4-tri-O-acetyl-6-deoxyhexopyranosyl)oxy]phenyl}-4H-chromene-6,7-diyl diacetate	C32H32O16	M-H	2.65	87983
671.41	x	0	0	n/a	n/a	n/a	n/a	10905921
672.14	x	0	0	n/a	n/a	n/a	n/a	40646
672.48	Blue	42.33	29.4	n/a	n/a	n/a	n/a	1092741
673.19	x	0	0	n/a	n/a	n/a	n/a	432151
673.35	x	0	0	n/a	n/a	n/a	n/a	349321
673.46	x	0	0	n/a	n/a	n/a	n/a	95446
674.2	x	0	0	5,12-Diacetoxy-6-(acetoxymethyl)-4-(benzoyloxy)-2,10,10-trimethyl-11-oxatricyclo[7.2.1.0~1,6~]dodec-7-yl nicotinate	C34H39NO11	M+K-2H	2.4	1835444
674.46	Green	16.67	8.08	n/a	n/a	n/a	n/a	650263
675.42	x	0	0	n/a	n/a	n/a	n/a	98605
676.41	x	0	0	n/a	n/a	n/a	n/a	18678610
677.45	Cyan	64	14.73	n/a	n/a	n/a	n/a	1595081
678.16	x	0	0	n/a	n/a	n/a	n/a	141091
679.01	x	0	0	n/a	n/a	n/a	n/a	892294

679.17	x	0	0	n/a	n/a	n/a	n/a	48097
679.46	Green	38.73	19.36	n/a	n/a	n/a	n/a	1245712
680.16	x	0	0	n/a	n/a	n/a	n/a	129799
680.46	Green	36.98	11.24	n/a	n/a	n/a	n/a	624076
680.95	x	0	0	n/a	n/a	n/a	n/a	109401
681.17	x	0	0	n/a	n/a	n/a	n/a	258921
681.3	x	0	0	Coproporphyrinogen III	C36H44N4O8	M+Na-2H	7.33	119374
681.4	Cyan	36.33	9.07	n/a	n/a	n/a	n/a	871528
682.05	x	0	0	n/a	n/a	n/a	n/a	69162
682.18	x	0	0	n/a	n/a	n/a	n/a	89449
682.94	x	0	0	n/a	n/a	n/a	n/a	82871
683.22	Blue	89.19	7.88	n/a	n/a	n/a	n/a	589981
684.18	x	0	0	n/a	n/a	n/a	n/a	305710
684.3	x	0	0	n/a	n/a	n/a	n/a	43765
684.54	Yellow	39.67	2.52	n/a	n/a	n/a	n/a	1040005
685.42	x	0	0	n/a	n/a	n/a	n/a	11061698
686.14	x	0	0	n/a	n/a	n/a	n/a	922996
686.48	Blue	39.33	7.02	n/a	n/a	n/a	n/a	1336607
687.36	x	0	0	n/a	n/a	n/a	n/a	449413
687.47	x	0	0	(7Z,19R,31R)-22,25,28-Trihydroxy-22,28-dioxido-16,34-dioxo-31-(palmitoyloxy)-17,21,23,27,29,33-hexaoxa-22lambda~5~,28lambda~5~-diphosphanonatetracont-7-en-19-yl (11Z)-11-octadecenoate	C75H142O17P2		-7.56	195876
688.49	Green	53.33	8.96	n/a	n/a	n/a	n/a	1080630
688.67	x	0	0	n/a	n/a	n/a	n/a	100704
688.95	x	0	0	n/a	n/a	n/a	n/a	27430
690.33	x	0	0	n/a	n/a	n/a	n/a	23170
690.47	Cyan	117.33	14.47	n/a	n/a	n/a	n/a	13377033
690.69	x	0	0	n/a	n/a	n/a	n/a	63140
691.18	x	0	0	n/a	n/a	n/a	n/a	162202
691.46	Cyan	53.33	5.03	n/a	n/a	n/a	n/a	6886111
692.16	x	0	0	n/a	n/a	n/a	n/a	53993
692.96	x	0	0	n/a	n/a	n/a	n/a	19465
693.18	x	0	0	n/a	n/a	n/a	n/a	84277
693.47	Cyan	33.96	11.39	n/a	n/a	n/a	n/a	8945784
694.47	Cyan	15.2	3.64	n/a	n/a	n/a	n/a	1692528
694.48	x	0	0	(19R,31R)-22,25,28-Trihydroxy-22,28-dioxido-16,34-dioxo-31-(palmitoyloxy)-17,21,23,27,29,33-hexaoxa-22lambda~5~,28lambda~5~-diphosphanonatetracontan-19-yl (9Z,12Z)-9,12-nonadecadienoate	C76H144O17P2	M-2H	-8.33	164457
694.99	x	0	0	n/a	n/a	n/a	n/a	144313
695.17	x	0	0	n/a	n/a	n/a	n/a	102247

695.31	x	0	0	n/a	n/a	n/a	n/a	32851
695.45	Cyan	5	1	n/a	n/a	n/a	n/a	773879
696.19	x	0	0	Amidepsine G	C34H37NO16	M-H2O-H	-8.99	760016
696.27	x	0	0	n/a	n/a	n/a	n/a	61075
696.37	Cyan	36	7	n/a	n/a	n/a	n/a	971169
696.5	Yellow	47.33	9.5	n/a	n/a	n/a	n/a	875459
696.63	x	0	0	n/a	n/a	n/a	n/a	230517
696.98	x	0	0	n/a	n/a	n/a	n/a	104254
697.3	x	0	0	N-(15-Benzyl-10-sec-butyl-14-hydroxy-3-isopropyl-7,13,13-trimethyl-2,5,9,12-tetraoxo-1,4,8,11-tetraoxacyclopentadecan-6-yl)-3-formamido-2-hydroxybenzamide	C36H46N2O12	M-H	2.15	414074
697.36	Cyan	40.33	5.03	n/a	n/a	n/a	n/a	686835
698.04	x	0	0	n/a	n/a	n/a	n/a	11047
698.13	x	0	0	n/a	n/a	n/a	n/a	72491
698.48	Green	39.33	7.51	n/a	n/a	n/a	n/a	927617
699.4	x	0	0	n/a	n/a	n/a	n/a	2945558
700.14	x	0	0	n/a	n/a	n/a	n/a	149187
700.49	Blue	47.33	11.37	n/a	n/a	n/a	n/a	982944
700.99	x	0	0	n/a	n/a	n/a	n/a	419932
701.5	Blue	23.33	7.57	(19R,31R,44Z)-22,25,28-Trihydroxy-22,28-dioxido-16,34-dioxo-19-(palmitoyloxy)-17,21,23,27,29,33-hexaoxa-22lambda~5~,28lambda~5~-diphosphahenpentacont-44-en-31-yl (11Z)-11-octadecenoate	C77H146O17P2	M-2H	-7.68	201699
701.64	x	0	0	n/a	n/a	n/a	n/a	152120
702.12	x	0	0	n/a	n/a	n/a	n/a	124935
702.5	Green	123.3	9.71	n/a	n/a	n/a	n/a	6150700
703.18	x	0	0	n/a	n/a	n/a	n/a	278378
703.34	x	0	0	n/a	n/a	n/a	n/a	41846
703.48	Green	46.52	47.1	n/a	n/a	n/a	n/a	1336962
705.47	Green	112.88	38.5	n/a	n/a	n/a	n/a	9103122
706.47	Green	73.11	38.54	n/a	n/a	n/a	n/a	1197726
707.19	x	0	0	n/a	n/a	n/a	n/a	240655
707.47	Green	91.24	33.99	n/a	n/a	n/a	n/a	147079
708.48	Green	45.82	22.46	n/a	n/a	n/a	n/a	539344
709.48	Green	17	4.58	n/a	n/a	n/a	n/a	381431
710.22	x	0	0	n/a	n/a	n/a	n/a	201266
711.38	Cyan	40	5.29	n/a	n/a	n/a	n/a	813958
711.75	x	0	0	n/a	n/a	n/a	n/a	185252
712.17	x	0	0	n/a	n/a	n/a	n/a	466398
713.32	x	0	0	n/a	n/a	n/a	n/a	225934
713.47	x	0	0	coleneuramide	C39H68N2O8	M+Na-2H	-5.86	19296

713.66	x	0	0	n/a	n/a	n/a	n/a	221912
714.04	x	0	0	UDP-N-acetyl-3-O-(1-carboxyvinyl)-D-glucosamine	C20H29N3O19P2	M+K-2H	2.37	31466
714.49	Green	23.95	7.19	(7Z,20R,32R,45Z)-23,26,29-Trihydroxy-23,29-dioxido-18,35-dioxo-20-[(palmitoyloxy)methyl]-19,22,24,28,30,34-hexaoxa-23lambda~5~,29lambda~5~-diphosphadopentaconta-7,45-dien-32-yl (11Z)-11-octadecenoate	C79H148O17P2	M-2H	-8.17	163052
716.07	x	0	0	n/a	n/a	n/a	n/a	124182
716.17	x	0	0	n/a	n/a	n/a	n/a	59385
717.47	Green	53	37.75	Phosphatidylglycerol(16:1/16:1)	C38H71O10P	M-H	1.61	1866563
718.74	x	0	0	n/a	n/a	n/a	n/a	272163
719.49	Green	125.49	8.47	n/a	n/a	n/a	n/a	15206300
719.71	x	0	0	n/a	n/a	n/a	n/a	39570
720.49	Green	118.56	14.02	n/a	n/a	n/a	n/a	5430073
721.49	Green	108.72	9.88	n/a	n/a	n/a	n/a	1519774
722.49	Green	42.08	22.79	n/a	n/a	n/a	n/a	21834
723.47	Green	6.2	1.16	n/a	n/a	n/a	n/a	499452
724.3	x	0	0	3-Formyl Rifamycin SV	C38H47NO13	M-H	6.65	106657
724.95	x	0	0	n/a	n/a	n/a	n/a	19599
725.42	Cyan	22.6	7.91	n/a	n/a	n/a	n/a	709055
726.1	x	0	0	n/a	n/a	n/a	n/a	48404
726.17	x	0	0	n/a	n/a	n/a	n/a	919778
726.42	x	0	0	n/a	n/a	n/a	n/a	19189
726.95	x	0	0	n/a	n/a	n/a	n/a	5417
727.16	x	0	0	n/a	n/a	n/a	n/a	73023
727.37	Cyan	15.44	6.79	n/a	n/a	n/a	n/a	1209048
727.5	x	0	0	n/a	n/a	n/a	n/a	90030
728.51	Green	78.99	22.72	(2R)-3-{[(2-Aminoethoxy)(hydroxy)phosphoryl]oxy}-2-[(1Z)-1-hexadecen-1-yloxy]propyl (4Z,7Z,10Z,13Z,16Z,19Z)-4,7,10,13,16,19-docosahexaenoate	C43H74NO7P	M-H2O-H	5.46	927659
728.73	x	0	0	n/a	n/a	n/a	n/a	153003
730.49	x	0	0	n/a	n/a	n/a	n/a	3300408
731.49	Green	39.72	19.4	n/a	n/a	n/a	n/a	1658298
733.5	Green	142	17.63	Phosphatidylglycerol(16:0/17:1)	C39H75O10P	M-H	3.48	12550294
734.14	x	0	0	n/a	n/a	n/a	n/a	203787
734.5	Green	136.57	25.61	n/a	n/a	n/a	n/a	19881
735.5	Green	130.56	9.17	n/a	n/a	n/a	n/a	1490050
735.68	x	0	0	n/a	n/a	n/a	n/a	148112
736.13	x	0	0	n/a	n/a	n/a	n/a	374720
736.45	Cyan	74.59	8.77	n/a	n/a	n/a	n/a	2055194
737.16	x	0	0	n/a	n/a	n/a	n/a	136544

737.45	Cyan	52.82	5.14	Spirangien A	C41H66O9	M+Cl	9.27	1167494
738.95	x	0	0	n/a	n/a	n/a	n/a	20313
739.43	Cyan	43.91	7.5	n/a	n/a	n/a	n/a	1280523
740.2	x	0	0	n/a	n/a	n/a	n/a	497743
740.45	Cyan	34.33	6.03	n/a	n/a	n/a	n/a	19557748
740.72	x	0	0	n/a	n/a	n/a	n/a	124052
741.15	x	0	0	n/a	n/a	n/a	n/a	23391
742.14	x	0	0	n/a	n/a	n/a	n/a	423454
742.31	x	0	0	n/a	n/a	n/a	n/a	64994
742.52	Green	48.82	5.07	n/a	n/a	n/a	n/a	442628
742.96	x	0	0	n/a	n/a	n/a	n/a	22161
743.49	Green	2.7	1.52	n/a	n/a	n/a	n/a	455579
744.3	x	0	0	n/a	n/a	n/a	n/a	135585
745.21	x	0	0	n/a	n/a	n/a	n/a	205363
745.48	x	0	0	1-Stearoyl-2-arachidonoyl-sn-glycero-3-phosphate	C41H73O8P	M+Na-2H	-3.86	4080619
745.5	Green	135.1	16.69	n/a	n/a	n/a	n/a	4741776
747.51	x	0	0	Azithromycin	C38H72N2O12	M-H	8.8	8449174
747.52	Green	127.24	22.97	Phosphatidylglycerol(16:0/18:1)	C40H11O10P	M-H	2.54	6307818
747.74	x	0	0	n/a	n/a	n/a	n/a	53529
748.2	x	0	0	n/a	n/a	n/a	n/a	564819
748.52	Green	111.69	35.04	n/a	n/a	n/a	n/a	2901563
748.63	x	0	0	n/a	n/a	n/a	n/a	540291
749.52	Green	86.33	29.75	n/a	n/a	n/a	n/a	960105
750.34	x	0	0	n/a	n/a	n/a	n/a	930680
750.47	Cyan	52.38	11.67	n/a	n/a	n/a	n/a	1299697
751.46	Cyan	34.67	5.88	Spirangien B	C42H68O9	M+Cl	1.46	702605
753.14	x	0	0	n/a	n/a	n/a	n/a	139941
753.46	Cyan	67.45	13.85	n/a	n/a	n/a	n/a	2636861
754.46	Cyan	39.11	8.88	n/a	n/a	n/a	n/a	910831
755.46	Cyan	14.98	4.32	n/a	n/a	n/a	n/a	625152
756.14	x	0	0	n/a	n/a	n/a	n/a	231439
757.48	Green	3	1	n/a	n/a	n/a	n/a	1664553
758.12	x	0	0	n/a	n/a	n/a	n/a	322537
758.31	x	0	0	n/a	n/a	n/a	n/a	15165
759.25	x	0	0	n/a	n/a	n/a	n/a	231579
759.41	x	0	0	bisglaucumlide C	C43H62O10	M+Na-2H	7.01	959458
759.52	Green	143.87	10.33	n/a	n/a	n/a	n/a	1758971
759.57	x	0	0	n/a	n/a	n/a	n/a	2587616
761.53	Green	141.82	15.51	n/a	n/a	n/a	n/a	6486586
762.15	x	0	0	n/a	n/a	n/a	n/a	236225
762.22	x	0	0	n/a	n/a	n/a	n/a	311720

762.53	Green	143.72	6.26	n/a	n/a	n/a	n/a	2416082
763.33	x	0	0	n/a	n/a	n/a	n/a	12523283
763.53	Green	97.79	9.55	n/a	n/a	n/a	n/a	33587
763.63	x	0	0	n/a	n/a	n/a	n/a	112038
764.13	x	0	0	n/a	n/a	n/a	n/a	432766
764.29	x	0	0	O-Phosphoviomycin	C25H44N13O13P	M-H	6.69	19133
765.47	Cyan	23.12	3.18	n/a	n/a	n/a	n/a	573465
767.21	x	0	0	n/a	n/a	n/a	n/a	143319
767.49	Cyan	25.88	11.46	n/a	n/a	n/a	n/a	3030700
768.13	x	0	0	n/a	n/a	n/a	n/a	218035
768.49	Cyan	24.77	6.33	n/a	n/a	n/a	n/a	958321
769.48	Cyan	17.44	9.64	n/a	n/a	n/a	n/a	498733
770.13	x	0	0	n/a	n/a	n/a	n/a	345989
771.49	Green	4	1	n/a	n/a	n/a	n/a	450183
771.62	x	0	0	2-Hydroxy-3-(icosanoyloxy)propyl (15Z)-15-tetracosenoate	C47H90O5	M+K-2H	-7.95	176928
773.53	Green	124.46	20.06	n/a	n/a	n/a	n/a	5757002
773.76	x	0	0	n/a	n/a	n/a	n/a	17593
774.53	Green	115.41	17.23	n/a	n/a	n/a	n/a	2515371
775.54	Green	123.27	9.85	n/a	n/a	n/a	n/a	1310346
775.65	x	0	0	n/a	n/a	n/a	n/a	218239
777.5	Green	23.67	12.1	n/a	n/a	n/a	n/a	425355
778.69	Blue	32	3.61	n/a	n/a	n/a	n/a	149912
778.94	x	0	0	n/a	n/a	n/a	n/a	107587
779.28	x	0	0	n/a	n/a	n/a	n/a	8297
779.47	Cyan	22.59	4	n/a	n/a	n/a	n/a	2644
780.11	x	0	0	n/a	n/a	n/a	n/a	282777
781.48	Cyan	85.64	8.92	n/a	n/a	n/a	n/a	4876096
782.48	Cyan	62.15	3.65	n/a	n/a	n/a	n/a	1255660
783.47	Cyan	24.54	2.39	n/a	n/a	n/a	n/a	654208
785.17	Black	9	1	n/a	n/a	n/a	n/a	372067
787.14	x	0	0	n/a	n/a	n/a	n/a	98012
787.26	x	0	0	n/a	n/a	n/a	n/a	489445
787.55	Green	124.16	14.33	n/a	n/a	n/a	n/a	4050308
788.55	Green	114.63	15.41	n/a	n/a	n/a	n/a	1045352
788.65	x	0	0	n/a	n/a	n/a	n/a	44166
789.54	Green	72.88	14.55	n/a	n/a	n/a	n/a	11484
789.78	x	0	0	n/a	n/a	n/a	n/a	15944
790.12	x	0	0	n/a	n/a	n/a	n/a	452420
790.69	Body	0.67	0.58	n/a	n/a	n/a	n/a	933688
791.48	Cyan	1.33	0.58	n/a	n/a	n/a	n/a	368105
792.71	Blue	58.33	9.76	n/a	n/a	n/a	n/a	2576257

793.71	Blue	37.09	12.06	n/a	n/a	n/a	n/a	1675945
795.5	Purple	27.13	5.74	n/a	n/a	n/a	n/a	2469764
796.5	Purple	13.08	1.87	n/a	n/a	n/a	n/a	528565
796.93	x	0	0	n/a	n/a	n/a	n/a	16412
797.46	Cyan	12.94	4.51	n/a	n/a	n/a	n/a	229495
798.13	x	0	0	n/a	n/a	n/a	n/a	316141
798.93	x	0	0	n/a	n/a	n/a	n/a	24964
799.44	Cyan	23.01	8.55	n/a	n/a	n/a	n/a	790343
799.94	x	0	0	n/a	n/a	n/a	n/a	81235
800.03	x	0	0	n/a	n/a	n/a	n/a	18080
800.28	x	0	0	n/a	n/a	n/a	n/a	22169
801.28	x	0	0	n/a	n/a	n/a	n/a	432721
801.5	x	0	0	(3xi)-1-O-[(2E,4E,6E,8E,10E,12E,14E,16E,18E,20E,22E)-23-Carboxy-2,6,10,15,19-pentamethyl-2,4,6,8,10,12,14,16,18,20,22-tetracosaundecaenoyl]-2-O-(12-methyltridecanoyl)-D-erythro-pentopyranose	C49H70O9	M-H	1.46	751241
801.55	Green	64.67	23.5	n/a	n/a	n/a	n/a	687193
803.17	Blue	87	17.29	n/a	n/a	n/a	n/a	610081
803.49	x	0	0	Tacrolimus	C44H69NO12	M-	3.87	967133
804.17	Blue	26.77	19.27	n/a	n/a	n/a	n/a	559819
805.41	x	0	0	N-Methyl-N-(10-methylundecanoyl)-D-seryl-D-alanyl-N-[(7S,10S,13S)-13-carboxy-3,18-dihydroxy-10-methyl-8,11-dioxo-9,12-diazatricyclo[13.3.1.1~2,6~]icosa-1(19),2(20),3,5,15,17-hexaen-7-yl]-N-methylglyci namide	C42H60N6O11	M-H2O-H	-6.83	7336013
806.11	x	0	0	n/a	n/a	n/a	n/a	248447
806.21	x	0	0	n/a	n/a	n/a	n/a	27704
806.71	Blue	17.2	7.82	n/a	n/a	n/a	n/a	621205
807.03	x	0	0	n/a	n/a	n/a	n/a	9877
807.11	x	0	0	n/a	n/a	n/a	n/a	64158
807.29	x	0	0	n/a	n/a	n/a	n/a	15821
807.63	x	0	0	n/a	n/a	n/a	n/a	74427
808.52	x	0	0	n/a	n/a	n/a	n/a	2550828
808.61	Green	56.27	48.02	(2R)-3-{[(2-Aminoethoxy)(hydroxy)phosphoryl]oxy}-2-[(1Z)-1-octadecen-1-yloxy]propyl docosanoate	C45H90NO7P	M+Na-2H	1.58	69676
808.95	x	0	0	n/a	n/a	n/a	n/a	16974
809.14	x	0	0	n/a	n/a	n/a	n/a	52738
809.29	x	0	0	n/a	n/a	n/a	n/a	41038
809.99	x	0	0	n/a	n/a	n/a	n/a	432810
810.54	Blue	13.33	1.15	n/a	n/a	n/a	n/a	86976
810.78	x	0	0	n/a	n/a	n/a	n/a	76156

812.11	x	0	0	n/a	n/a	n/a	n/a	158923
813.44	Cyan	39.67	4.04	n/a	n/a	n/a	n/a	1253528
814.17	x	0	0	n/a	n/a	n/a	n/a	73091
814.45	Cyan	18.33	3.06	Myxochromid A2	C44H63N7O9	M-H2O-H	6.98	704755
816.29	Green	42	19.29	n/a	n/a	n/a	n/a	34025
816.79	x	0	0	n/a	n/a	n/a	n/a	270197
817.51	Yellow	80.33	88.91	n/a	n/a	n/a	n/a	14750752
817.76	x	0	0	n/a	n/a	n/a	n/a	57482
818.21	x	0	0	n/a	n/a	n/a	n/a	22000
819.15	Blue	48.67	8.62	n/a	n/a	n/a	n/a	423555
820.02	x	0	0	n/a	n/a	n/a	n/a	18238
820.27	x	0	0	n/a	n/a	n/a	n/a	25226
820.94	x	0	0	n/a	n/a	n/a	n/a	115783
821.28	x	0	0	Argyrin F	C40H44N10O9S1	M-H2O-H	6.4	9141
821.61	Green	40.67	21.46	n/a	n/a	n/a	n/a	9395
821.67	x	0	0	n/a	n/a	n/a	n/a	27801
822.62	x	0	0	N-[(2S,3R)-1-(beta-D-erythro-Hexopyranosyloxy)-3-hydroxy-2-octadecanyl]docosanamide	C46H91NO8	M+K-2H	0.27	65250
822.94	x	0	0	n/a	n/a	n/a	n/a	61041
822.96	Green	60	21.63	n/a	n/a	n/a	n/a	99544
823.24	x	0	0	n/a	n/a	n/a	n/a	307914
823.3	x	0	0	Argyrin A	C40H44N10O8S1	M-H	3.15	38276
824.56	Blue	43.77	14.37	n/a	n/a	n/a	n/a	715146
825.56	Blue	23.73	17.51	n/a	n/a	n/a	n/a	532158
826.56	Blue	6	2.65	n/a	n/a	n/a	n/a	390795
828.05	Blue	19.33	4.51	n/a	n/a	n/a	n/a	355856
830.29	Green	41	17.78	n/a	n/a	n/a	n/a	12393
830.96	x	0	0	c832	C84H125N15O20	M-2H	5.58	349370
831.5	Yellow	45.05	11.44	n/a	n/a	n/a	n/a	18341261
831.74	x	0	0	2,3-Dipalmito-1-olein	C53H100O6	M-H	-2.98	74536
832.5	Yellow	24.83	5.92	n/a	n/a	n/a	n/a	538266
833.51	Yellow	15.99	10.14	n/a	n/a	n/a	n/a	424995
835.28	x	0	0	n/a	n/a	n/a	n/a	19874
835.62	Green	35.86	12.4	n/a	n/a	n/a	n/a	408077
836.63	x	0	0	N-[(2S,3S,4R,8E)-1-(L-glycero-Hexopyranosyloxy)-3,4-dihydroxy-8-octadecen-2-yl]-2-hydroxydocosanamide	C46H89NO10	M+Na-2H	5.33	116776
836.96	Green	41.91	17.76	n/a	n/a	n/a	n/a	182702
837.3	x	0	0	n/a	n/a	n/a	n/a	73885
838.47	Cyan	1.33	2.31	n/a	n/a	n/a	n/a	430393
839.49	Cyan	1.33	0.58	n/a	n/a	n/a	n/a	450183
840.12	x	0	0	n/a	n/a	n/a	n/a	57682
841.14	Blue	19.67	4.51	n/a	n/a	n/a	n/a	326305

841.46	x	0	0	n/a	n/a	n/a	n/a	1090408
841.94	x	0	0	n/a	n/a	n/a	n/a	40276
842.94	x	0	0	1-[5-(2-Iodophenyl)-1,3,4-thiadiazol-2-yl]-3-phenylurea	C15H11IN4OS	2M-H	4.42	44789
844.3	Green	34	10.82	N-{[1-({1-({(E)-[5-(2,4-Dioxo-3,4-dihydro-1(2H)-pyrimidinyl)-4-hydroxydihydro-2(3H)-furanylidene]methyl}amino)-3-[(3-hydroxyphenylalanyl)(methyl)amino]-1-oxo-2-butanyl}amino)-4-methyl-1-oxo-2-pentanyl]carbamoyl}tryptophan	C41H51N9O11	M-H	1.41	36768
844.46	x	0	0	Myxochromid A3	C45H63N7O9	M-H	9.6	327387
845.48	Yellow	32.33	11.02	n/a	n/a	n/a	n/a	386473
846.18	x	0	0	n/a	n/a	n/a	n/a	322456
846.3	x	0	0	n/a	n/a	n/a	n/a	14639
847.49	x	0	0	n/a	n/a	n/a	n/a	2754314
848.22	x	0	0	n/a	n/a	n/a	n/a	348551
848.92	x	0	0	n/a	n/a	n/a	n/a	40360
849.28	x	0	0	precorrin-1	C41H46N4O16	M-H	-0.71	35472
850.28	x	0	0	n/a	n/a	n/a	n/a	309342
850.66	Yellow	43.38	14	(2R)-3-{[(2-Aminoethoxy)(hydroxy)phosphoryl]oxy}-2-(icosanoyloxy)propyl (13Z)-13-docosenoate	C47H92NO8P	M+Na-2H	1.14	186066
850.97	x	0	0	n/a	n/a	n/a	n/a	124077
851.3	x	0	0	n/a	n/a	n/a	n/a	89731
851.66	Yellow	29.07	4.26	n/a	n/a	n/a	n/a	1107343
853.53	Cyan	3.33	1.53	n/a	n/a	n/a	n/a	510236
855.51	Blue	7.67	5.03	n/a	n/a	n/a	n/a	358738
857.5	Yellow	3.67	1.53	n/a	n/a	n/a	n/a	268607
857.96	x	0	0	n/a	n/a	n/a	n/a	63696
858.3	x	0	0	n/a	n/a	n/a	n/a	47772
858.47	x	0	0	n/a	n/a	n/a	n/a	21362
858.63	x	0	0	n/a	n/a	n/a	n/a	30786
859.5	x	0	0	n/a	n/a	n/a	n/a	1608299
859.93	x	0	0	n/a	n/a	n/a	n/a	48383
861.14	Blue	14	1.73	n/a	n/a	n/a	n/a	312246
862.66	Yellow	49.58	5.02	n/a	n/a	n/a	n/a	1647707
863.29	x	0	0	n/a	n/a	n/a	n/a	93686
863.48	x	0	0	n/a	n/a	n/a	n/a	3262791
864.66	Yellow	53.09	7.02	n/a	n/a	n/a	n/a	1536538
864.97	x	0	0	2-(1,3-Dioxo-2,3-dihydro-1H-inden-2-yl)-6,8-quinolinedisulfonic acid	C18H11NO8S2	2M-H	-6.76	69056
865.31	x	0	0	n/a	n/a	n/a	n/a	57642
865.5	x	0	0	n/a	n/a	n/a	n/a	13253093
865.66	Yellow	24.48	7.46	n/a	n/a	n/a	n/a	673212
867.54	Yellow	6	4.36	n/a	n/a	n/a	n/a	440829

869.51	Purple	13	2.65	n/a	n/a	n/a	n/a	502688
871.08	x	0	0	n/a	n/a	n/a	n/a	196394
871.71	Green	43.67	4.25	n/a	n/a	n/a	n/a	398356
871.96	x	0	0	n/a	n/a	n/a	n/a	30921
872.3	x	0	0	n/a	n/a	n/a	n/a	36776
872.63	x	0	0	n/a	n/a	n/a	n/a	19166
873.5	Green	1.02	0.32	n/a	n/a	n/a	n/a	379631
873.68	x	0	0	n/a	n/a	n/a	n/a	104458
874.63	x	0	0	(2R)-3-{[(2-Aminoethoxy)(hydroxy)phosphoryl]oxy}-2-[(4Z,7Z,10Z,13Z,16Z)-4,7,10,13,16-docosapentaenoyloxy]propyl (15Z)-15-tetracosenoate	C51H90NO8P	M-H	-1.14	275387
876.58	x	0	0	n/a	n/a	n/a	n/a	1316384
876.66	Yellow	67.72	11.08	n/a	n/a	n/a	n/a	1772913
877.29	x	0	0	1,3,4,6-Tetra-O-acetylhex-2-ulofuranosyl 2,3,4-tri-O-acetyl-6-O-tritylhexopyranoside	C45H50O18	M-H	-2.73	35320
878.67	Yellow	51.84	3.47	n/a	n/a	n/a	n/a	866166
879.23	x	0	0	n/a	n/a	n/a	n/a	224080
879.5	x	0	0	n/a	n/a	n/a	n/a	4103805
879.67	Yellow	20.01	1.75	n/a	n/a	n/a	n/a	532158
880.43	x	0	0	N-{[(4S,7R,10S,13R,18R)-18-Benzyl-4-(1H-indol-3-ylmethyl)-7-isobutyl-10-isopropyl-5-methyl-3,6,9,12,19-pentaoxo-1,2,5,11-tetraazacyclononadecan-13-yl]carbamoyl}-L-isoleucine	C46H65N7O8	M+K-2H	-5.44	78792
881.55	Cyan	5	1	n/a	n/a	n/a	n/a	511674
882.57	Yellow	2	1	n/a	n/a	n/a	n/a	447305
883.55	Cyan	1	0	n/a	n/a	n/a	n/a	433992
886.56	Purple	30.58	8.17	(12R)-18-Amino-15-hydroxy-1-(3-methyl-5-pentyl-2-furyl)-15-oxido-9-oxo-10,14,16-trioxa-15lambda~5~-phosphaoctadecan-12-yl 13-(3,4-dimethyl-5-pentyl-2-furyl)tridecanoate	C48H84NO10P	M+Na-2H	5.78	28366603
886.81	x	0	0	n/a	n/a	n/a	n/a	161685
888.37	x	0	0	n/a	n/a	n/a	n/a	339088
888.56	Purple	3.69	1.47	n/a	n/a	n/a	n/a	448384
890.67	Yellow	56	11.53	n/a	n/a	n/a	n/a	1278748
892.3	Blue	64.69	8.54	Microsclerodermins (Cl)	C41H48ClN9O12	M-H	8.71	505923
893.3	Blue	28.98	8.83	n/a	n/a	n/a	n/a	374588
894.3	Blue	9.47	9.66	n/a	n/a	n/a	n/a	378667
894.5	x	0	0	n/a	n/a	n/a	n/a	3364438
896.64	Blue	1.67	1.53	n/a	n/a	n/a	n/a	400877
897.56	Yellow	4	1	n/a	n/a	n/a	n/a	336758
897.84	x	0	0	n/a	n/a	n/a	n/a	175288
899.54	Yellow	4	1	n/a	n/a	n/a	n/a	428234
901.18	Blue	15.33	12.66	coenzyme alpha-F420-3	C34H43N6O21P	M-H	7.94	754578

902.55	Green	2.33	2.08	n/a	n/a	n/a	n/a	464213
903.54	Green	0.67	0.58	n/a	n/a	n/a	n/a	475002
904.55	x	0	0	n/a	n/a	n/a	n/a	588449
905.25	x	0	0	n/a	n/a	n/a	n/a	162309
905.53	Cyan	7	4.58	n/a	n/a	n/a	n/a	520300
905.74	x	0	0	n/a	n/a	n/a	n/a	235694
906.56	x	0	0	n/a	n/a	n/a	n/a	3920941
906.7	Yellow	6.67	1.53	n/a	n/a	n/a	n/a	391515
908.82	x	0	0	n/a	n/a	n/a	n/a	134192
909.56	Cyan	5.67	0.58	n/a	n/a	n/a	n/a	404837
909.61	x	0	0	n/a	n/a	n/a	n/a	82706
909.9	x	0	0	n/a	n/a	n/a	n/a	102952
910.06	x	0	0	sulfoacetyl-CoA	C23H38N7O20P3S2	M+Na-2H	6.74	189733
911.58	Green	7	3.61	n/a	n/a	n/a	n/a	351172
912.58	Green	3.67	1.53	n/a	n/a	n/a	n/a	415277
913.55	Green	0.33	0.58	n/a	n/a	n/a	n/a	312967
914.55	Green	0.33	0.58	n/a	n/a	n/a	n/a	302511
916.52	x	0	0	n/a	n/a	n/a	n/a	711053
916.78	x	0	0	n/a	n/a	n/a	n/a	290108
917.16	Blue	9	5.57	(2Z,5E)-2-(Benzylimino)-5-(5-methoxy-3-methyl-1,3-benzothiazol-2(3H)-ylidene)-3-phenyl-1,3-thiazolidin-4-one	C25H21N3O2S2	2M-H	-9.06	291511
918.57	x	0	0	n/a	n/a	n/a	n/a	491243
918.69	Yellow	12.33	9.45	n/a	n/a	n/a	n/a	471766
920.58	x	0	0	n/a	n/a	n/a	n/a	3410962
921.72	Green	39.67	3.51	n/a	n/a	n/a	n/a	391875
923.14	Blue	25.89	14	n/a	n/a	n/a	n/a	436151
924.13	Blue	7.94	5.19	n/a	n/a	n/a	n/a	304314
925.56	Green	3.14	1.21	n/a	n/a	n/a	n/a	426074
926.05	x	0	0	n/a	n/a	n/a	n/a	105566
928.55	Green	1.75	0.66	n/a	n/a	n/a	n/a	302511
928.82	x	0	0	n/a	n/a	n/a	n/a	86947
929.56	Green	0.92	0.88	n/a	n/a	n/a	n/a	521018
930.56	Green	0.93	0.89	n/a	n/a	n/a	n/a	286546
932.6	x	0	0	n/a	n/a	n/a	n/a	303305
933.19	x	0	0	S-{1-[5-(6-Amino-9H-purin-9-yl)-4-hydroxy-3-(phosphonooxy)tetrahydro-2-furanyl]-3,5,9-trihydroxy-8,8-dimethyl-3,5-dioxido-10,14-dioxo-2,4,6-trioxa-11,15-diaza-3lambda~5~,5lambda~5~-diphosphaheptadecan-17-yl} 4-(1H-indol-3-yl)butanethioate	C33H47N8O17P3S	M-H2O-H	8.27	120247
933.54	Yellow	8.33	4.93	n/a	n/a	n/a	n/a	769941
934.54	Yellow	7.67	4.51	n/a	n/a	n/a	n/a	3553259
937.26	x	0	0	n/a	n/a	n/a	n/a	191269

939.12	Blue	24.67	10.69	n/a	n/a	n/a	n/a	458098
939.83	x	0	0	n/a	n/a	n/a	n/a	315289
940.68	Green	10.67	6.43	n/a	n/a	n/a	n/a	300347
942.57	Green	3.67	1.53	n/a	n/a	n/a	n/a	397636
943.64	x	0	0	n/a	n/a	n/a	n/a	1615933
945.11	Blue	17	8.89	n/a	n/a	n/a	n/a	405917
947.81	x	0	0	n/a	n/a	n/a	n/a	233814
948.6	x	0	0	n/a	n/a	n/a	n/a	2139632
948.71	Green	17.02	4.4	n/a	n/a	n/a	n/a	329910
949.15	x	0	0	n/a	n/a	n/a	n/a	27562
950.57	Green	2.43	1.69	n/a	n/a	n/a	n/a	409877
950.82	x	0	0	n/a	n/a	n/a	n/a	442711
952.57	x	0	0	n/a	n/a	n/a	n/a	2009578
952.73	Green	40.26	8.39	n/a	n/a	n/a	n/a	376749
955.57	Green	1.08	1.01	n/a	n/a	n/a	n/a	393675
958.81	x	0	0	n/a	n/a	n/a	n/a	382981
960.61	x	0	0	n/a	n/a	n/a	n/a	195355
961.09	Blue	21.67	11.24	n/a	n/a	n/a	n/a	579928
961.81	x	0	0	n/a	n/a	n/a	n/a	392967
962.61	x	0	0	n/a	n/a	n/a	n/a	1306996
964.57	Green	4.55	2.36	n/a	n/a	n/a	n/a	335676
966.58	Green	1.92	1.89	n/a	n/a	n/a	n/a	2828646
966.8	x	0	0	n/a	n/a	n/a	n/a	261615
967.66	Green	8.34	2.53	n/a	n/a	n/a	n/a	303232
969.8	x	0	0	n/a	n/a	n/a	n/a	419156
970.59	Green	2.1	1.15	n/a	n/a	n/a	n/a	323782
972.19	Blue	3.33	1.53	n/a	n/a	n/a	n/a	383592
972.79	x	0	0	n/a	n/a	n/a	n/a	411968
974.86	x	0	0	n/a	n/a	n/a	n/a	141019
975.64	x	0	0	n/a	n/a	n/a	n/a	1485681
976.8	x	0	0	n/a	n/a	n/a	n/a	517649
977.68	Green	2.67	1.53	n/a	n/a	n/a	n/a	299987
979.6	Green	4	2	n/a	n/a	n/a	n/a	335676
980.79	x	0	0	n/a	n/a	n/a	n/a	429472
982.58	x	0	0	n/a	n/a	n/a	n/a	1179993
983.22	Green	18.15	3.23	n/a	n/a	n/a	n/a	419596
984.29	x	0	0	n/a	n/a	n/a	n/a	127236
984.59	Green	1.63	0.55	n/a	n/a	n/a	n/a	428594
986.28	x	0	0	n/a	n/a	n/a	n/a	180744
987.24	Green	37.99	39.01	n/a	n/a	n/a	n/a	347569
989.54	x	0	0	n/a	n/a	n/a	n/a	2337708
989.66	Black	6.44	2.22	n/a	n/a	n/a	n/a	790701

990.3	x	0	0	n/a	n/a	n/a	n/a	294706
990.65	Black	5.34	2.09	n/a	n/a	n/a	n/a	414557
992.58	Green	5	3.61	n/a	n/a	n/a	n/a	420316
993.29	x	0	0	n/a	n/a	n/a	n/a	168421
994.03	x	0	0	n/a	n/a	n/a	n/a	62402
994.22	Green	15	7.55	n/a	n/a	n/a	n/a	432192
994.4	x	0	0	n/a	n/a	n/a	n/a	195639
994.6	x	0	0	n/a	n/a	n/a	n/a	253405
995.2	Green	6.67	1.53	n/a	n/a	n/a	n/a	352613
995.78	x	0	0	n/a	n/a	n/a	n/a	88693
996.78	x	0	0	n/a	n/a	n/a	n/a	175038
997.11	Blue	4	1	n/a	n/a	n/a	n/a	293135
998.58	Green	0.67	0.58	n/a	n/a	n/a	n/a	323422
999.29	x	0	0	n/a	n/a	n/a	n/a	347664
1002.33	x	0	0	n/a	n/a	n/a	n/a	400098
1002.74	Green	40.81	0.7	n/a	n/a	n/a	n/a	392235
1003.67	x	0	0	n/a	n/a	n/a	n/a	453899
1004.29	x	0	0	n/a	n/a	n/a	n/a	179550
1006.77	x	0	0	n/a	n/a	n/a	n/a	80760
1007.78	x	0	0	n/a	n/a	n/a	n/a	180830
1009.7	Green	18.43	5.67	n/a	n/a	n/a	n/a	275101
1010.28	x	0	0	n/a	n/a	n/a	n/a	291493
1012.26	Blue	12.59	11.38	n/a	n/a	n/a	n/a	417796
1014.24	Green	25.94	5.21	n/a	n/a	n/a	n/a	372427
1014.79	x	0	0	n/a	n/a	n/a	n/a	412079
1016.37	x	0	0	N~2~-Formyl-L-glutaminyl-N-[(2S,6S,9S,12S,16S,19E)-6-[(2S)-2-butanyl]-16-[(5-hydroxy-1H-indol-3-yl)methyl]-2-(methoxymethyl)-9-methyl-4,5,8,11,15,18-hexaoxo-23-thia-3,7,10,14,17,24-hexaazabicyclo[19.2.1]tetracosa-1(24),19,21-trien-12-yl]-L-isoleucinamide	C45H61N11O12S	M+K-2H	-3.66	170509
1020.28	x	0	0	n/a	n/a	n/a	n/a	146185
1021.5	x	0	0	1,2-dioctanoyl-sn-glycero-3-phosphoserine	C22H42NO10P	2M-H	0.18	165643
1021.72	Green	24.19	6.65	n/a	n/a	n/a	n/a	350451
1022.78	x	0	0	n/a	n/a	n/a	n/a	268715
1025.68	Green	9.13	2.71	n/a	n/a	n/a	n/a	334595
1025.91	x	0	0	n/a	n/a	n/a	n/a	262900
1026.28	x	0	0	n/a	n/a	n/a	n/a	203559
1030.77	x	0	0	n/a	n/a	n/a	n/a	215069
1032.7	Green	11.88	2.51	n/a	n/a	n/a	n/a	352613
1033.77	x	0	0	n/a	n/a	n/a	n/a	240294
1034.22	Blue	26.87	14.17	n/a	n/a	n/a	n/a	285201

1036.77	x	0	0	n/a	n/a	n/a	n/a	174660
1040.27	x	0	0	n/a	n/a	n/a	n/a	416741
1040.71	Green	18	3.11	n/a	n/a	n/a	n/a	444067
1046.78	x	0	0	n/a	n/a	n/a	n/a	98081
1049.77	x	0	0	n/a	n/a	n/a	n/a	325216
1050.18	Blue	15.01	4.4	n/a	n/a	n/a	n/a	346848
1051.99	x	0	0	n/a	n/a	n/a	n/a	86158
1053.53	x	0	0	1-O-[(3beta,5xi,9xi,18xi)-3-{[2-O-(6-Deoxy-alpha-L-mannopyranosyl)-L-arabinopyranosyl]oxy}-23,28-dioxoolean-12-en-28-yl]-6-O-beta-L-glucopyranosyl-L-glucopyranose	C53H84O22	M-H2O-H	-2.11	78116
1055.27	x	0	0	n/a	n/a	n/a	n/a	295064
1059.78	x	0	0	n/a	n/a	n/a	n/a	189890
1063.27	x	0	0	n/a	n/a	n/a	n/a	207341
1066.27	x	0	0	n/a	n/a	n/a	n/a	354583
1073.27	x	0	0	n/a	n/a	n/a	n/a	65815
1074.26	x	0	0	n/a	n/a	n/a	n/a	317865
1078.76	x	0	0	n/a	n/a	n/a	n/a	205893
1081.38	x	0	0	n/a	n/a	n/a	n/a	115993
1081.71	x	0	0	n/a	n/a	n/a	n/a	49650
1082.26	x	0	0	n/a	n/a	n/a	n/a	171583
1085.26	x	0	0	n/a	n/a	n/a	n/a	266565
1088.71	x	0	0	n/a	n/a	n/a	n/a	35387
1089.04	x	0	0	n/a	n/a	n/a	n/a	44553
1091.23	Green	15.05	3.49	n/a	n/a	n/a	n/a	322701
1092.77	x	0	0	n/a	n/a	n/a	n/a	356957
1093.69	x	0	0	n/a	n/a	n/a	n/a	39645
1094.03	x	0	0	n/a	n/a	n/a	n/a	73603
1094.37	x	0	0	n/a	n/a	n/a	n/a	32197
1101.69	x	0	0	n/a	n/a	n/a	n/a	10440
1107.5	x	0	0	Stalagmoside V	C55H82O24	M-H2O-H	1.03	365268
1108.86	x	0	0	n/a	n/a	n/a	n/a	231391
1109.53	Green	15.47	6.78	n/a	n/a	n/a	n/a	480037
1110.54	Green	8.97	5.63	n/a	n/a	n/a	n/a	399436
1112.25	x	0	0	n/a	n/a	n/a	n/a	117873
1124.78	x	0	0	n/a	n/a	n/a	n/a	107619
1126.84	x	0	0	n/a	n/a	n/a	n/a	144446
1131.51	Green	20.67	10.07	n/a	n/a	n/a	n/a	5912367
1132.27	x	0	0	n/a	n/a	n/a	n/a	105751
1133.53	Green	4.39	2.15	n/a	n/a	n/a	n/a	319096
1142.84	x	0	0	n/a	n/a	n/a	n/a	130752
1147.48	x	0	0	n/a	n/a	n/a	n/a	414024
1153.5	Green	10.49	6.69	Aesculioside IIe	C54H84O24	M+K-2H	-4.21	56747

1154.5	Green	4.94	2.55	n/a	n/a	n/a	n/a	300347
1158.79	x	0	0	n/a	n/a	n/a	n/a	214795
1192.84	x	0	0	n/a	n/a	n/a	n/a	134730
1197.45	x	0	0	n/a	n/a	n/a	n/a	145206

B1.2 Supplemental Figures

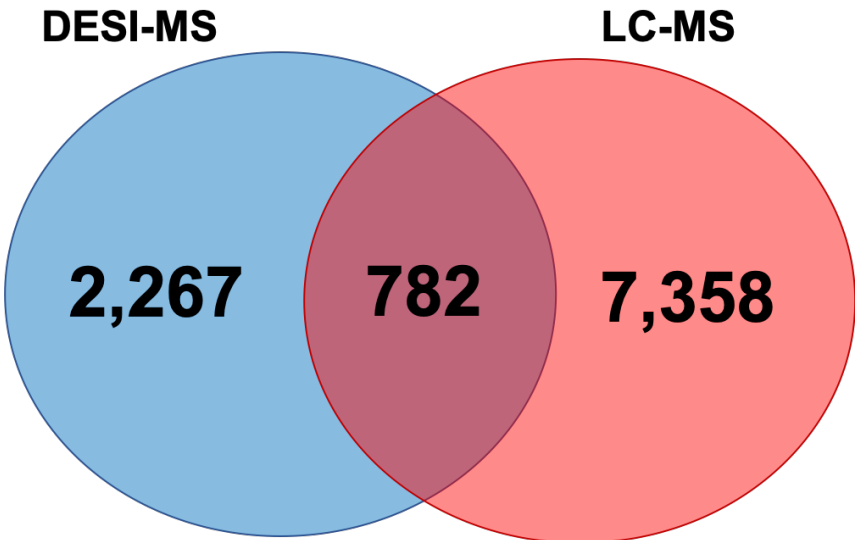

Figure B.1. Venn Diagram showing the number conserved and unique features between LC-MS and DESI-MS analysis of microbial co-cultures.

Acquisition parameters for the generated data:

Liquid chromatography-mass spectrometry (LC-MS) experiments were performed on a Waters Synapt G2 HDMS (Milford, MA, USA) mass spectrometer equipped with a Waters nanoAcquity UPLC system and autosampler (Milford, MA, USA). Metabolites were separated on a reverse phase 1 mm × 100 mm HSS T3 C_{18} column packed with 1.8-µm particles (Waters, Milford, MA, USA) held at 45°C. Liquid chromatography was performed using a 30-min gradient at a flow rate of 75 µL min^{-1} using mobile phase A (0.1% formic acid in H_2O) and mobile phase B (0.1% formic acid in ACN). The following elution gradient was used for analysis: 0 min, 99% A; 1 min, 99% A; 10 min, 40% A; 20 min, 1% A; 22 min, 1% A; 25 min, 99% A.

LC-MS analyses were run using high-resolution mode, with a capillary voltage of – 0.8 kV, source temperature at 100°C, sample cone voltage at 30 V, extraction cone voltage at 5 V, source gas flow of 400 mL min^{-1}, desolvation gas temperature of 325°C, and He cell flow of 180 mL min^{-1}. The data were acquired in negative ion mode from 50 to 2000 Da with a 1-s scan time; leucine enkephalin was used as the lock mass (*m/z* 554.2615). All analytes were analyzed using MS^E with an energy ramp from 10 to 40 eV and an injection volume of 5 µL.

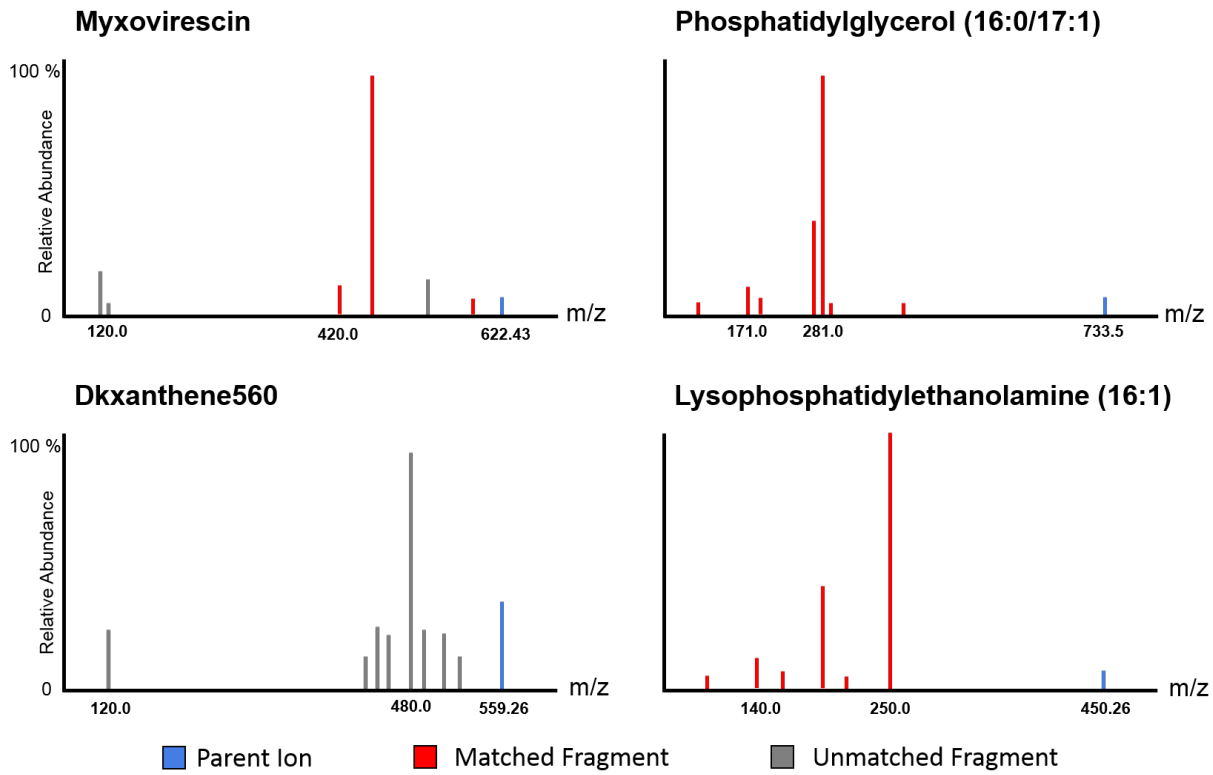

Figure B.2. Fragmentation spectra of identified metabolites

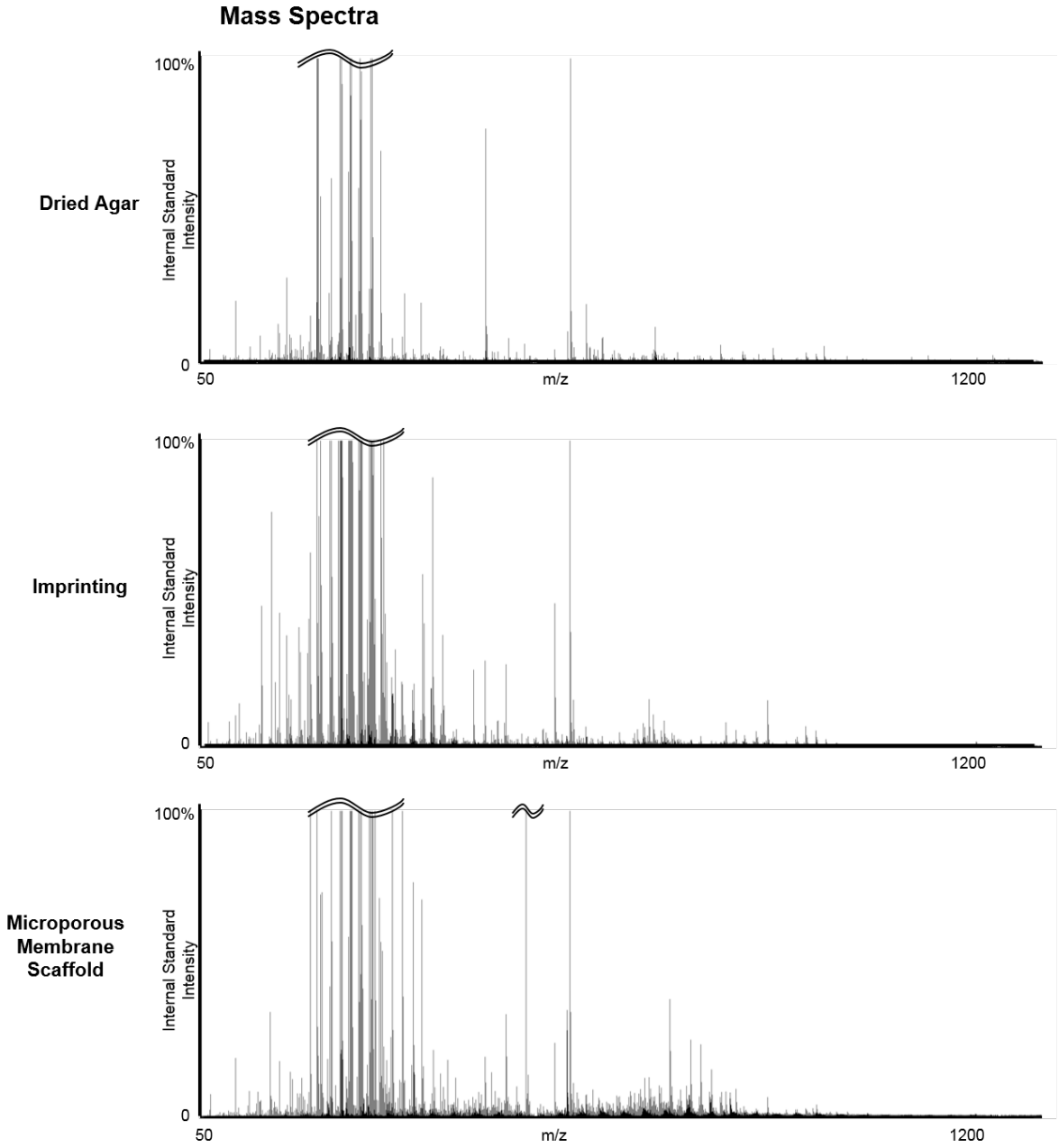

Figure B.3. Average mass spectra of dried agar, imprinting, and nylon membrane sampling methods. Intensities are shown with the internal standard and lock mass leucine-enkephalin (m/z 554.26) intensity representing 100%.

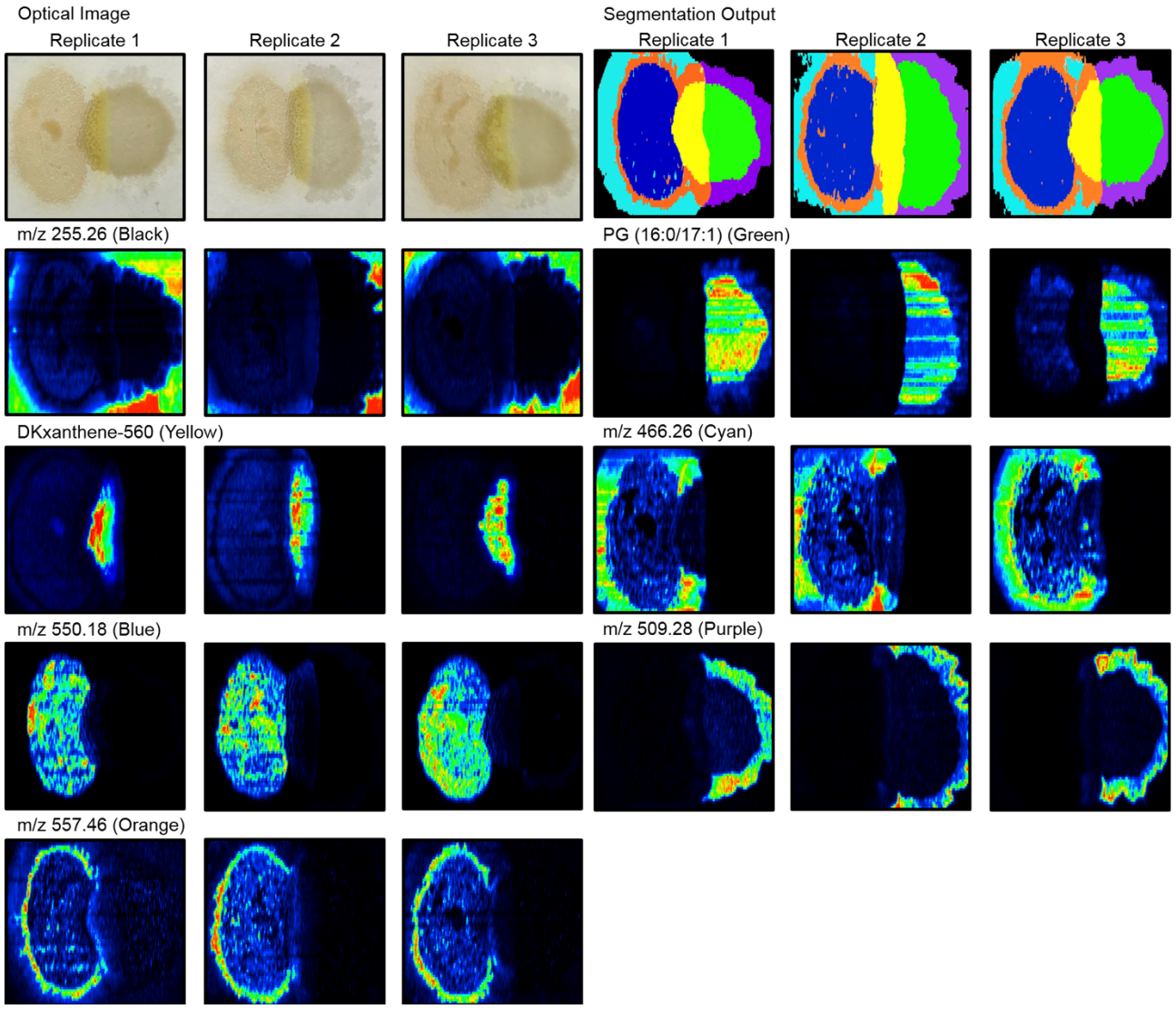

Figure B.4. Biological replicates of unsupervised segmentation from MMS DESI-IMS. The ion image of the primary contributing feature to each segment is shown across replicates with the segment denoted in parentheses by color.

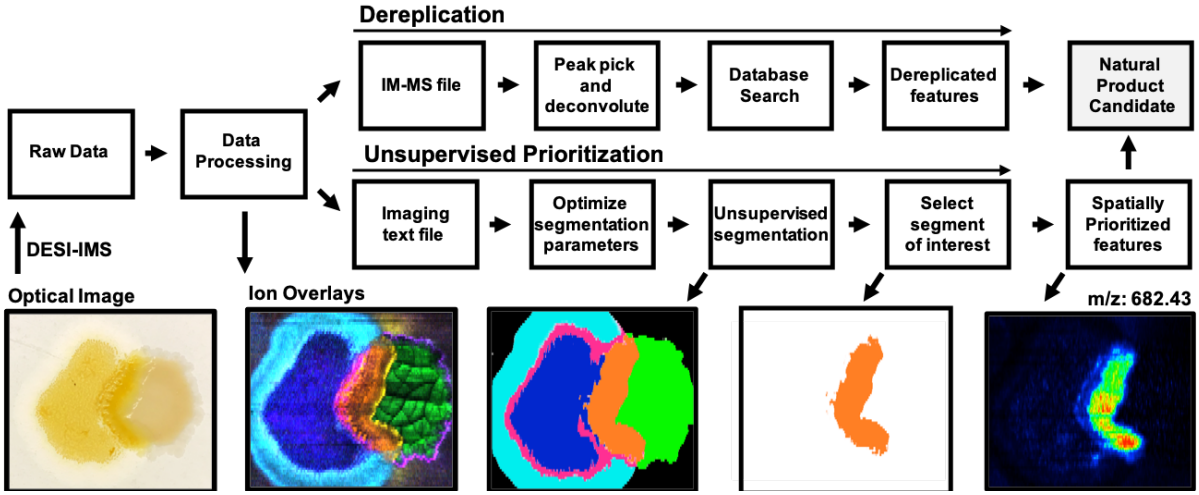

Figure B.5. Natural product discovery workflow using unsupervised segmentation and dereplication.

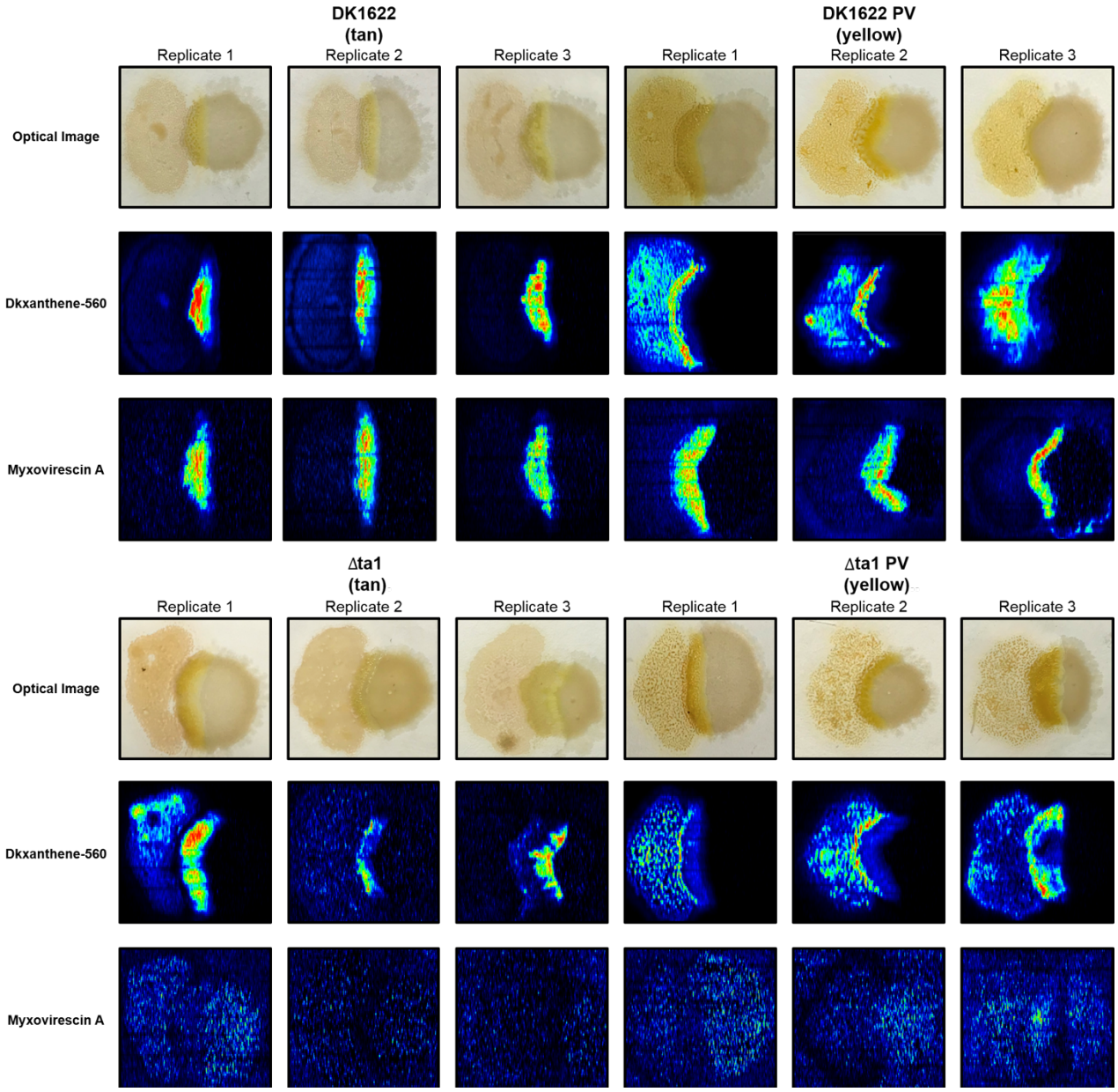

Figure B.6. Biological replicates of WT and *M. xanthus Δta1* strains and respective phase variants production of reported natural products Myxovirescin A and DKxanthene-560.

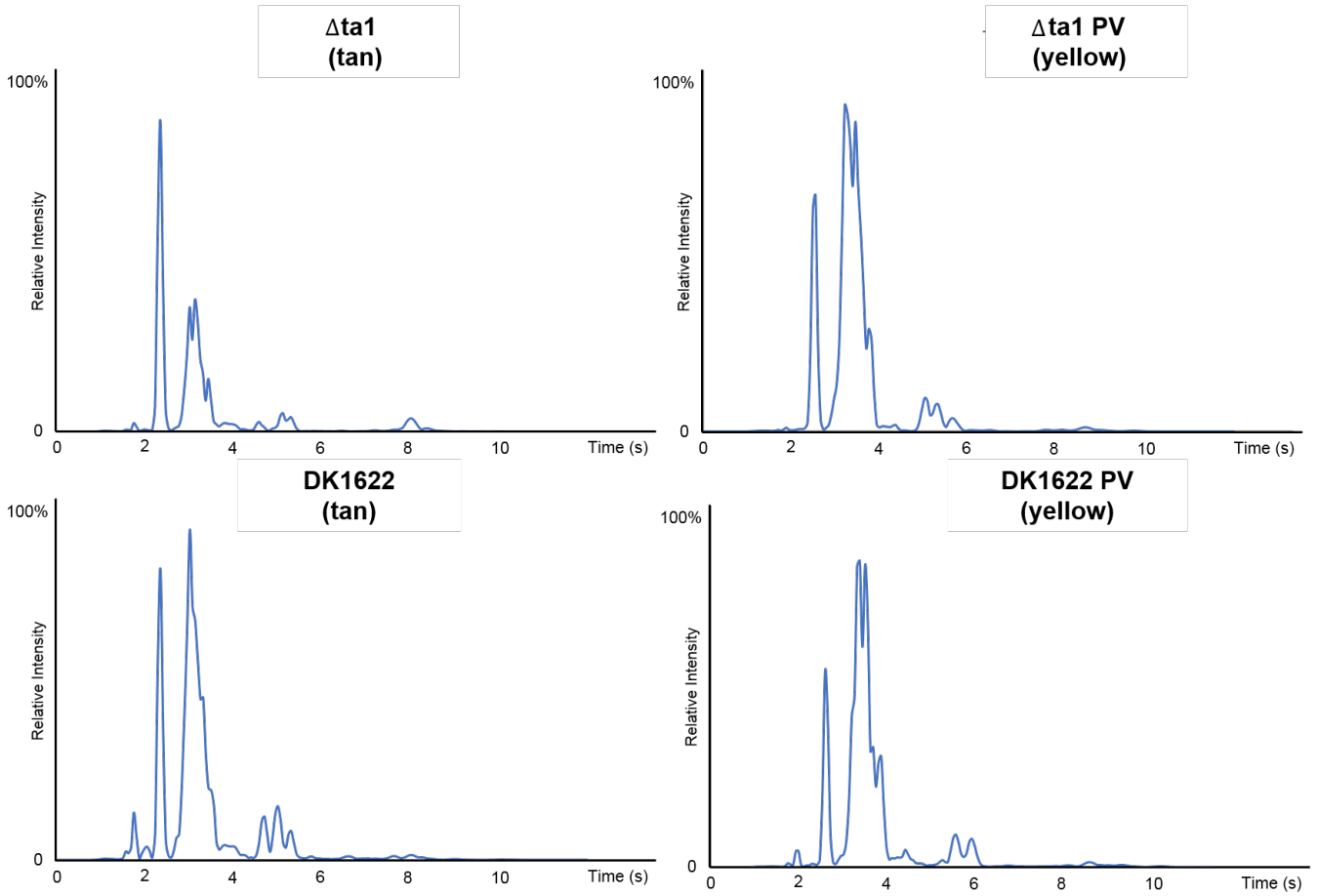

Figure B.7. Drift time vs relative intensity of WT and *M. xanthus* Δta1 and respective phase variants.

APPENDIX C

SUPPLEMENTARY MATERIALS FOR CHAPTER 3

Accelerating Strain Engineering using Desorption Electrospray Ionization-Imaging Mass Spectrometry and Untargeted Molecular Analysis of Intact Microbial Colonies.

Berkley M. Ellis,[1-5] Piyoosh Babele,[6] Jody C. May,[1-5] Carl H. Johnson,[7,8] Brian F. Pfleger,[9] Jamey D. Young,[6,7] and John A. McLean*[1-5]

[1]Department of Chemistry, Vanderbilt University, Nashville, TN USA; [2]Center for Innovative Technology, Vanderbilt University, Nashville, TN USA; [3]Institute of Chemical Biology, Vanderbilt University, Nashville, TN USA; [4]Institute for Integrative Biosystems Research and Education, Vanderbilt University, Nashville, TN USA ; [5]Vanderbilt-Ingram Cancer Center, Vanderbilt University, Nashville, TN USA; [6]Department of Chemical and Biomolecular Engineering, Vanderbilt University, Nashville, TN USA,; [7]Department of Molecular Physiology and Biophysics, Vanderbilt University, Nashville, TN USA; [8]Department of Biological Sciences, Vanderbilt University, Nashville, TN USA; [9]Department of Chemical and Biological Engineering, University of Wisconsin, Madison, WI USA

Abstract

Synthetic biology is no longer limited by reading and writing DNA, rather it is inhibited by what to write. Directed evolution and screening strain libraries are techniques proven to identify genetic sequences encoding enhanced performance. The previous bottleneck for these workflows were generating strain libraries, however the advances in genomic sciences have yielded technologies capable of generating libraries up to 10^{10} genetic variants. At a rate of 10^2 samples per day, the current rate-limiting step in synthetic biology workflows are analytical methods determining the resulting phenotypes. To address this issue, we have developed a desorption electrospray ionization-imaging mass spectrometry (DESI-IMS) screening assay that directly

samples microorganisms. This technology increases the throughput of metabolic measurements by reducing sample preparation and analyzing organisms in a multiplexed fashion. To further accelerate synthetic biology workflows, we utilized untargeted acquisitions and unsupervised analytics to provide multiple targets for future engineering strategies within a single acquisition. We demonstrate the utility of the developed method using *Escherichia coli* strains engineered to overproduce free fatty acids. Using unsupervised segmentation, we determined discrete metabolic phenotypes associated with each strain, which includes the primary product, relative production levels, and specificity within biosynthetic production. The determined metabolic phenotypes additionally detail the broader biology of the microorganisms. Within our *E. coli* panel, we measured changes in membrane lipid saturation, which affects cell viability. In sum, we present an analytical method to accelerate synthetic biology workflows through rapid, untargeted, and multiplexed analyses.

C.1.1 Supplemental Figures

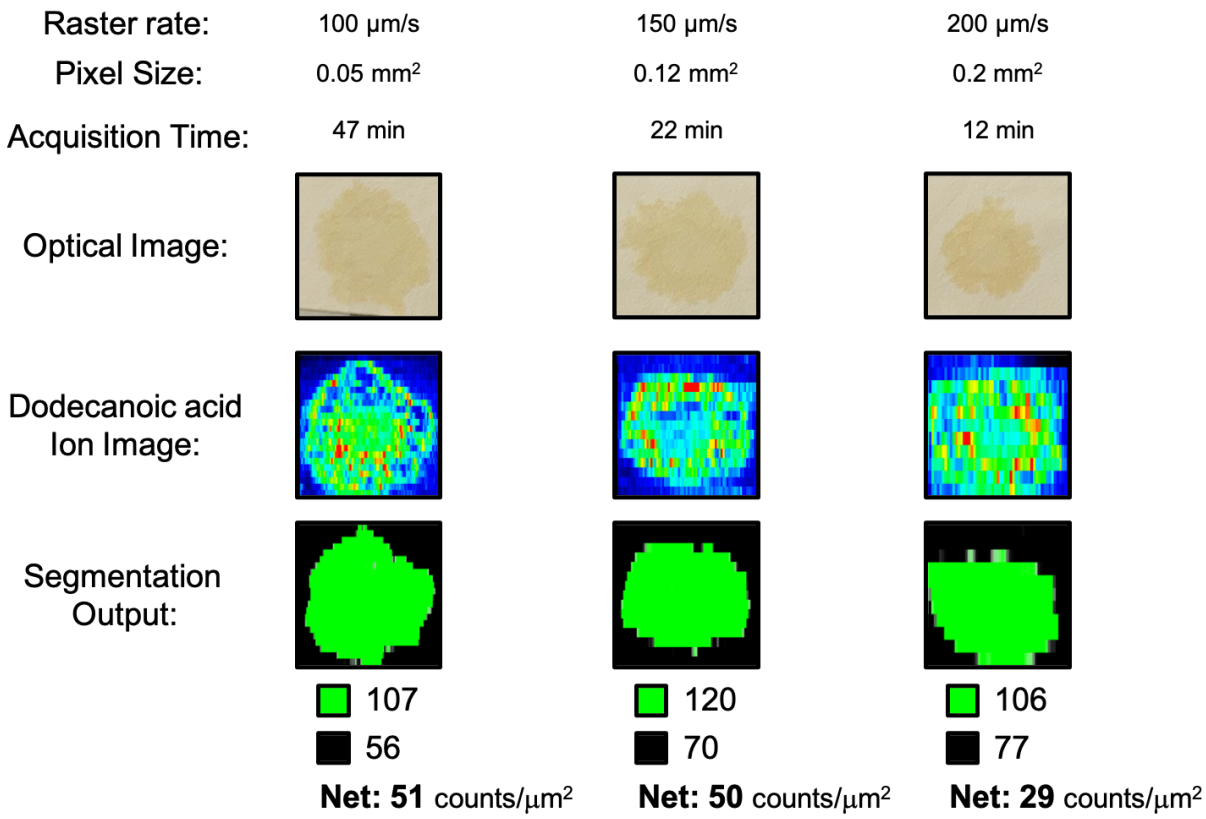

Figure C.1. Evaluation of raster rate on sampling time and dodecanoic acid measurement. Lower raster rates and smaller pixels equate to more resolved images, but longer acquisitions. Increasing raster rate from 100 µm/s to 150 µm/s had a negligible effect on the amount of dodecanoic acid measured from the colony when compared to the background (as defined by unsupervised segmentation). Increasing raster rate to 200 µm/s had an effect on measured amounts of dodecanoic acid.

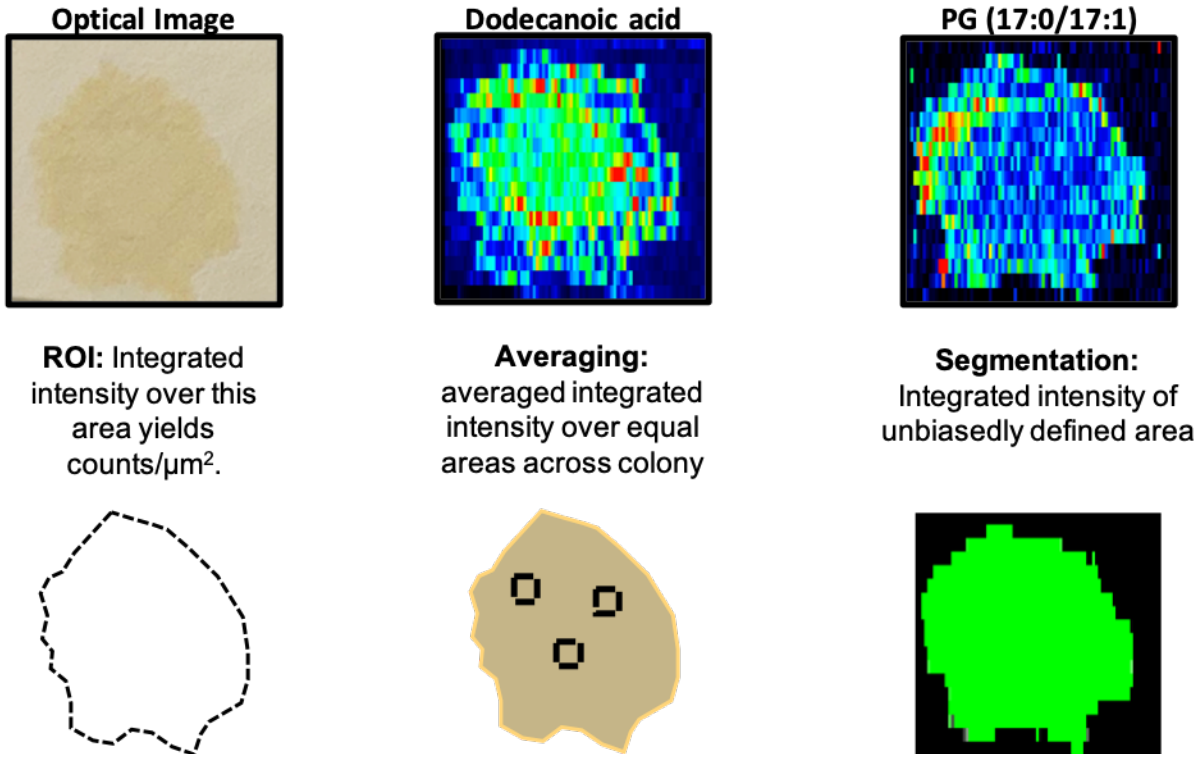

Data Analysis Method	Average Counts/μm² (n=3)	Signal-to-noise ratio	Net Counts/μm²
ROI	322.3 ± 11	29.3	216.7
Averaging	332.7 ± 27.3	12.2	243.8
Segmentation	333 ± 15	21.8	219.3

Figure C.2. We compared average counts/μm², signal-to-noise ratio, and net counts/μm² of dodecanoic acid from TY05 colonies using the three IMS data analytics methods represented above. Notably, we observe comparable results between segmentation and ROI averaging. While ROI has better performance metrics, it requires user input to define colony areas. Unsupervised segmentation achieves similar output while defining colony areas unbiasedly

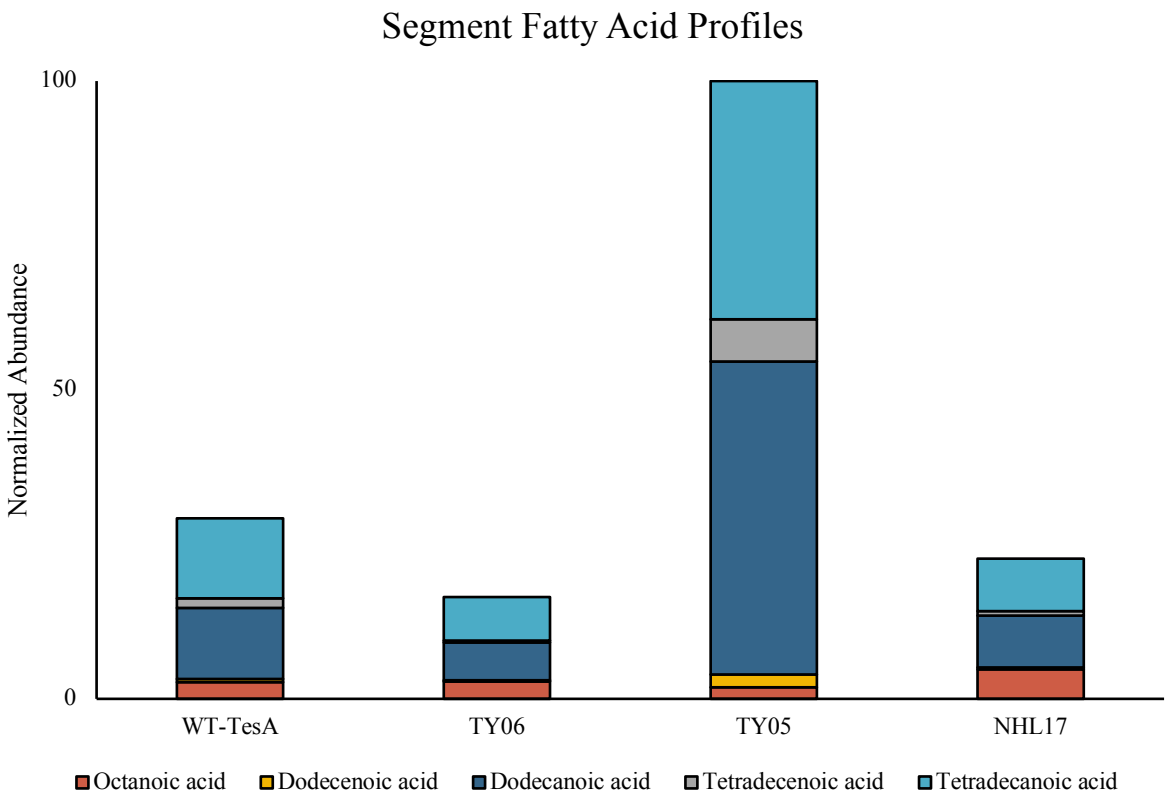

Figure C.3. Segment fatty acid profiles. The IMS areas associated with segments validated via PCR genotyping were integrated to yield comprehensive fatty acid profiles.

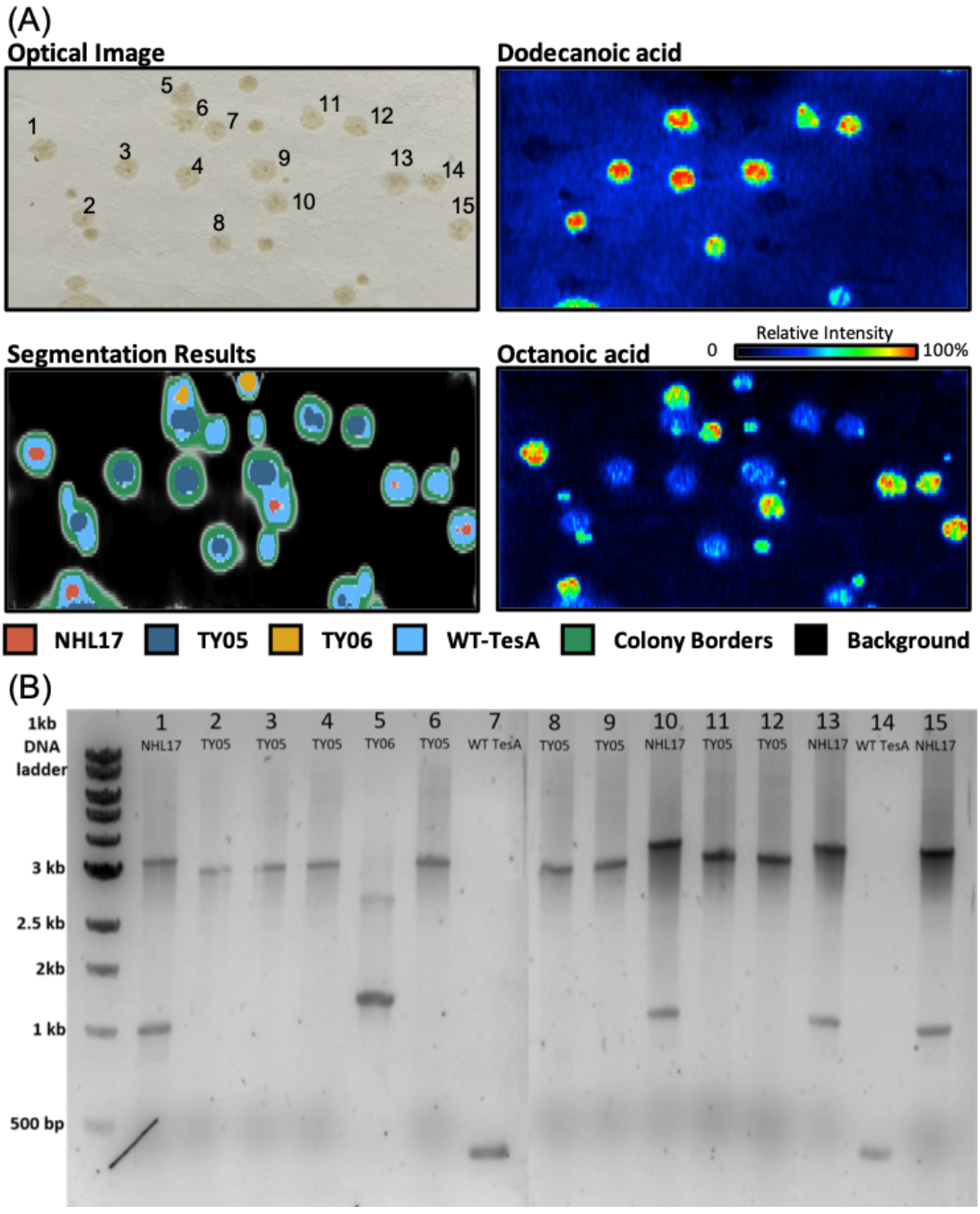

Figure C.4. Confirming unsupervised segmentation results using PCR genotyping. (A) Optical image highlighting colony numbers. Segmentation results highlight the colony areas and identities. Dodecanoic acid and Octanoic acid highlight the primary biosynthetic products contributing to phenotypes. (B) Numbered colonies were streaked on a fresh LB media plate. These replicate colonies were subjected to PCR genotyping instead of original colonies as DESI-IMS may perturb the sample integrity. Colonies that are not numbered formed after this picking process and thus were not analyzed via PCR analysis. PCR primers for each strain are found in Table C.1.

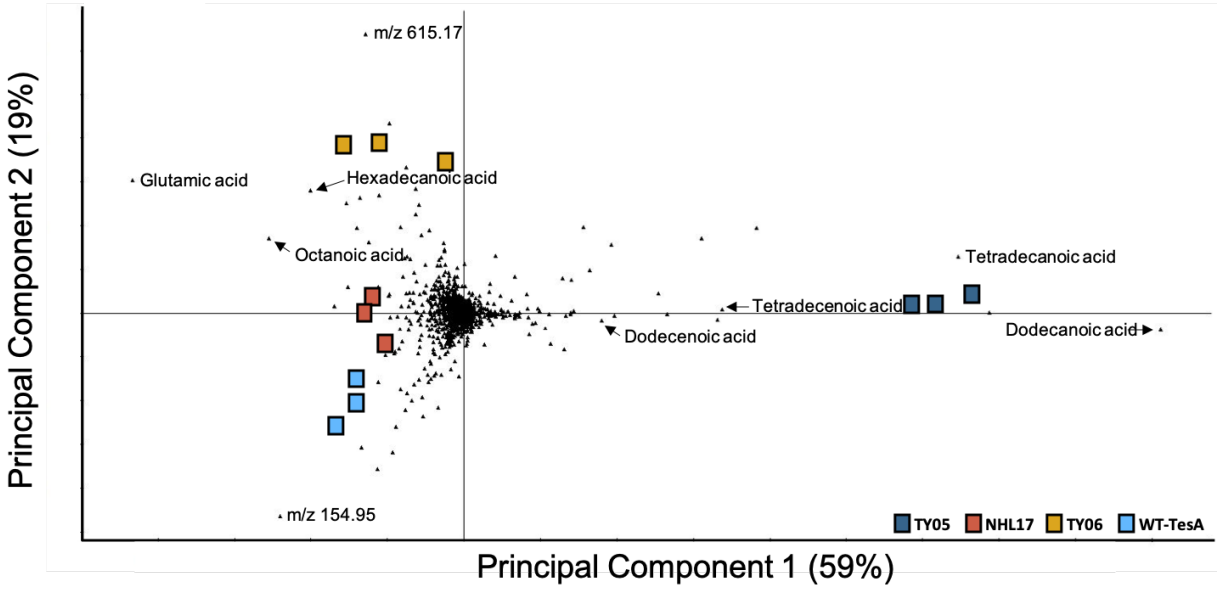

Figure C.5. PCA Loadings plot highlighting features contributing to strain metabolic phenotypes.

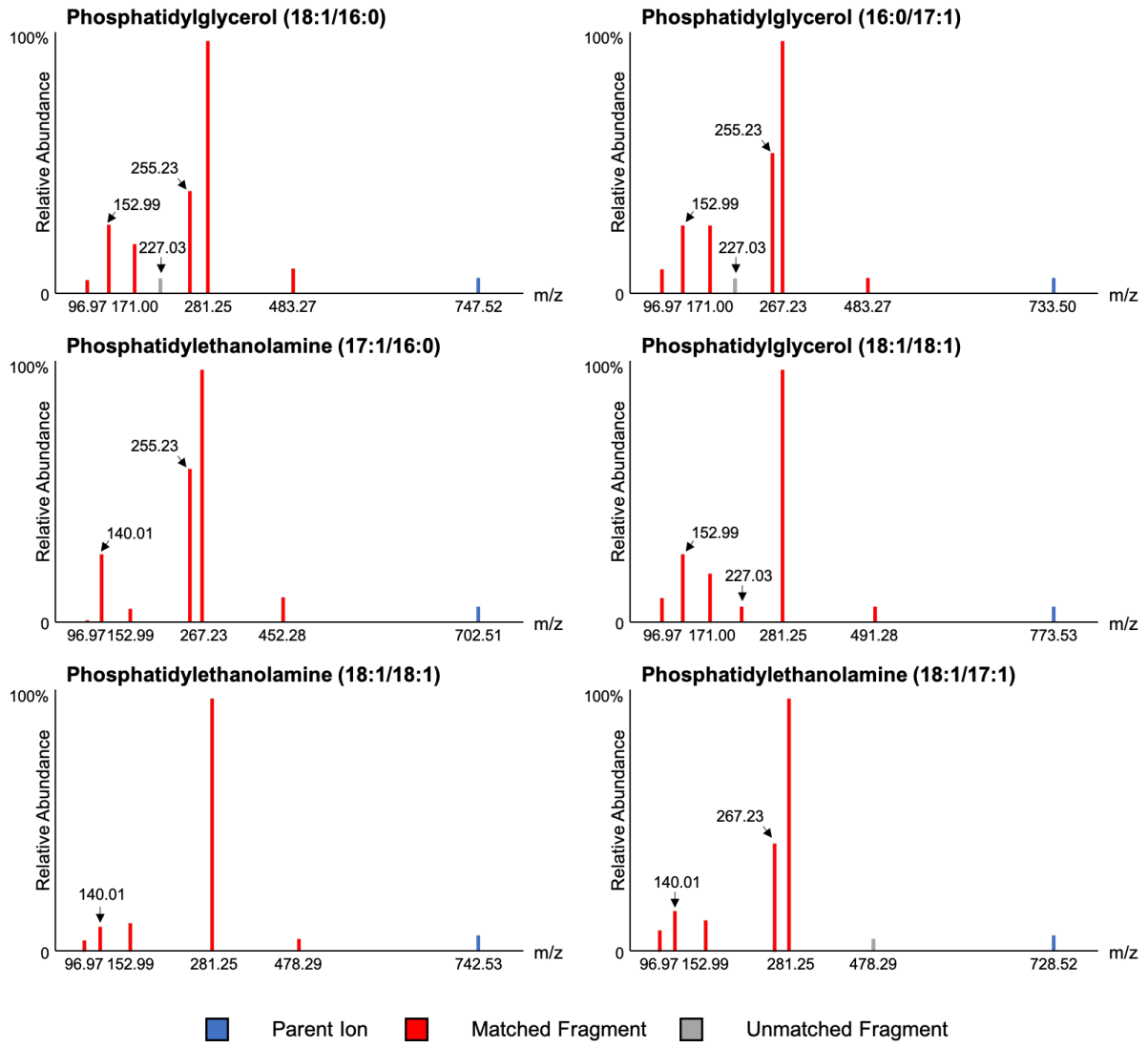

Figure C.6. MS/MS Spectra of Identified Lipids. DESI-MS/MS was performed by directly sampling colonies using the microporous membrane scaffold method. Only features that localized to colony areas were considered as fragment ions. All MS/MS experiments were performed at collision energies of 30 V.

C.1.2 Supplemental Tables

Table C.1: List of *E.coli* strains, genotype and primer used for their validation.

Strains	Genotype/construct	Primers
pBAD18-tesA WT	pBAD18 carrying WT tesA under P_{BAD} control, Amp^R	Forward (TesA-seq-FW) GCCTGCCTTGTTGAATGATAA Reverse(TesA-seq-RV) AATACCGTCATCCTGCATCC
NHL17	K12 MG1655 ΔaraBAD ΔfadD::trc-CpFatB1.2-M4-287 (C8-specific *Cuphea palustris* FatB1 thioesterase)	Forward (rNHL115) GCATCGTCCGTGGTAATCATTTG Reverse(rNHL93) GCATTTATGCCGATGTGAACGG
TY05	K-12 MG1655 ΔfadDEAB::trcBTE (acyl-ACP thioesterase from *Umbellularia californica*)	Forward (fadABKO_colPCR_fwd) GGAGTGAATAAGTAACGCATCC Reverse (fadABKO_colPCR_rv) GCTGTCGCGTCTTATCGTGC
TY06	K-12 MG1655 DfadDEAB::trcBTEH204A	Forward (rNHL229) AGGCAAATTCTGTTTTATCAGACC Reverse (gCRM323) GCACTCCCGTTCTGGATAATG

APPENDIX D

SUPPLEMENTARY MATERIALS FOR CHAPTER 4

Chiral Separation of Diastereomers of the Cyclic Nonapeptides Vasopressin and Desmopressin by Uniform Field Ion Mobility Mass Spectrometry

Shawn T. Phillips, Berkley M. Ellis, James N. Dodds, Jody C. May, and John A. McLean*

Department of Chemistry, Center for Innovative Technology, Vanderbilt Institute of Chemical Biology, and Vanderbilt Institute for Integrative Biosystems Research and Education, Vanderbilt-Ingram Cancer Center, Vanderbilt University, Nashville, TN 37235-1822

Comments on Modeling Ion Mobility Distributions Presented in this Work

In this Supporting Information we provide additional spectra to support our conformational analysis described in the main text. Supplemental Figure S1 details the fragmentation spectra associated with both conformers of 8L-vasopressin and Supplemental Figure S2 illustrates the observed two conformations of 8L-vasopressin, yet in helium drift gas, which is more closely aligned to experimental conditions in our computation methods.

D.1.1 Supplemental Tables

Table D.1 A summary of drift tube CCS measurements of nonapeptides.

Nonapeptide		**Ion Form**	**Mass (Da)**	**$^{DT}CCS_{N2}$ (Å^2)**	**$^{DT}CCS_{He}$ (Å^2)**
8L-Vasopressin - A - B	8L-VP	$[M+H]^+$	1084	302.2 ± 0.2 310.4 ± 0.6	219 ± (0.9) 224 ± (1.4)
8D-Vasopressin	8D-VP	$[M+H]^+$	1084	309.8 ± 0.2	226 ± (1.1)
8L-Desmopressin	8L-DP	$[M+H]^+$	1069	307.8 ± 0.5	225 ± (1.2)
8D-Desmopressin	8D-DP	$[M+H]^+$	1069	314.4 ± 0.4	230 ± (1.1)

The nitrogen values in this table correspond to three replicate measurements (N=3) from separate days. Helium measurements were from a single set of experiments (uncertainty given in parenthesis, which is much higher in helium compared to nitrogen). The x axis was converted from drift time to CCS in the main text using the single field method described by Stow *et. al.* (*Anal. Chem.* **2017**, *89*, 9048-9055).

D.1.2 Supplemental Figures

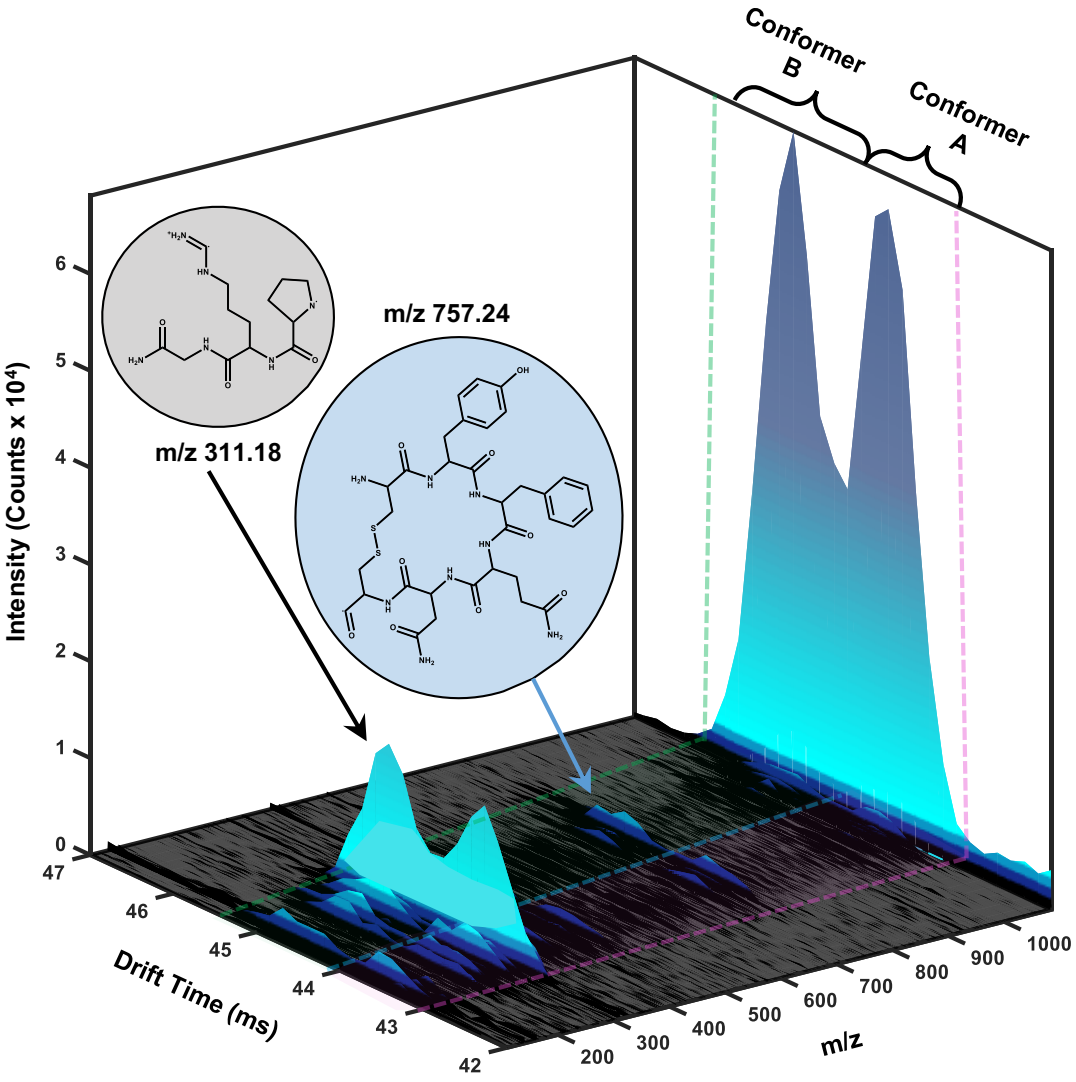

Figure D.1. Ion mobility fragmentation data for 8L-vasopressin. Both conformers have the same fragmentation spectra, providing increased confidence that both distributions at m/z 1084 are from the same parent ion, and are not a contaminant.

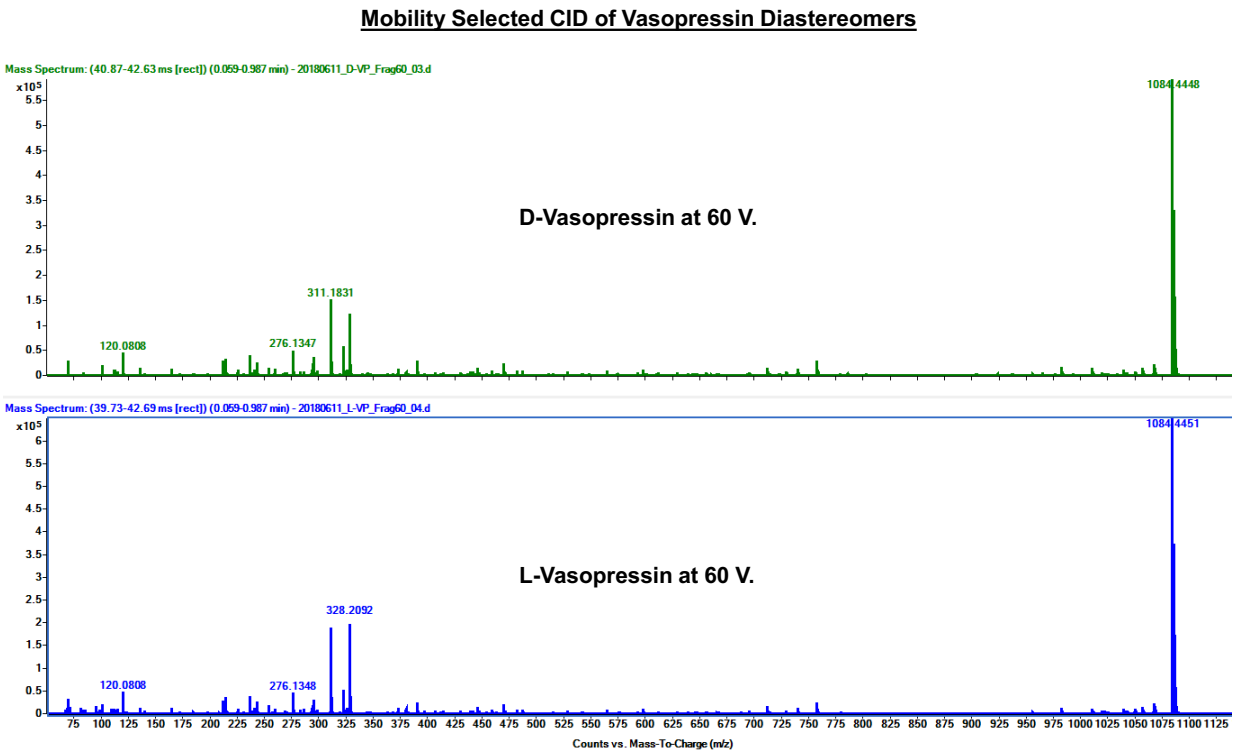

Figure D.2. Mobility selected mass spectra for 8D- (Top) and 8L- (Bottom) vasopressin diastereomers for 60 V (laboratory frame) CID. While both stereoisomers have the same fragmentation spectra, and hence does not eliminate the possibility of some "D" vasopressin as a contaminant in "L" VP from the manufacturer, this information provides additional confidence that the secondary conformer is not an unrelated molecule with the same molecular formula as 8L-VP.

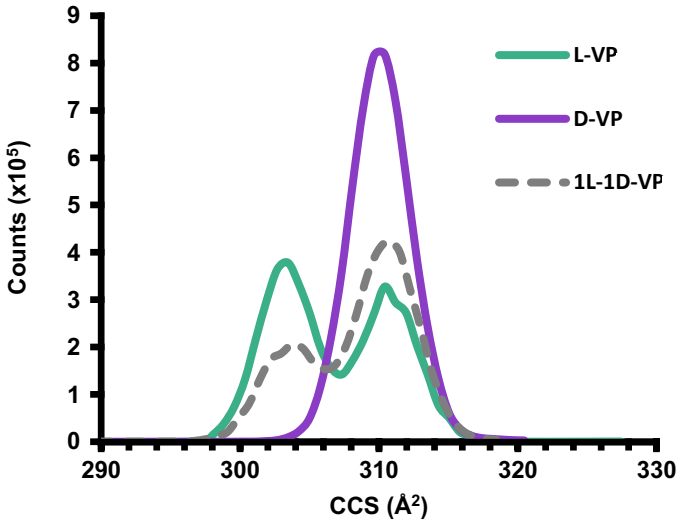

Figure D.3. Ion mobility spectra for the protonated $[M+H]^+$ Vasopressin diasteromers (L and D) in addition to a 1:1 mixture (gray dashed trace). The IM distribution for 8D-VP and the larger conformer of 8L-VP have essentially the same measured CCS. As more 8D-VP is added to a solution of 8L-VP (see gray trace), the distribution at higher CCS (*ca.* 310 Å^2) increases in abundance in comparison to the distribution of 8L-VP at lower CCS (*ca.* 304 Å^2). This observation helps support the claim that the two peaks observed for 8L-VP originate solely from the 8L-VP sample.

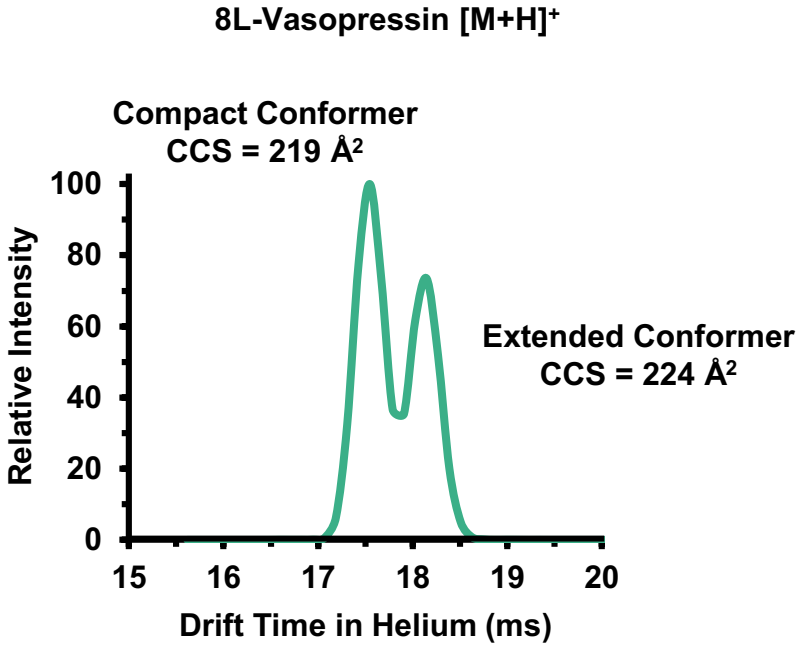

Figure D.4. Drift time distributions for singly-protonated 8L-vasopressin obtained when conducting the IM separation in helium drift gas. A with nitrogen drift gas (Figure 2B of the main text), two distinct conformational populations are observed in helium. These helium-based CCS measurements more closely align with the computational results.

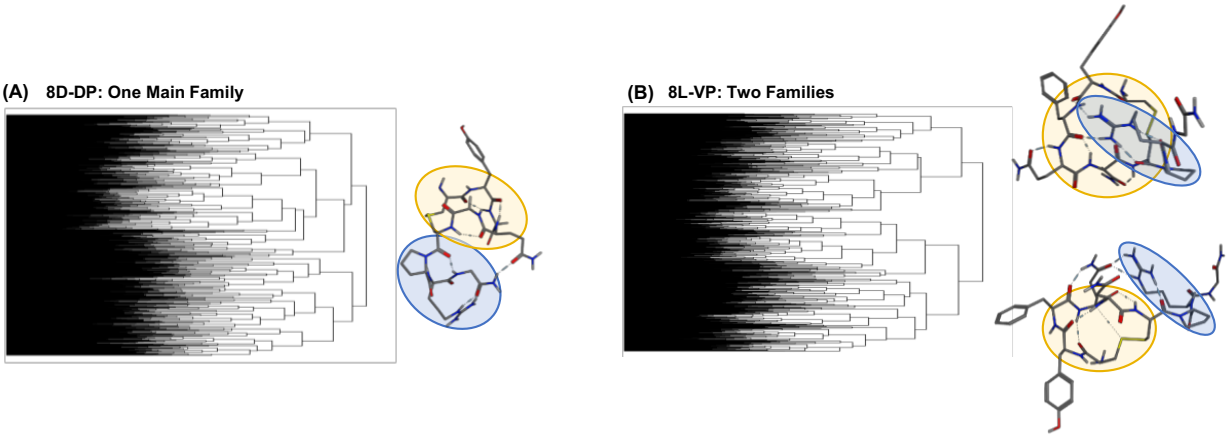

Figure D.5. RMSD Clustering analysis was performed such that the 3,000 structures for each isomer were reduced to 6 main families on the basis of previous studies on vasopressin. **(A)** 8D-Vasopressin exhibits one dominant family, while 8L-Vasopressin has two main families **(B)**. These results are mirrored in the conformation analysis and drift spectra.

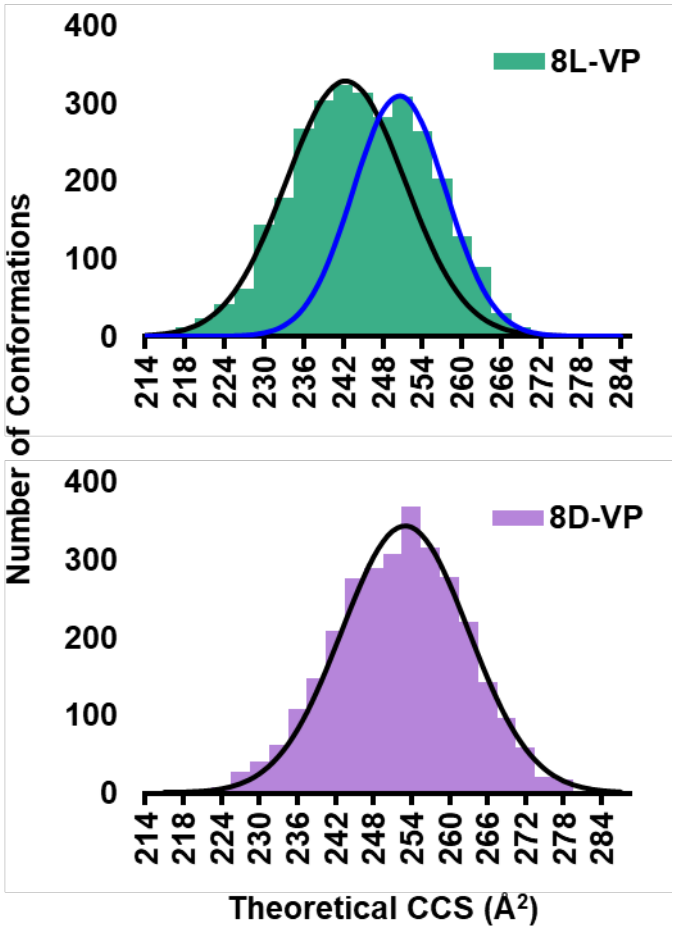

Figure D.6. Distribution of theoretical structures based on the calculated CCS. Here, normal distributions are overlaid across the histograms to illustrate that two structural families were observed for 8L-VP whereas only one primary structural family at higher CCS is observed for 8D-VP.